TEXAS TECH UNIVERSITY
Multidisciplinary Research in Transportation™

Design Guidance for Low-Water Crossings in Areas of Extreme Bed Mobility, Edwards Plateau, Texas

David B. Thompson, Theodore G. Cleveland, Xing Fang, Keh-Han Wang

Notice

The United States Government and the State of Texas do not endorse products or manufacturers. Trade or manufacturers' names appear herein solely because they are considered essential to the object of this report.

Technical Report Documentation Page

1. Report No.: FHWA/TX–08/0–4695–3	2. Government Accession No.:	3. Recipient's Catalog No.:

4. Title and Subtitle:
    Design Guidance for Low-Water Crossings in Areas of Extreme Bed Mobility, Edwards Plateau, Texas
		5. Report Date:
		    March 23, 2009

		6. Performing Organization Code:
7. Author(s): David B. Thompson, Theodore G. Cleveland, Xing Fang,and Keh-Han Wang		8. Performing Organization Report No. 0–4695–4

9. Performing Organization Name and Address:
    Texas Tech University
    College of Engineering
    Box 41023
    Lubbock, Texas 79409-1023
		10. Work Unit No. (TRAIS):

		11. Contract or Grant No. : Project 0–4695–01–2

12. Sponsoring Agency Name and Address
    Texas Department of Transportation
    Research and Technology Implementation Office
    P. O. Box 5080
    Austin, TX 78763-5080
		13. Type of Report and Period Cover:
		Technical Report: September 2003 – August 2008

		14. Sponsoring Agency Code:

16. Abstract:

The purpose of this report is to present results from a combination of field and laboratory investigations of mobility of gravel to cobble sized materials in Texas streams on the Edwards Plateau. TxDOT uses low-water crossings for many of the roadways in the region, particularly where the streams are ephemeral. When the streambed mobilizes, instances of roadway loss of service, either by deposition of large amounts of bed materials or by structural failure associated with streambed mobilization are relatively common. The objectives of the project were to determine the mechanics of streambed mobilization and develop design guidelines (approaches) to mitigate damage associated with streambed mobilization events. Numerical models were developed and a GIS approach was used to demonstrate how area subject to streambed mobilization can be identified through application of these tools. Physical models were used to demonstrate the mechanics of streambed mobilization and test current design solutions. The physical model identified the mechanics for culvert "self-clearing" and that a porous roadbed results in changes to the flow dynamics that affect bedload deposition in the low-water crossing area. An offset three-culvert design was identified by TxDOT engineers as an alternative to the more-common box culvert.

17. Key Words Hydraulics, bed mobility, sediment transport, low-water crossings	18. Distribution Statement No restrictions. Document available to public through National Technical Information Service, Springfield, VA 22161, www.ntis.gov		

19. Security Classif. (of this report)
    Unclassified
	20. Security Classif. (of this page)
	    Unclassified
		21. No. Pages
		184
			22. Price

This page intentionally left blank.

Design Guidance for Low-Water Crossings
In Areas of Extreme Bed Mobility,
Edwards Plateau, Texas

by
David B. Thompson, R.O. Anderson Engineering, Inc.
Theodore G. Cleveland, Texas Tech University
Xing Fang, Auburn University
Keh-Han Wang, University of Houston

with contributions by,
William H. Asquith, U.S. Geological Survey
Franklin T. Heitmuller, U.S. Geological Survey
Meghan C. Roussel, U.S. Geological Survey

AUTHOR'S DISCLAIMER

The contents of this report reflect the views of the authors who are responsible for the facts and the accuracy of the data presented herein. The contents do not necessarily reflect the official view of policies of the Texas Department of Transportation or the Federal Highway Administration. This report does not constitute a standard, specification, or regulation.

PATENT DISCLAIMER

There was no invention or discovery conceived or first actually reduced to practice in the course of or under this contract, including any art, method, process, machine, manufacture, design or composition of matter, or any new useful improvement thereof, or any variety of plant which is or may be patentable under the patent laws of the United States of America or any foreign country.

ENGINEERING DISCLAIMER

Not intended for construction, bidding, or permit purposes.

TRADE NAMES AND MANUFACTURERS' NAMES

The United States Government and the State of Texas do not endorse products or manufacturers. Trade or manufacturers' names appear herein solely because they are considered essential to the object of this report.

This page intentionally left blank.

Acknowledgements

---

[1] Dr. Fang was at Lamar University for the majority of the duration of this project. He is now located at Auburn University.

[2] Dr. Cleveland was at University of Houston for the majority of the project duration. He is now located at Texas Tech University.

CONTENTS

LIST OF TABLES

LIST OF FIGURES

1. Background

1.1. Introduction

Stream crossings are generally designed with culverts or bridge structures to pass hydrologic events of ten-percent annual exceedance frequency, more or less[1]. A *low-water crossing* is a road crossing of a stream channel where the structure is designed to convey only relatively frequent hydrologic events. Events greater than the design standard are allowed to pass over the structure.

In most geographic areas, traffic is only periodically impacted by flows overtopping low-water crossings. The period of overtopping is limited to a few hours up to a day or two. After the overtopping event recedes, traffic can resume use the low-water crossing in a normal fashion after local maintenance crews examine the structure to ensure no damage occurred during the hydrologic event. Low-water crossings are seen as an economic alternative to more substantial structures in regions where most flood flows are relatively small and where loss of service for a short period of time does not significantly impact the local populace.

However, in the hill country region of the Edwards Plateau of Texas, the experience is different from other Texas locations. Some streams mobilize and transport large quantities of relatively coarse bed material. At low-water crossings, this material may be deposited on the right-of-way or on the highway. Furthermore, substantial erosion at or near the structure may occur and numerous structure failures were reported by Texas Department of Transportation (TxDOT) District personnel.

Low-water crossings in as many as 17 Texas counties in the hill country region may be affected. Specifically, the Junction, Texas region experiences many of these failures. Therefore, initial focus of project research was directed toward highways in Edwards, Kimble, and Real Counties.

A photographic example of such a problem is shown in Figure 1.1. The amount of transported material is evident from the photograph. In addition, the asphaltic-concrete wear course was stripped from a substantial portion of the crossing. In some areas, the highway foundation was lost to erosion as well. The image depicted in Figure 1.1 is characteristic of problems of this type.

Because of structural and depositional failure modes, TxDOT personnel sought guidance on design of low-water structures and on mitigation of depositional processes. As a result, TxDOT Research Project 0–4695 was initiated to review the literature, reconnoiter several sites that exhibited prob-

---

[1] The design exceedance frequency depends on the highway class — primary highways are designed for less-frequent events than off-system highways.

Figure 1.1: Paks crossing of Johnson Fork on FM 2169 after a flood event in 2000.

lem behaviors, determine what further research would be fruitful, and execute the resulting research plan.

The initial research program was established with a two-year duration to establish whether or not to continue studies past the first two years. Initial objectives were:

1. To conduct a review of the professional literature treating streambed mobility,

2. To review TxDOT Maintenance Management Information System (MMIS) records to attempt to quantify the actual costs associated with streambed mobility problems,

3. To conduct field studies at three locations along Johnson Fork Creek,

4. To execute qualitative physical model studies of materials recovered from field investigations, and

5. To develop a research plan to address issues raised during the initial research phase.

The literature review is documented by Heitmuller and others (2005). The interim report was produced by Thompson (2004). After review of the interim report, the TxDOT project management team met with the research team and a work plan was developed to proceed with a second phase of the research project.

1.2. Objectives

Project objectives fell under two broad questions.

1. Why are some stream crossings subject to significant bed-mobility events?

2. What engineering solutions are appropriate for stream crossings subject to significant bed-mobility events?

1.3. Purpose

The purpose of this report is to document results of TxDOT Research Project 0–4695 and present guidelines developed to assist TxDOT designers in dealing with low-water crossing design in areas of significant streambed mobility.

2. PROCEDURE

Because of the phased approach to the project research, two work plans were developed. The first, or initial work plan included: a limited field investigation, a review of TxDOT maintenance records from several counties in the affected geographic area, a literature review, a qualitative physical model, and initial qualitative numerical modeling. A significant objective of the initial phase of project research was to determine the justification for investing additional TxDOT resources in further research (based on the outcomes of initial project activities), then given that additional investment in project research was justified, development of a second-phase work plan to complete project objectives.

The procedures for the first and second phase of the project are developed in the following sections of this report. These components of this report are largely extracted from the original project agreement (technical proposal) and modifications to project agreement (development of the technical proposal).

2.1. Development of the Work Plan

The development of Project 0–4695 was different than many other TxDOT research projects. In the research team's proposal, a substantial amount of work (and associated expense) was proposed. Because of the nature of this particular problem, neither the research team nor the TxDOT project management team were certain that project goals would be met. The nature of the research problem was such that it was more "researchy" than many TxDOT research problems. As a result, a phased approach was developed by the research team in conjunction with the TxDOT project management team in which a two-year study would be undertaken to clarify the nature of subsequent research, should the project move forward to more in-depth work.

2.1.1. Initial Work Plan

The initial work plan was developed in response to a request from the TxDOT project management team. The initial proposal developed in response to the request for proposal was substantial and not typical for TxDOT research projects. This was because the research team believed the nature and scope of the problem were substantial and did not fit the typical research problem statement developed by TxDOT engineers. Therefore, in cooperation with TxDOT personnel, a revised work plan was developed:

4

1. Conduct a review of the professional literature treating streambed mobility,

2. Review TxDOT MMIS records for Edwards, Real, and Kimble Counties to attempt to quantify the actual costs associated with streambed mobility problems,

3. Conduct field studies at three locations along Johnson Fork,

4. Execute trial physical model studies of materials recovered from field investigations, and

5. Develop a research plan to address issues raised during the initial research phase.

At the end of the first two years (the initial phase of the research project), an interim report (Thompson, 2004) was delivered. The research plan developed as part of that work would be reviewed by TxDOT personnel and a determination to continue the research project would be made.

2.1.2. Modified Work Plan

Based on the work completed in the initial phase of the research project, a revised work plan was developed and presented as a modification to the original proposal. The additional tasks included an examination of the geomorphology of area streams, physical modeling of potential structures to be used for stream crossings, numerical modeling of selected stream crossings from the field investigations, and monitoring of selected sites. The additional tasks of the modified work plan were:

1. Conduct a geomorphologic assessment of a portion of the affected area,

2. Continue physical modeling experiments to evaluate selected potential design approaches,

3. Expand detailed numerical modeling experiments to assess the utility of numerical models (such as HEC-RAS) for evaluating bed-mobility and assist development of appropriate designs, and

4. Continuous monitoring of one or more selected sites during project activities to provide additional data for interpretation of modeling results.

2.2. Literature Review

The literature review comprised three components: (1) To review TxDOT maintenance records (MMIS) and extract information about maintenance issues associated with mobile-bed streams, (2) to review the professional literature was examined to determine what, if any, work related to project objectives was conducted by other researchers, and (3) make a preliminary determination of the geographic extent of the problem. Results from the literature review are documented by Heitmuller and others (2005). Results from the MMIS review are presented in Section 3.1. Appropriate literature is referenced as needed in the following sections of this report.

2.3. Field Investigation

A field investigation was conducted at three sites where crossing instability was associated with bed mobility of the stream. The three sites were located on Johnson Fork Creek at the Paks, Guzman, and Lowlands crossings one site on the Nueces River at the Ben Williams crossing. The objectives of field studies were to examine a variety of different mechanics for determining bed grain-size distributions, collect survey data (particularly slope), and generally gather field information for later use in modeling activities. Results from field investigations are presented in Section 3.3.

2.4. Qualitative Laboratory and Numerical Modeling

2.4.1. Qualitative physical model

It was important to determine, on a qualitative basis, whether or not laboratory hydraulic study of several TxDOT designs or models of existing structures reproduce the observed problems of bedload deposition, bedload abrasion, and bedload-induced failure of TxDOT structures. The intent of physical (laboratory) modeling is to reproduce the field-observed phenomenon in a laboratory over a short test section. The intent of the qualitative physical modeling developed as part of the research project is to determine what kinds of forces are involved in bed mobility of gravel-cobble stream beds.

For example, in high magnitude, fast rising floods, there are unusual hydraulic drag forces on bed materials and there also is an underflow (porous flow) component. It is possible that sufficient buoyancy forces are generated over the whole bed such that bed sediment mobilization is enhanced. Furthermore, it is possible that these flows entrain significant amounts of soil (not rock) so that the viscosity and density of the working fluid may be increased.

The results extracted from the qualitative physical modeling were used in the design of more detailed experiments. An illustration of the complex hydraulics that will require modeling is shown in Figure 2.2 — in the figure gravel choked a significant portion of the low-water conveyance potential of the structure.

2.4.2. Screening Model

Parker's (Parker, 1990) method for the estimation of surface-based bedload transport is expressed in Equations 2.1 and 2.2. This approach is an extension of the substrate-based bedload transport model developed from the data of Oak Creek in Oregon (Parker and others, 1982). Parker's equation can be used to estimate bedload $Q_{Gi}, (ML^{-1}T^{-1})$ over the channel width for each size group of particles defined in the particle size distribution (surface layer) in a gravel-bed stream, and then compute the total bedload transport rate (W) based on the fraction of particles (F_i) in each size

group.

$$W = \sum Q_{Gi} F_i, \tag{2.1}$$

$$\frac{R g p_i Q_{Gi}}{B u_*^3} = \alpha F_i G \left[\omega \phi_{sgo} \left(\frac{\overline{D_i}}{D_{sg}} \right)^{-\beta} \right], \tag{2.2}$$

where g is acceleration of gravity (LT^{-2}), R is the submerged specific gravity for gravel and equals to $(\rho_s/\rho - 1)$ (ρ_s is density of sediment and ρ is the density of water), Q_{Gi} is volumetric bedload (gravel) transport rate ($ML^{-1}T^{-1}$) for ith size group of bedload, B is channel width (L), u_* is shear velocity (LT^{-1}), $\overline{D_i}$ is the mean grain size of the ith size group (L), p_i is the volumetric fraction of the ith size group in bedload, F_i is the volumetric fraction of the ith size group in the surface layer, D_{sg} is geometric mean grain size of the surface layer, ϕ_{sgo} is normalized Shields stress, ω is a function of the normalized Shields stress ϕ_{sgo} and the arithmetic standard deviation of the surface layer. The coefficients α and β are given as: $\alpha = 0.00218$ and $\beta = 0.0951$ (Parker, 1990). The parameter ω is a function of the normalized Shields stress ϕ_{sgo},

$$\omega = 1 + \frac{\sigma_0}{\sigma_s} (\omega_0 - 1), \tag{2.3}$$

where σ_0 and ω_0 are determined as functions of ϕ_{sgo} (Parker, 1990) and are listed in Table 2.1.

The normalized Shields stress, ϕ_{sgo}, is acquired by dividing the surface-based Shields stress τ_{sg}^* by the reference stress τ_{rsgo}^*,

$$\phi_{sgo} = \frac{\tau_{sg}^*}{\tau_{rsgo}^*}, \tag{2.4}$$

where the reference Shields stress, $\tau_{rsgo}^* = 0.0386$ (Parker, 1990). The surface-based Shields stress, τ_{sg}^*, is defined as

$$\tau_{sg}^* = \frac{u_*^2}{R G D_{sg}}. \tag{2.5}$$

Shear velocity, u_*, is calculated using or assuming mean or normal flow conditions in the channel and is given as

$$u_* = \sqrt{ghS}, \tag{2.6}$$

where S is the channel bed slope or the channel energy slope, and h is the mean water depth in the river.

The function G was developed from analysis of Oak Creek data for estimating gravel transport and is given by Parker (1990) as

$$G(\phi) = \begin{cases} 5474 \left(1 - \frac{0.853}{\phi} \right)^{4.5} & \phi > 1.59, \\ \exp \left[14.2(\phi - 1) - 9.28(\phi - 1)^2 \right] & 1 \le \phi \le 1.59, \\ \phi^{14.2} & \phi < 1, \end{cases} \tag{2.7}$$

Table 2.1: Relations between ϕ_{sgo} and parameters σ_0 and ω_0 (Parker, 1990).

ϕ_{sgo}	σ_0	ω_0
0.6684	1.011	0.8157
0.7639	1.011	0.8157
0.8601	1.01	0.8182
0.9096	1.008	0.8233
0.9615	1.004	0.8333
1.000	0.9997	0.8439
1.055	0.9903	0.8621
1.108	0.9789	0.8825
1.197	0.9567	0.9214
1.302	0.9273	0.9723
1.407	0.8964	1.025
1.529	0.8604	1.083
1.641	0.8287	1.13
1.702	0.8123	1.153
1.832	0.7796	1.196
1.937	0.7554	1.225
2.044	0.7326	1.25
2.261	0.6928	1.287
2.499	0.6585	1.313
2.732	0.6345	1.333
2.993	0.615	1.352
3.477	0.5877	1.38
4.075	0.564	1.403
4.469	0.5523	1.414
5.016	0.5395	1.426
6.158	0.5209	1.444
7.821	0.5045	1.458
10.06	0.4917	1.469
14.38	0.479	1.48
19.97	0.4712	1.486
25.79	0.4668	1.49
38.57	0.462	1.493
68.74	0.4578	1.497
91.95	0.4564	1.498
231.2	0.4541	1.499
2320	0.4527	1.50

where

$$\phi = \omega \phi_{sgo} \left(\frac{\overline{D_i}}{D_{sg}} \right)^{-\beta}. \tag{2.8}$$

For the case of a complex channel cross section in a floodplain, the cross section is divided into the main channel, plus the left and right overbank areas of the floodplain. It is further assumed that no bedload transport occurs on overbank areas of the floodplain. Parker's surface-based bedload equation for prismatic channels (rectangular or trapezoidal geometry) is modified

$$u_*^2 = gR_{hc}S, \tag{2.9}$$

$$\frac{RQ_{Gi}p_i}{A_c Su} = \alpha F_i G \left[\omega \phi_{sgo} \left(\frac{\overline{D_i}}{D_{sg}} \right)^{-\beta} \right], \tag{2.10}$$

where A_c denotes the flow area in the main channel, R_{hc} denotes the hydraulic radius of the flow in the main channel.

In this study, the surface-layer particles are the objective of the analysis. Therefore, they are treated as the bedload particles in the study area, so p_i equals F_i in Equations 2.1 and 2.2,

$$W = \sum Q_{Gi} F_i, \tag{2.11}$$

$$\frac{RgQ_{Gi}}{Bu_*^3} = \alpha G \left[\omega \phi_{sgo} \left(\frac{\overline{D_i}}{D_{sg}} \right)^{-\beta} \right], \tag{2.12}$$

The calculation steps for implementation Parker's equation are shown in Figure 2.1. In Figure 2.1, the first layer is model input data, which includes three parts of information: (1) channel geometry including bed slope or energy slope and channel discharge; (2) grain size distribution; and (3) grain specific gravity. The second layer data are computed flow parameters, including mean flow velocity and water depth in the channel for a specific discharge or discharges and characteristic parameters for the grain size distribution. Remaining layers follow the discussion for Equations 2.1–2.12 to implement Parker's method for estimating gravel transport rate. Mean channel flow velocity and flow depth are computed from the channel geometry and the channel discharge by assuming steady, uniform (normal) flow. Grain size characteristics, such as grain size d_{90} and geometric mean value of gravel, are computed from the grain size distribution and used as model input data. Based on these results, the principal model parameter for Parker's method, channel shear velocity u_* (the third layer), is computed using the SurGTAM spreadsheet program.

After channel shear velocity (the third layer), grain geometric mean value (the second layer) and grain specific gravity (the first layer) are obtained, the model required parameters for Parker's method, such as the parameter ω (Equation 2.3), Shields stress τ_{rsgo}^* (Equation 2.5), normalized Shields stress ϕ_{sgo} (Equations 2.9 and 2.10), the function G (Equation 2.7) are computed using SurGTAM. Finally, these parameters are used in Parker's method (Equations 2.11 and 2.12) to calculate the gravel transport rate Q_{Gi} for the ith size group and bedload W for all size groups over the channel width.

9

Channel geometry
Channel discharge

Grain size distribution

Submerged specific gravity: $R=(\rho_s/\rho-1)$
acceleration of gravity: g

Flow velocity: u
Water depth: h

Particle distribution: D_{s90}

Geometric mean grain size of the surface layer: D_{sg}

Roughness height:
$K_s = 2 D_{s90}$

Shear velocity: u*
$u/u_* = 2.5 \ln(11h/Ks)$

Surface based shield stress: $\tau_{sg}*$
$= u_*^2/(RgD_{sg})$

Normalized shield stress:
$\Phi_{sgo} = \tau_{sg}*/\tau_{rsgo}*$
(where $\tau_{rsgo}* = 0.0386$)

ω_0, σ_0 (from Parker 1990a Figure)

Mean grain size of the i-th size group: $\overline{Di}$

$\omega = 1 + (\sigma_0/\sigma_s)(\omega_0 - 1)$

$\Psi = \left[\omega \phi_{sgo} \left(\frac{\overline{D_i}}{D_{sg}} \right)^{-\beta} \right]$

Volumetric fractions of different size groups: Fi
$\alpha = 0.0218$
$\beta = 0.0951$
Percent finer values: p_i
Channel Width: B

$G(\Psi)$

Volumetric bedload (gravel) transport rate: Q_G

$$\frac{R\ g\ p_i\ Q_{Gi}}{B\ u_*^3} = \alpha\ F_i\ G \left[\omega\ \phi_{sgo} \left(\frac{\overline{D_i}}{D_{sg}} \right)^{-\beta} \right]$$

Figure 2.1: Flow chart for implementing Parker's bedload transport model.

2.5. Geomorphology

Geomorphologic and hydraulic data collection and analysis of river and stream channels in the Edwards Plateau would enhance the understanding of processes contributing to bedload transport and deposition at low-water crossings. These data facilitates modeling efforts and laboratory flume research. Geomorphology and channel hydraulics can be examined in the field and through computational analysis. Field research can further be subdivided into discrete measurements and continuous monitoring. This section addresses all field activities except continuous monitoring. The interpretation of geomorphologic and hydraulic data and the application of these findings in models and laboratory experiments could result in optimal design criteria for low-water crossings.

Geomorphic field research includes channel surveying, particle-size analyses, geophysics, and techniques to estimate bedload transport rates and scour. Surveys of channel cross-section and slope provide data for calculating shear stresses at the channel bed and the power of flows to mobilize and transport gravel. Surveys may also be used to compare pre-flood and post-flood channel conditions. Particle-size analyses are necessary to determine the proportion of material transported during a given flow. Particle-tracing techniques could be used to directly measure gravel transport rates and trajectories. Geophysical techniques, namely electromagnetic resistivity (ER), are used to distinguish subsurface pores from solid rock. A geophysical survey of channels in the study area could provide volumetric estimates of gravel and void space, possibly even distinguishing between water- or solid-filled void space. Other devices could be used to determine depth of scour during floods. This information could be used to indicate channel reaches subject to relatively high rates of gravel mobilization and transport.

Hydraulic field research consists of indirect methods of measuring peak flood discharges, structural assessments, and assessment of pressure fluctuations at the channel bed. Indirect peak discharge measurements provide a quantitative association between structural damage and the magnitude of floods. Structural assessment of low-water crossings includes location of culverts, height above the channel bed, orientation to flow, and general arrangement. It is anticipated that these characteristics affect the structural integrity of low-water crossings during floods. Additionally, the installation of stress sensors at the channel bed could reveal the forces necessary to mobilize bed material or damage the structure.

Computational methods for geomorphologic and hydraulic characterization are comparatively rapid and accurate procedures to characterize river basins and channel reaches. Geographic information systems (GIS) and digital aerial photography enable mapping of channel position and gravel-bar migration through time. Channel sinuosity, meander bend curvature, and other geomorphic parameters can be measured using aerial photography. Digital elevation models (DEM) can be used to determine a variety of basin characteristics, including drainage area and basin slope. Coupled with geographic positioning system (GPS) data from field activities, computational methods provide a powerful tool for assessing the spatial patterns of low-water crossing susceptibility and condition.

Geomorphologic and hydraulic field research at low-water crossings is an important contribution to numerical models and laboratory experiments involving bedload transport. Discrete field assessments at numerous locations throughout the Edwards Plateau increase the chances for observation

of changes at low-water crossings following floods. Coupled with computational methods, field analyses would provide the information necessary to accurately model processes at low-water crossings and prescribe techniques for optimal structural design.

2.6. Physical modeling

The purpose of the physical model studies was to qualitatively determine

- Whether or not laboratory hydraulic studies of models of existing structures can reproduce observed problems of bedload deposition, bedload abrasion, and bedload induced failure, and

- Whether there are design elements than can mitigate these phenomenon.

A collateral goal was to gather additional scientific knowledge, even if only observational, about the mobilization, deposition, and solids accommodation through a low-water crossing structure.

The intent was to reproduce the phenomenon in a laboratory over a short test section using small models to determine what kinds of forces are involved in bed mobility of gravel-cobble stream beds. For example, in high-magnitude, fast-rising floods there are unusual hydraulic drag forces on the bed materials and there also is an underflow (porous flow) component. It is possible that sufficient buoyant forces are generated over the bed such that bed-particle mobilization is enhanced. Furthermore, these flows entrain significant amounts of soil (not rock) such that the viscosity and density of the working fluid may be increased.

An illustration of the complex hydraulics that inspired the modeling is displayed in Figure 2.2. The Figure 2.2 image was captured in 2003. In the image, gravel choked a significant portion of the low-water conveyance potential of the structure.

The source of gravel in the image is a combination of bed-material mobilization by the hydraulic action of the river combined with maintenance activities comprising movement of gravel deposits from the low-water crossing after an event. Although gravel present in the culverts might result from maintenance activities (clearing the deposits), the on-site observations by research and Tx-DOT personnel indicated that the gravel is too far inside the culvert to be attributed entirely to maintenance activities.

Other complex issues are illustrated in Figures 2.3 and 2.4. These images are from circa 2007. They were captured during a large rainfall event. In the first image the water surface is just at the roadway and overtopping of the roadway was imminent (flow is from left to right in the image). On the downstream side of the crossing the river still has significant flow capacity. More interesting is the line of vortices on the upstream side captured in Figure 2.4. These vortices persisted for several minutes while being observed. Vortex size is not apparent from the images. Furthermore, these vortices were not only formed by debris but one could observe reasonably large stones (and other debris) dislodging near the vortex and travel through the structure.

Figure 2.2: RR 335 at Ben Williams Ranch crossing Nueces River about 12 miles northeast from Barksdale, Edwards County, Texas. (Near the Real County line). Upstream side near river. All culverts have gravel deposit except for the southern four culverts which currently (03-09-2003) are passing flow. The other culverts also pass some flow, but behave as porous medium.

Figure 2.3: US 374 Northwest from Telegraph, Texas (between Junction and Rocksprings, Texas). Image is on a tributary of the South Llano River.

Figure 2.4: US 374 Northwest from Telegraph, Texas (between Junction and Rocksprings, Texas). Image is on a tributary of the South Llano River. Notice the vortices near the front left of the image at the water-roadway interface.

It is this very potential (to accommodate water and solids) that is the focus of the scientific and practical aspects of the physical model studies.

2.6.1. Physical Model Studies — General Approach

The general approach was to construct and instrument a flume for semi-quantitative modeling of generic low water crossing structures.

Quoting from the proposal:

> The University of Houston has two options for physical modeling of low-water crossings. The first option is a flume that is 4 feet wide and about 16 to 30 feet long. The flume has adjustable slopes and sufficient flow rates. It is unknown at this time how the bed-load will be modeled in the flume. The second option is a glass-walled wave tank measuring about 120 ft long and 4 ft wide; the tank is readily adapted to flow studies such as required by the proposed research.
>
> Texas Tech University has a 15-ft tilting flume that can be used for qualitative exper-

iments. However, it is proposed that Tech technicians build a longer flume as part of the project so that aquarium gravel is of the approximate scale of the gravel beds of the problem streams. Then a control system can be fabricated that will introduce a floodwave similar to those experienced by the prototype.

Ultimately, the second UH option was selected, that is adapt an existing tank to perform the studies. The task was undertaken in November 2006. The flume was operational in February 2007 and experiments were conducted for the remainder of that year and partly into 2008.

2.6.2. Experimental Design

The experiments were conducted in a purpose-built wooden flume resting on top of an existing wave tank. The flume was 48-feet long, 3-feet wide, and 2-feet deep. Flow was provided by six $\frac{3}{4}$ HP sump pumps with isolation valves and the head tank to dissipate flow fluctuations. A small viewing window was cut into the side of the flume to capture images during the experiments.

A digital video recording system was purpose-built to support the research — when fully functional the DVR system could capture images on 4 channels at 30 frames per second. One DVR interface failed during the study so only 3 channels were ultimately used.

A pressure transducer/data logger system was operated independently to measure water depth during the experiments. These devices, while convenient, experienced huge instrument drifts (they could not maintain a zero) so, where used the video images are required to correct the depth measurements. The researchers believe that the depth loggers correctly capture depth variation, but because every restart produced a different zero reading, the data need to be corrected (by the independently-captured video images). As with the video system, these level instruments are also field portable, and with the caveat regarding establishing accurate reference levels, should be valuable tools for field instrumentation.

Velocity measurements were made by means of drift tracers. An acoustic system was developed for the research but was not successfully operated in the wooden flume.

Within the flume the test section contained one of several model crossings:

1. No crossing — a reference case.

2. Rectangular culvert — two different sizes.

3. 2-Barrel circular culvert.

4. 4-barrel circular culvert.

5. Porous abutment with rectangular culvert.

Figure 2.5 is a sketch of the experimental conditions for a no-structure configuration. In this configuration the entire experimental channel comprised the solids materials, with or without a

throttle upstream of the test section[1]. Water depths were measured upstream from the nozzle
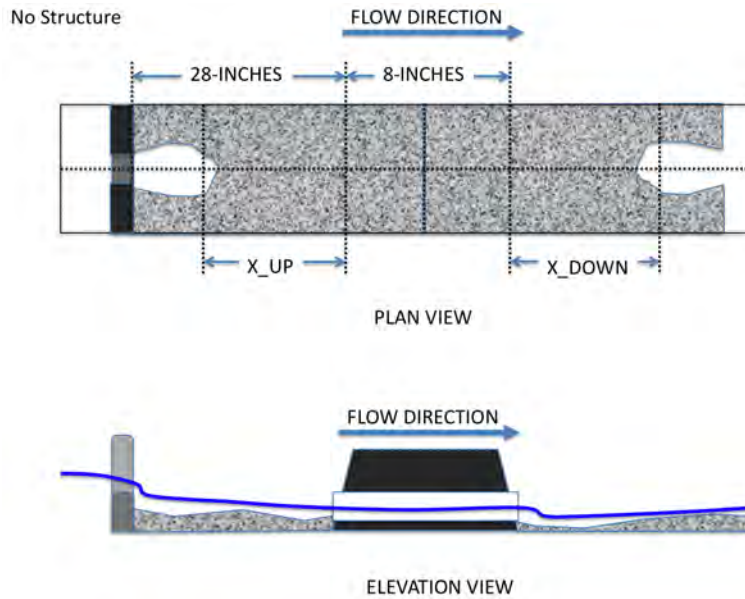

Figure 2.5: Sketch of Physical Model Experimental Configuration — No Structure Case.

section, then just upstream and just downstream from the crossing model. The water depths upstream and downstream from the model were measured both from the bottom of the flume and at the solids bed[2].

The distances labeled X_{UP} and X_{DOWN} correspond to distances measured over time in a single experiment to determine the rate of solids movement from nozzle towards the crossing model, and the rate of "headcut" downstream of the model. The researchers observed that the downstream headcut must propagate to the crossing for a clogged culvert to "self-clear."

The physical arrangement was kept the same in all experiments, roughly one channel-width upstream from the test section formed the solids source for the experiments, and one channel-width downstream from the test section was a repository (that is, pre-placed solids). In these sketches small erosion pits are depicted at the upstream and downstream end of the test section. These pits always formed during the experiments and the distances from the edge of the pits and the test section (X_{UP} and X_{DOWN}) were measured at the beginning and end of each experiment, and occasionally during experiments.

---

[1]The throttle in these sketches is depicted as the slot on the left of the test section. Discharge is from left to right in the figure. On the left is a "nozzle" or "throttle" section that was used to induce sufficient velocity to mobilize the solids upstream from the crossing model. The throttle was used to induce supercritical flow to guarantee bed mobilization for the experiments. Un-throttled experiments were also conducted — the interpretation is essentially the same, but the time scale is greatly reduced using the throttle.

[2]This measurement configuration was an attempt to quantify depth above the visible bed as well and depth above an impervious barrier. These measurements, were they reliable, would enable an estimate of the portion of discharge that is flowing in the porous (and mobile) bed as opposed to the portion of discharge flowing as open conduit flow.

Figure 2.6 is a sketch of the experimental conditions for a rectangular culvert configuration. Two different culvert widths were used in the experiments, $\approx$ 3 and $\approx$ 5 inches, to allow some variable cross sectional flow area for comparison to the circular culvert cases. In addition to different widths the culverts were modeled using a "glass" top and without a top. The top simulates the roadway and is the more realistic model — interpretation of results is based on glass-top models because they represent field conditions. The topless experiments were conducted to learn more about clogging and clearing of culverts in the idealized geometry[3].
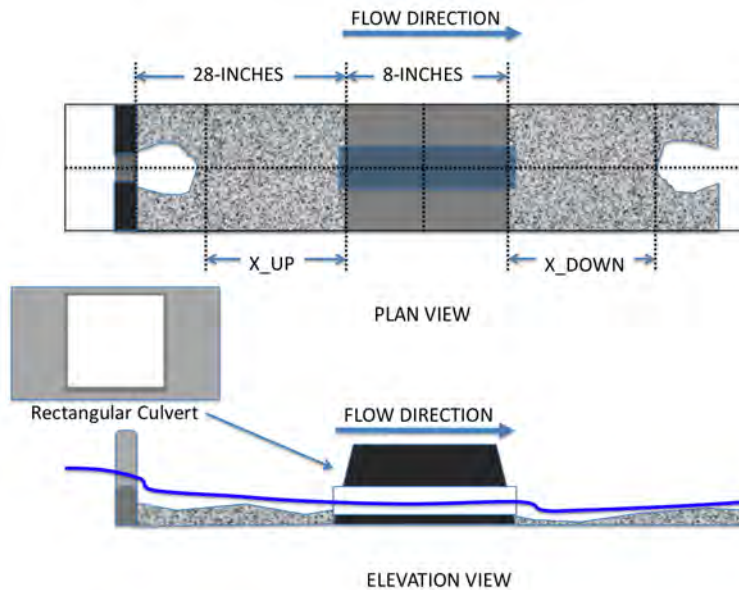

Figure 2.6: Sketch of Physical Model Experimental Configuration — Rectangular Culvert.

Figure 2.7 is an image of a typical rectangular culvert model. The small bricks create the smaller of the two flow openings studied. The larger width model openings present the same cross sectional area as the 2-barrel circular culvert.

Figure 2.8 is a sketch of the experimental conditions for a 2-barrel circular culvert configuration. The circular culverts present the same flow area as the wide box culvert model, thus the projected area seen by the water is unchanged. Circular culvert models were constructed from wood blocks with large diameter ($\approx$ 3+ inches) holes bored through the blocks. The holes were drilled slightly off-center so that the top of the block could be shaved and covered with glass to image inside of the culvert[4].

Figure 2.9 is an image of a typical 2-barrel circular culvert model. This particular image is looking downstream in the test section. In this particular image there are some solids in the culvert but otherwise this culvert is clear of solids. There is also some evidence of prior flow downstream with a slightly sinuous flow channel moving downstream from the model. When such models

---

[3]The glass-top models were difficult to capture enough high-quality imagery for publication purposes.

[4]The process of shaving and mounting a viewing glass was not completed.

Figure 2.7: Image of Physical Model Experimental Configuration — Rectangular Culvert (cover removed). Note the eroded materials upstream and downstream (an upstream moving headcut) and the material removed just downstream of the rectangular section as well as the model roadbed. Flow was from the right to the left.
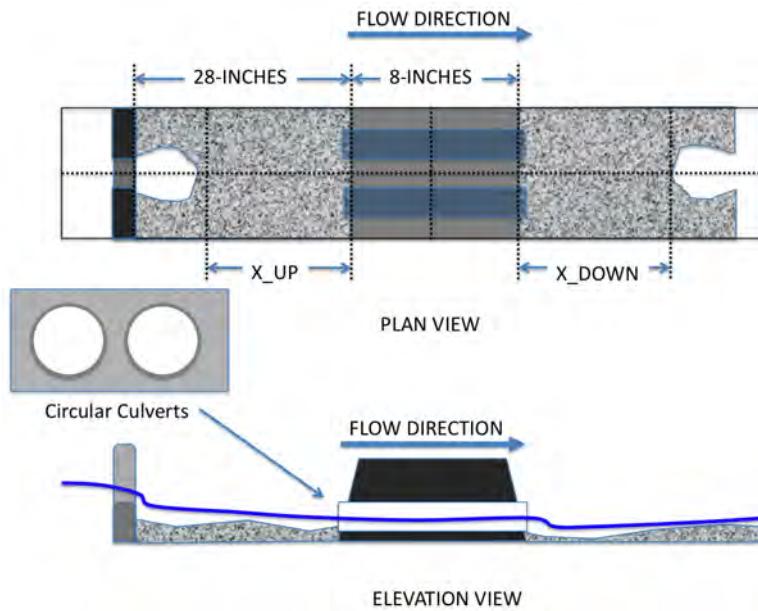

Figure 2.8: Sketch of Physical Model Experimental Configuration — 2-Barrel Circular Culvert.

became clogged, the openings were not visible and the solids generally formed a nearly uniform surface across the flow path. The cross sectional area of flow is roughly equivalent to the flow area presented by the large rectangular culvert.

Figure 2.9: Image of Physical Model Experimental Configuration — 2-Barrel Circular Culvert. This image is from an actual experiment — water is running through the culvert in the image (downstream is into the image.)

Figure 2.10 is a sketch of the experimental conditions for a 4-barrel circular culvert configuration. The 4-barrel circular culvert presents twice the flow area as the wide box culvert model[5].

Figure 2.11 is an image of a typical 4-barrel circular culvert model. This particular image is looking upstream in the test section. In this particular image this culvert is clear of solids.

Figure 2.12 is a sketch of the experimental conditions for a rectangular opening-porous abutment configuration. This configuration was suggested as plausible for low-water crossings after reading Kerenyi and others (2003). In that report the researchers postulated the existence of stagnation points at the structure-water contact that that these locations would be where clogging would be expected to begin. The idea of moving the stagnation point inside of a porous structure so that the velocities at approach are not zero was the main inspiration for this kind of experiment.

The porous structures were build by placing stones in a wire frame[6]. These stone-filled frames entirely replaced the solid abutments used in the other physical models. Only a box culvert was studied as other geometries were perceived as being too difficult to construct in practice.

Figure 2.13 is an image the porous-abutment model. In the image the presence of the porous abutment is evident. The glass-top roadway is also displayed in the image. In this particular

---

[5]These models were anticipated to carry more water and solids before clogging.
[6]A gabion is a reasonable representation for visualization of how the models were constructed.
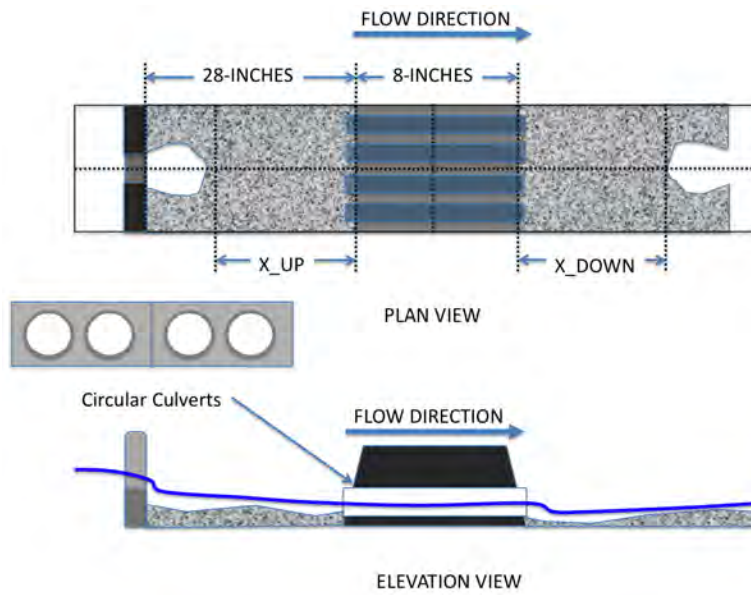
Figure 2.10: Sketch of Physical Model Experimental Configuration — 4-Barrel Circular Culvert.

Figure 2.11: Image of Model Experimental Configuration — 4-Barrel Circular Culvert. Flow downstream is into the image.
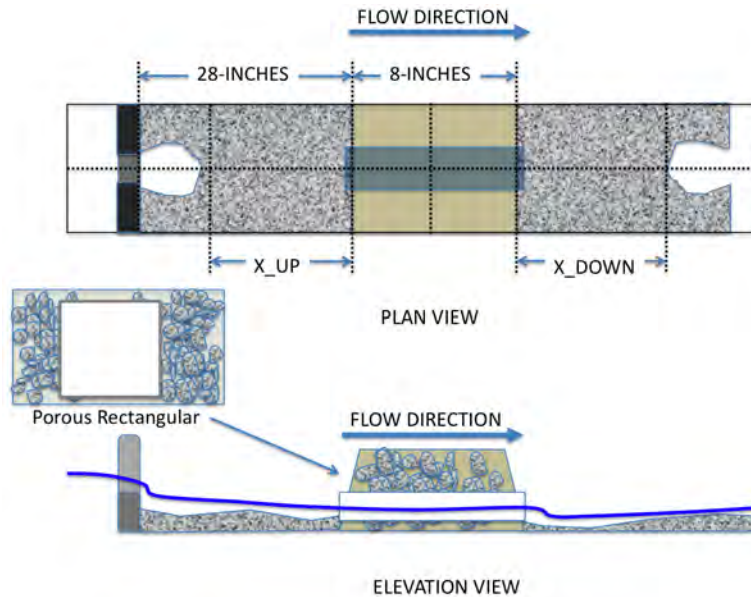
Figure 2.12: Sketch of Physical Model Experimental Configuration — Porous Culvert.

image the water flow through the rectangular section is visible. However, when the structure is submerged, image clarity is reduced substantially. Also pictured is the nested water-level sensors, which are housed in the vertical pipes to the upper right of the image. The vertical pipes are perforated at the bottom and serve as stilling wells. To the lower left in the image is one of the three image-collection cameras. Another camera is housed on the opposite side of the window to the left in the image and the third is upstream from the stilling wells (and not in the picture). These camera locations were used for all the experiments, regardless of model. The stilling wells for depth measurements were located at the same points for all experiments as well.

2.7. Numerical Modeling

The flowchart presented as Figure 2.14 represents the analytical procedure followed by University of Houston researchers for the detailed numerical modeling for this study. The approach included four major steps: Flood event data (statistical) analysis, watershed stability analysis using a geographical information system (GIS), hydrologic modeling with HEC-HMS (2008), and hydraulic modeling using HEC-RAS (2008) to derive flow hydrographs and flow characteristics for the channel stability studies.

The statistical analysis of the flood event data consisted in downloading the peak streamflow data for as many years as were available. The data were used to determine the risk of damages in terms of the return period of the flood event used in this study. The spatial analysis of the corresponding rainfall event was done using GIS. This helped compute subsequent runoff volumes and sediment yields for each subbasin. Significant sediment yield in the subbasin in which the LWCs are located

Figure 2.13: Image of Physical Model Experimental Configuration — Porous Culvert. Plastic cover representing roadbed in-place in this image.

justifies the channel analysis study. The MUSLE model was selected in the computation of sediment loads for data availability and the nature of the site, which is vast, composed of diverse geological formations, and is located in an arid region where storms are short high-intensity events.

For the channel stability analysis, HEC-GeoRAS (Ackerman, 2005), which is loaded in GIS as an extension was used to digitize the Johnson Fork drainage line. Cross-section and land use data were exported to both HEC-HMS (hydrologic modeling) and HEC-RAS (hydraulic analysis). The flow hydrograph obtain from the HEC-HMS was inputted into the HEC-RAS to determine steady and unsteady flow characteristics of the channel and compute the bedload. The water-surface elevation was also exported back to the GIS to plot the floodplain for reference.

2.7.1. Watershed Stability Analysis

GIS Modeling

The Hydrologic Unit Code (HUC) of the Llano River watershed was obtained from the National Hydrography Dataset (NHD, 2006). The Llano River watershed is HUC 12090204. The Llano River watershed is shown superimposed on a county map in Figure 2.15. The HUC was used to retrieve the 30-meter resolution Digital Elevation Model (DEM) mosaic for the watershed from the Better Assessment Science Integrating Point & Nonpoint Sources (BASIN) program[7]. The derived raster was used to derive the drainage network and delineate the 57 subwatersheds, displayed on Figure 2.16. Land-use and geologic data were acquired from the Texas Natural Resources Information

---

[7]Available from `http://www.epa.gov/waterscience/basins/` at the time of this writing.
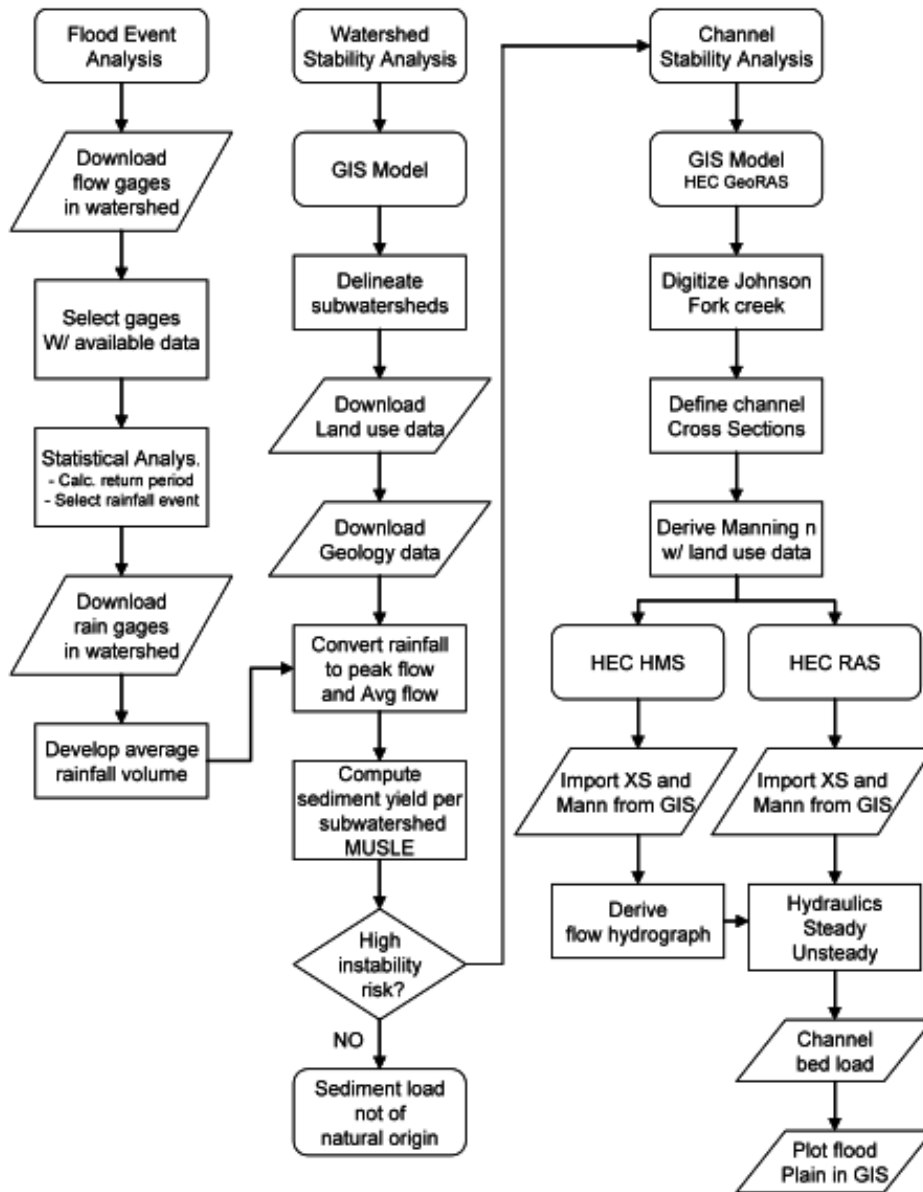
Figure 2.14: Flowchart of the analysis protocol used for the detailed numerical modeling developed by University of Houston researchers (Wang and Krou, 2008).

System[8]. These digital layers were managed with GIS for the MUSLE model application.
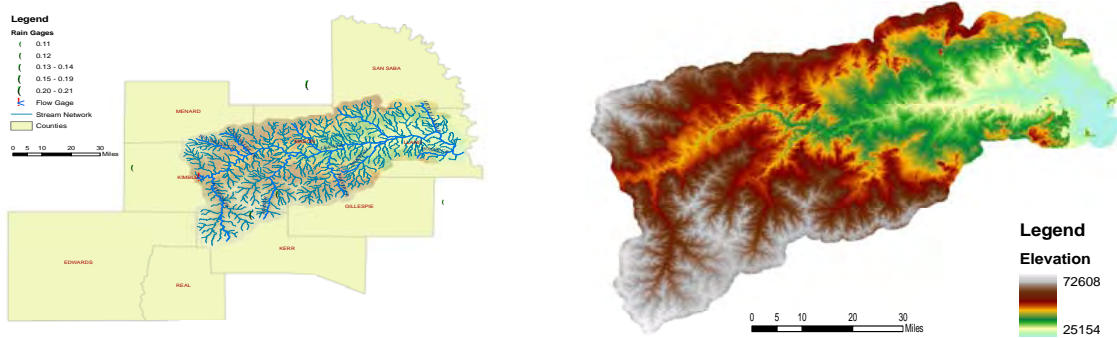

Figure 2.15: Llano River watershed superimposed with selected Texas counties and 30-meter DEM for the Llano River watershed (Wang and Krou, 2008).
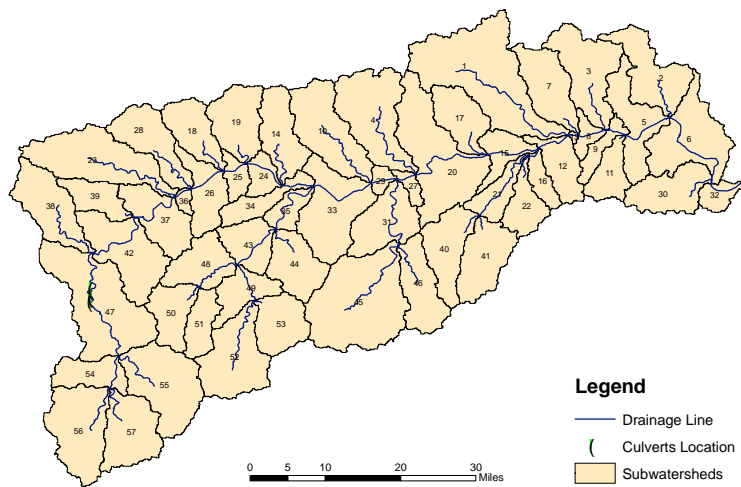

Figure 2.16: Subdivided Llano River watersheds (Wang and Krou, 2008).

MUSLE

The Modified Uniform Soil Loss Equation (MUSLE) model was used in GIS to estimate the sediment yield for the selected storm event. MUSLE is

$$Y_s = \alpha \left(Q_v Q_p \right)^\beta KLSCP, \tag{2.13}$$

where Y_s is the sediment yield (tons), Q_y is the runoff volume (acre-feet), Q_p is the peak discharge (cfs) for the event, K is the soil erodibility factor, LS is the topographic factor, C is the cropping-management factor, and P is the erosion-control practice factor. The coefficients α and β are

---

[8]Available from http://www.tnris.state.tx.us/DigitalData/data_cat.htm at the time of this writing.

calibration coefficients with values of 95 and 0.56, respectively, for Texas (Simons and Sentürk, 1992). Results are presented in Table C.4 in Appendix C.

Runoff Volume and Peak Flow

An estimate of the event runoff volume and the event peak discharge are required for application of MUSLE. These variables were estimated using NRCS methods. The runoff curve number (CN) depends on soil association and on land-use/land-cover classification. Because of the texture of watershed soils, Hydrologic Soil Group D was selected. Values of CN for the land-use/land-cover complexes extant on the watersheds are listed in Table C.2 in Appendix C. For a simplified calculation of the runoff volume, the subbasins were subdivided into 2,484 parcels by overlaying the subwatersheds, land-use, and geologic layers. This method has the advantage of allowing direct calculations without computing the distribution (percentage) of each type of land use or geologic feature.

Peak flows are given for subbasins and not parcels. Simple summation of individual peak discharges from subbasins does not produce the watershed peak discharge. Therefore, a FORTRAN program was developed to compute curve numbers for the parcels within each of the 57 subbasins. A watershed curve number was computed using the areally-weighted average. Runoff volume for the event rainfall is computed using

$$Q_v = \frac{(P - 0.2S)^2}{P + 0.8S},\tag{2.14}$$

where Q is the runoff volume (in), P is the event precipitation depth (in), and S is the watershed maximum potential retention (in). Watershed maximum potential retention is computed using

$$S = \frac{1000}{CN} - 10,\tag{2.15}$$

where CN is the watershed curve number.

Peak flow was calculated using

$$t_l = \frac{L^{0.8}(S + 1)}{1900S_0},\tag{2.16}$$

$$T_p = \frac{D}{2} + t_l,\tag{2.17}$$

$$Q_p = \frac{484A}{T_p},\tag{2.18}$$

where t_l is the lag time (hr), L is the length to divide (ft, computed using the GIS model), S_0 is the average watershed slope (dimensionless), D is the rainfall duration (hr, 95-60 = 35 hr), T_p is the time to peak (hr), and A is the watershed drainage area (mi^2). The slope and area of each unit are determined by the GIS model.

Soil erodibility is represented in the MUSLE approach using what is called the K factor. The soil erodibility factors used for this application are listed in Table C.3 in Appendix C, based on

Wischmeier and Smith (1978). The topographic factor in MUSLE, LS, is estimated as

$$LS = \left(\frac{\lambda}{72.6}\right)^n \left(\frac{430 \sin^2 \theta + 305.6\theta + 0.43}{6.613}\right), \tag{2.19}$$

where λ is the slope length to the watershed divide, θ is the slope angle, and n is dependent on slope. The exponent $n = 0.3$ for $\theta \leq 3\%$, $n = 0.4$ for $\theta = 3\%$, and $n = 0.5$ for $\theta \geq 3\%$. Soil erodibility and topographic factors were calculated for each parcel and area-averaged to obtain values for the enveloping subbasin.

The cropping-management factor C is the product of the canopy cover, mulch, close-growing vegetation, and residual effects of the land use. Wischmeier and Smith (1978) provides the method and curves to estimate those values. Results are shown in Table C.2 in Appendix C. The erosion-control practice factor, P, was assumed to be 1.0 because no erosion-control practice is known to be applied in the watershed.

Channel Stability Analysis

The results from the watershed analysis are displayed on Figure 2.17. The culverts are located in an area with significant sediment mobility, thereby justifying the channel stability study. Five sub-watersheds upstream from Johnson Fork Creek were extracted from the Llano watershed layer for modeling and are displayed on Figure 2.18. `HEC-GeoRAS` (Ackerman, 2005) was used to define the Johnson Fork Creek channel alignment and develop the cross sections for hyrdaulic modeling with `HEC-RAS` (U.S. Army Corps of Engineers, 2002). Cross-sections with an average length of 1,500 meters were developed and are displayed on Figure 2.19. The cross-sections, along with extracted Mannings coefficient, n, and channel lengths were transferred to `HEC-RAS`. These parameters were also transferred to `HEC-HMS` for hydrologic modeling.

2.7.2. Frequency Analysis

USGS streamgaging station 08150000— Llano River near Junction, Texas, was selected for flood frequency analysis. A plot of annual maximum discharges for the period of record is displayed on Figure 2.20. Annual maximum discharges were obtained from the USGS water-data website[9], which contains water resources data for the entire nation. Return periods were calculated using procedures documented by U.S. Interagency Advisory Committee on Water Data (1982). The Pearson Type III distribution was fit to logarithms of the annual maximum discharge.

$$y_i = \ln q_i, \tag{2.20}$$

where y_i is the logarithm of the annual maximum discharge, q_i. The mean and standard deviation, $\overline{y_i}$ and s_y, are computed in the standard way. The skew coefficient is given by

$$C_s = \frac{n \sum (y_i - \overline{y})^3}{(n-1)(n-2)s_y^3}, \tag{2.21}$$

[9]The website is `http://waterdata.usgs.gov/nwis` at the time of this writing.
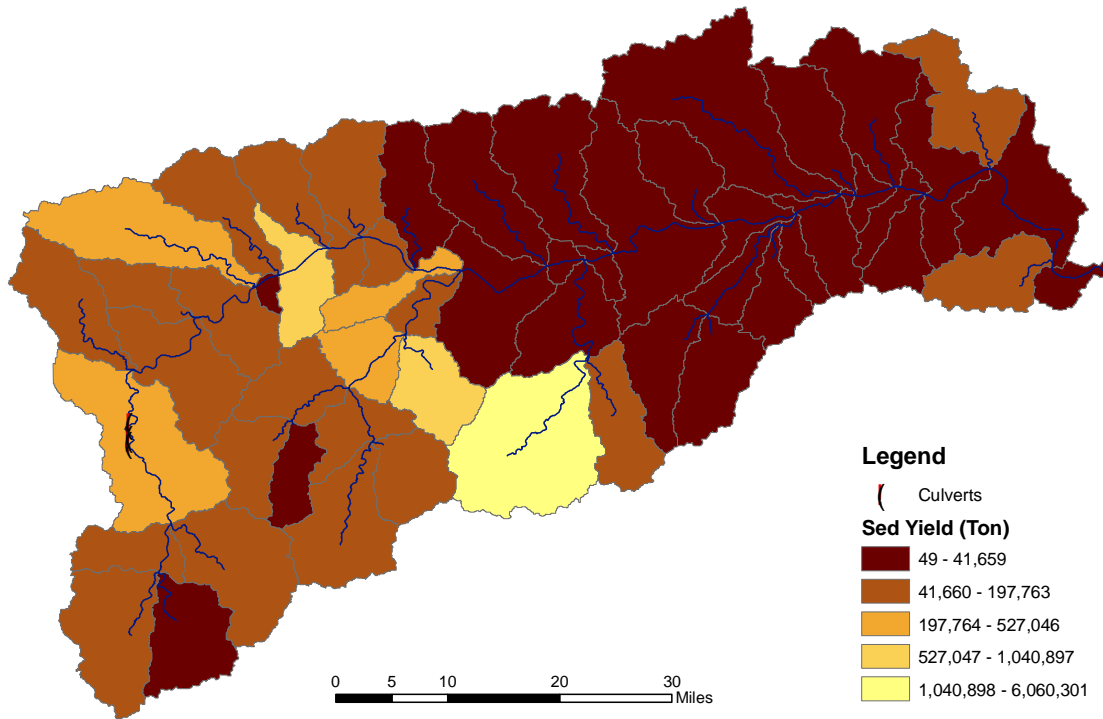
Figure 2.17: Sediment generation from the Llano River watershed (Wang and Krou, 2008).

where n is the number of observations in the sample. The estimate of the log-discharge for a T-year event is

$$y_T = \overline{y} + s_y K_T, \tag{2.22}$$

where K_T is *frequency factor* and is determined from a table of values dependent on the skew coefficient, C_s. Tables of K_T are presented in most hydrologic textbooks[10] and in U.S. Interagency Advisory Committee on Water Data (1982). The expected discharge for a T-year return period is

$$q_T = \exp y_T. \tag{2.23}$$

Results from fitting a Pearson Type III distribution to the logarithms of annual peak flow data from the Llano River are presented in Table C.6 in Appendix C. The peak discharge with a 100-year return period is about 432,000 cfs. The peak discharge with a return period of 5 years is about 53,200 cfs. The November 2, 2000 flood event selected for the study has an estimated return period of about 18 years.

---

[10]Chow and others (1988) is an example.

Figure 2.18: Subwatersheds used by University of Houston researchers for development of HEC-HMS model (Wang and Krou, 2008).

2.7.3. Hydrologic Modeling

Rainfall data for the selected flood event (November 2, 2000) were obtained from the National Climatic Data Center (NCDC) of the National Oceanic and Atmospheric Administration[11]. Raingages with Cooperative Station Identification (COOPID) numbers 411017, 413270, 414670, 415312, and 417243 were retained because they are located within or near the boundaries of the study watershed. Rainfall hyetographs for the study event are presented in Appendix C. The event duration was determined to be 35 hrs (beginning on 11/02/00 at 12:00 PM and ending on 11/03/00 at 11:00 PM). The inverse direct weight (IDW) method was used to calculate the average rainfall intensity and the rainfall volume, which was 5.43 inches. The calculation details are listed in Table C.1 of Appendix C.

The hyetograph to distribute watershed rainfall for the hydrologic modeling was taken from Station 414670, located in Junction, Texas. The location of Station 414670 is shown on Figure 2.18. The rainfall distribution from Station 414670 is presented in Table C.1 in Appendix C. The hyetograph from Station 414670 was used as the watershed hyetograph, with rainfall depths from the other raingages used to determine the basin average precipitation.

---

[11]These data were obtained from the internet.
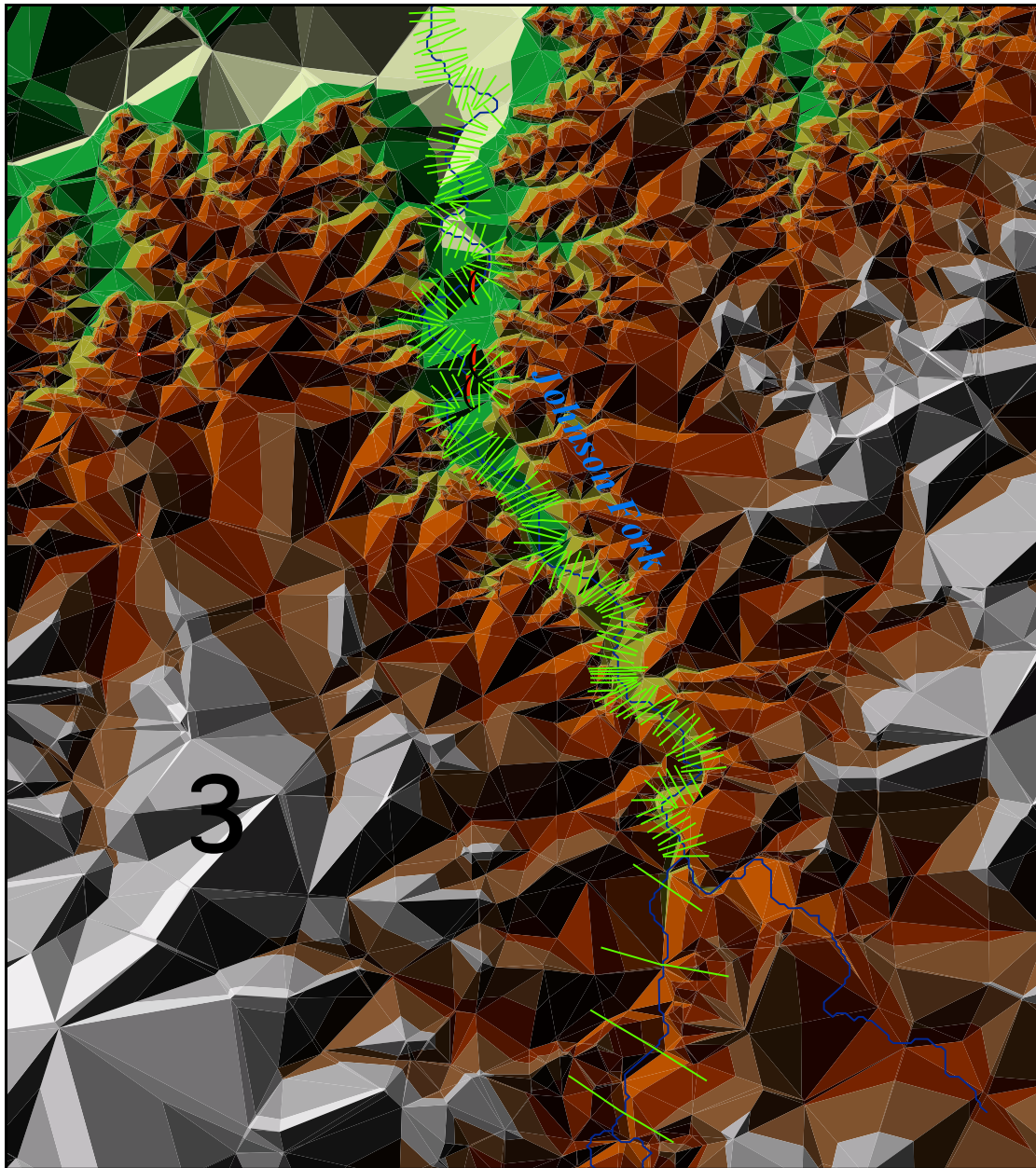
Legend

Culverts

X-Sections

0   1.5   3   6   9
Miles

Figure 2.19: Location of cross sections for University of Houston researchers' modeling of Johnson Fork Creek using HEC-RAS (Wang and Krou, 2008).
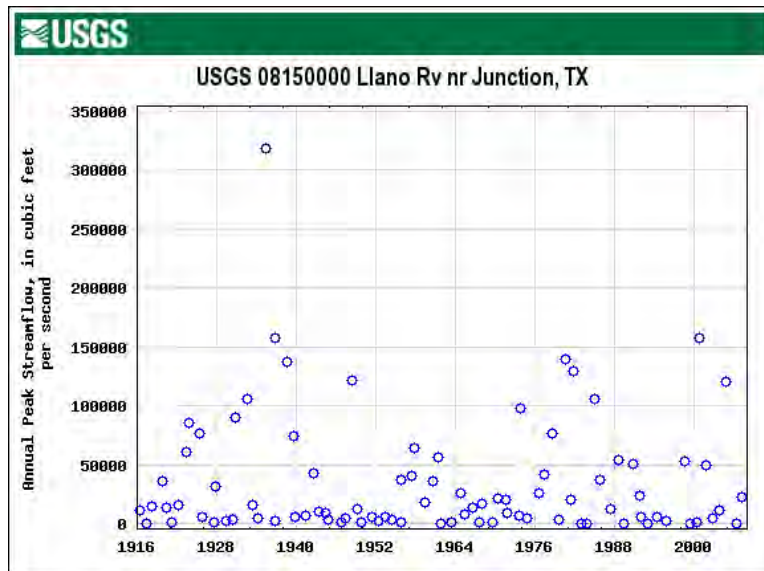
Figure 2.20: Annual maximum discharge from USGS Streamgage 0815000, Llano River near Junction, Texas, for the period of record.

The model consisted of overland and channel routings with five subbasins and two main channels, as shown on Figure 2.18. The channels were subdivided into four sections each taking cross-section variations into account. The SCS (now NRCS) and Muskingum-Cunge methods were used for overland and channel routings, respectively. The Muskingum-Cunge method is detailed in Bedient and Huber (2002). The channel of interest is the section of Johnson Fork Creek located in the subwatershed which hosts the culverts.

2.7.4. Hydraulic Modeling

Channel hydraulic routing in `HEC-RAS` was modeled for 31 sections (Table C.7 in Appendix C) in a closed system where there was no overland flow input along the channel. Using the runoff hydrograph at the outlet of the subbasin for the routing would have underestimated the magnitude of the transport mechanism within the channel. On the other hand, the runoff hydrograph of the inlet of the subbasin would have overestimated that magnitude. An average runoff hydrograph, compiled from the flows in the channel segments, were therefore used as inflow hydrograph for `HEC-RAS` simulations.

2.7.5. Sediment Transport Computation

The bed-load transport process and volume are regulated by the channel geometry and water-sediment velocity along with sediment concentration and particle size distribution. The channel geometry and the unsteady state hydraulic characteristics were obtained from the `HEC-RAS` model.

Particle size distributions were obtained through sampling and analysis of the stream bed. The bed-load transport rate at each cross section were then computed and used to derive the time variation of channel bottom elevations. A key step in calculating the variation of channel bottom elevations calculation is the determination of the sediment-size and flow-velocity dependent maximum degradation depth and transport capacity at each cross-section.

Sampling Method

For this project, sediment samples were taken from the river bed using the grid method (Bunte, 1992; Kondolf, 1997) and the volumetric technique (Church and others, 1987; Melis and others, 1997). Sample analysis suggested by Simons and Sentürk (1992) and Yang (2003) were used to determine the particle size distribution of the river bed. To implement the grid sampling method, which is a surface sampling technique, the target area was divided into squares with a survey tape stretched across the river bed. A total of 100 pebbles were sampled, each at mesh points three feet apart (Green, 2003). A frequency-by-number record was established following the 1941-Krumbein phi-scale (Casagli and others, 2003; Kondolf, 1997). For application of the volumetric sampling method, samples from three successive deeper layers of the bed material were collected. The samples were collected by shoveling a two-foot square near the low-water crossing. Each layer was as thick of the largest stone protrusion into the bed, which resulted in two-inch thick sheets. A classical sieving method was performed to sort particles according to size.

The river bed particle size characteristics obtained from sieve analysis are listed in Table C.8 in Appendix C. The grid sampling technique produced a finer size particle distribution than the volumetric sampling method. However, the resulting distributions are more coarse than those sampled at the sub-layers. The median diameter d_{50} obtained from grid sampling, which is 24.2 mm, is close to the average of d_{50} of the three layers sampled using the volumetric method, which is 26.8 mm. The second layer from the volumetric sampling was used for calculation. That layer represents better the whole array of particle sizes with the least amount of fine sediment sifted by the river base flow.

Maximum Degradation Depth

When a channel degrades, fine materials are transported much more quickly than coarse materials. The result is a coarsening of the river bed. Degradation stops when the coarse sediment covers the bed entirely and protects the finer deposits beneath it, as shown schematically in Figure 2.21. The coarse layer at the surface is called the armor. Usually, more than one armor layer is necessary to prevent the fine material underneath from being eroded. The maximum degradation depth is (Yang, 2003)

$$Y_d = Y_a \left(\frac{1}{\Delta p} - 1 \right), \tag{2.24}$$

where Δp is the decimal percentage of material larger than the armoring size and Y_a is the armoring thickness, such as $Y_a = 3d$, with the armoring size. The armoring size d was obtained by averaging

31

the armor particle-sizes computed following the Meyer-Peter and Müller (d_MP), Mavis and Laushey (d_ML), and Yang (d_Y) methods. Those methods are shown as

$$d_\mathrm{MP} = \frac{SD}{0.19 \left(\frac{n}{d_{90}^{1/6}} \right)^{1.5}}, \tag{2.25}$$

$$d_\mathrm{ML} = \left(\frac{0.7V}{0.51} \right)^2, \tag{2.26}$$

$$d_\mathrm{Y} = \left(\frac{1}{6.01} \frac{V}{2.05} \right)^2, \tag{2.27}$$

where S is the stream gradient, D (ft) is the mean flow depth, n is Manning's roughness coefficient, d_{90} (mm) is the bed material size for 90% finer, and V (ft/s) is the mean flow velocity at the cross section.
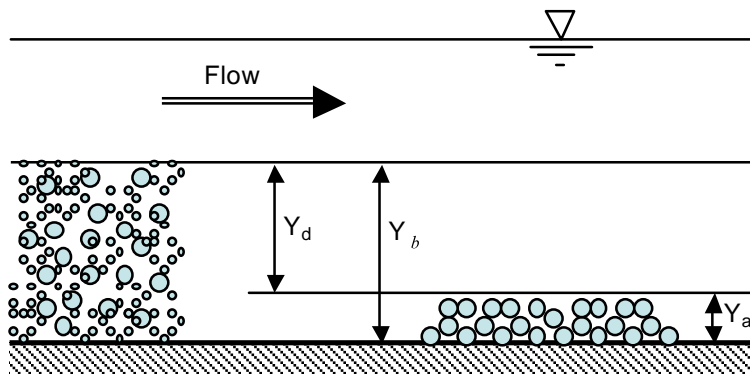
Figure 2.21: Schematic of the streambed armoring process (Wang and Krou, 2008).

Transport Capacity

The fluvial bed particle size distribution and size characteristics, specifically the $d_{15.9}$, d_{35}, d_{50}, d_{65}, $d_{84.1}$, d_{90}, and the geometric mean d_g, determined from analysis of samples obtained by the grid and volumetric methods were used to compute bed-load transports, given the channel cross-section and runoff hydrograph. In this section, Einstein, Parker and others, and Meyer-Peter-Müller bedload transport concepts are summarized. Einstein (1950), Parker and others (1982), Simons and Sentürk (1992), and Yang (2003) provide a more detailed theoretical development. Any assumption or approximation made in coding the calculation sequences is also mentioned.

Einstein Probabilistic Approach Theoretically, movement of a river bed sediment is initiated when the drag force applied by the stream flow exceed some critical value. In coarse fluvial processes, bed-load transport is observed to occur in a much higher rate than suspended transport. However, observation of particle movement in nature is very difficult and the beginning of motion is not well

defined because it is related to other not well known factors that make it appear random in space and time. That phenomenon prompted Einstein (1950) to avoid the incipient motion criteria in establishing bed-load transport precepts. Recalling the turbulent nature of natural stream flows, Einstein related the transport process to the probability that a turbulent flow fluctuation would produce an instantaneous lift force large enough to trigger a particle motion (Einstein, 1950; Simons and Sentürk, 1992; Yang, 2003). Through the probability of a particle being eroded from the bed Einstein established a relation between the transport rate Φ_* on individual particles and intensity of shear stress Ψ_* of that particle as

$$\Phi_* = \frac{1}{A_*} \frac{1 - 0.5\left[\text{erf}(b) - \text{erf}(a)\right]}{0.5\left[\text{erf}(b) - \text{erf}(a)\right]}, \tag{2.28}$$

where $A_* = 43.5$, and a and b are functions of Ψ_*.

In computing bed-load transport using Einstein's theory, use of four empirical curves from Einstein's work is required. Einstein's empirical curves are the logarithmic velocity distribution correction factor χ, V/U'''^* attributable to channel irregularities (V is stream velocity and U'''^* is shear velocity due to form roughness), hiding correction factor ξ, and the lifting correction factor Y.

Parker Equal Mobility Approach   Based on field data and assuming that in gravel bed stream bedload transport is essentially due to the movement of exposed particles at the surface, Parker and others (1982) found that surface grains have an equal probability of transport regardless of their size. The bed-load volume is therefore approximated by that of a representative grain size of the bed surface particle size distribution. For this project, d_{50} is used to characterize the bedload discharge W^* as a function of the dimensionless shear stress ϕ_{50}

$$W^* = \begin{cases} 0.0025 e^{14.2(\phi_{50}-1)-9.28(\phi_{50}-1)^2} & 0.95 < \phi_{50} < 1.65, \\ 11.2\left(1 - \frac{0.822}{\phi_{50}}\right)^{4.5} & 1.65 < \phi_{50}. \end{cases} \tag{2.29}$$

The dimensionless shear stress ϕ_{50} is

$$\phi_{50} = \frac{\gamma}{\gamma_s - \gamma} \frac{DS}{0.0875 d_{50}}. \tag{2.30}$$

The bedload q_b per unit channel width is

$$q_b = \sum q_{bi},$$
$$= \sum \frac{\gamma}{\gamma_s - \gamma} DS \sqrt{gDS} p_i W_i^*, \tag{2.31}$$

where q_{bi} and p_i are the bedload and fraction by weight for the size fraction d_i, g is the gravitational constant, D and S are the depth and slope of the channel, and γ and γ_s are the specific weight of water and sediment. In this study, for each flowrate, the channel depth was obtained by applying the Manning formula. The roughness coefficient n used in the formula was obtained from Einstein's bed-load calculation method mentioned above. By the equal mobility principle, the dimensionless bed-load transport W_i^* is identical in every size fraction d_i so that $W_i^* = W^*$. Because $\sum p_i = 1$,

$$q_b = \frac{\gamma}{\gamma_s - \gamma} DS \sqrt{gDS} W^*. \tag{2.32}$$

33

Meyer-Peter and Müller Energy Slope Approach   The Meyer-Peter and Müller approach can be used to calculate the bedload of coarse material with particle sizes greater than 3 mm (Yang, 2003). This approach assumes that part of the energy slope of a fluvial flow is the result of the stream energy used for solid transport. According to the 1923-Strickler formula, the total energy slope S is related to the velocity V and hydraulic radius R_s of the stream by

$$S = \frac{V^2}{K_s^2 R_s^{4/3}}. \tag{2.33}$$

The energy slope due to sediment transport through skin friction is

$$S_r = \frac{V^2}{K_r^2 R_s^{4/3}}, \tag{2.34}$$

where K_s and K_r are compound resistance coefficients. K_r was determined as

$$K_r = \frac{26}{d_{90}^{1/6}}. \tag{2.35}$$

Equations 2.33 and 2.34, adjusted for experimental results, give

$$S_r = \left(\frac{K_s}{K_r}\right)^{3/2} S. \tag{2.36}$$

Meyer-Peter and Müller established the wet bedload rate q_b as a function of the total energy slope S, which is due to solid transport. The equation was expressed in metric units as

$$\gamma \left(\frac{K_s}{K_r}\right)^{3/2} RS = 0.045 \left(\gamma_s - \gamma\right) d_{35} + 0.25 \rho^{1/3} q_b^{2/3}. \tag{2.37}$$

Following Equation 2.36, Equation 2.37 can be rewritten

$$\gamma RS_r = 0.045 \left(\gamma_s - \gamma\right) d_{50} + 0.25 \rho^{1/3} q_b^{2/3}. \tag{2.38}$$

The dry weight of the sediment load is given by

$$q_{b,\text{dry}} = \frac{\gamma_s}{\gamma_s - \gamma} q_b, \tag{2.39}$$

where ρ is the density of water, and γ and γ_s are the specific weight of water and sediment, respectively. Equation 2.33 shows that when the flow velocity is zero, the total energy slope is also zero nullifying the energy slope imparted to the sediment transport. However, from Equation 2.38 there would still be a residual bedload, which is in contradiction with the fact that for a stable channel incipient motion is due to flow velocity. When the flow velocity is approximately zero, the transport capacity was adjusted such that the bedload transport rate was also approximately zero.

Channel Bottom Elevation The channel bottom elevation variation attributed to aggradation and degradation was calculated using bedload volume fluxes in and out of each segment. A segment is the channel section defined by two consecutive cross-sections (Figure 2.22). The bedload volume flux $Fq_{i,t}$ through a cross-section (i) within a period of time Δt is given by

$$Fq_{i,t} = q_{(b,\mathrm{dry}),t}\Delta t, \tag{2.40}$$

and the depth variation $\Delta Y_{i,t}$ of segment i due to sediment load is

$$\Delta Y_{i,t} = \frac{Fq_{i-1} - Fq_i}{L_i W_{i,t}}, \tag{2.41}$$

where segment i is defined by cross sections $(i-1)$ and (i) with L_i the segment length and $W_{i,t}$ the average top width of the bounding cross sections. If $\Delta Y_{i,t}$ is positive, aggradation occurs; otherwise degradation occurs. The new channel bottom elevation at cross section (i) is

$$E_{(i-1,t+1)} = E_{(i-1,t)} + \Delta Y_{i,t}$$
$$E_{(i,t+1)} = E(i,t) + \Delta Y_{i,t} \tag{2.42}$$
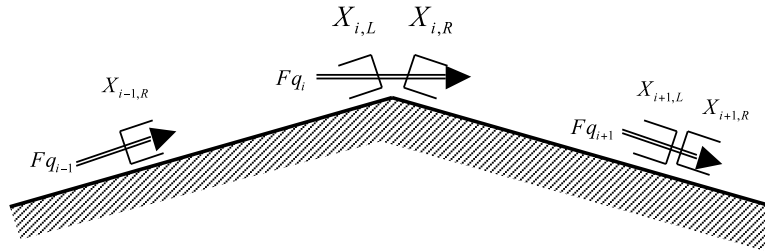
Figure 2.22: Schematic of bed flux through channel segments (Wang and Krou, 2008).

Because aggradation and degradation depend on the slope, flow area, and Manning's coefficient of segments according to the formulae, there will be two values of depth variation at each cross-section, namely values given by the segments upstream (segment(i)) and downstream (segment$(i+1)$) of the cross-section(i). Cross-sections were then divided into left and right (Figure 2.22)) and the correct bottom channel elevation was averaged.

In the case of channel aggradation Equation 2.42 was applied with an additional constraint. Only the cross-section with the lowest elevation received a sediment depth increment. When the difference of elevation is below 1%, both cross-sections receive the increment. Channel degradation is limited by the maximum degradation depth, which also limits the volume of available sediment to be transported downstream. The bedload volume flux out of the segment was then adjusted from that sediment volume deficit before using it as input to the downstream section.

2.8. Continuous Monitoring of Selected Sites

Bed mobility is a sufficiently transient phenomenon that attended field monitoring would be difficult if not impossible. Unattended monitoring is therefore indicated. Of the available tools, video

imaging (as in the laboratory experiments), channel stage (either with staff gage in the video window or with data-logging transducers), and some surface velocity measurements are reasonable. With the exception of a prototype video system that was only briefly deployed, none of the field monitoring was accomplished for a variety of reasons. The tools considered as well as some limitations are presented here to document for future engineers the thinking at the time of the project and perhaps provide ideas for future studies should the need emerge.

2.8.1. Video Image Collection

Video monitoring of the low-water crossings during flood events could provide critical information as to the hydraulic state of the channel as well as the local hydraulics proximal to the low-water crossing structures. Even rudimentary image analysis software, while labor intensive, can provide estimates of surface velocity, and possible capture of significant mobilization events. Comparative analysis of before/after imagery can allow some estimate of mass moved. Nighttime video monitoring at the time the research project was executed was not possible[12].

A prototype video monitoring system was deployed to assess various recording methods, installation methods, risk of vandalism, power requirements, and data retrieval. Ultimately vandalism and privacy-rights concerns required removal of the system.

2.8.2. Stage Recording

Stage monitoring of the low-water crossings could provide valuable information to the depth-of-water conditions in the stream. Furthermore, the rate of change of stage will be valuable in assessing the unsteady nature of the flood wave — these data will benefit the physical and numerical modeling tasks of the proposed project. Low-water crossings are a non-typical environment for stage sensing. Several technologies were considered viable.

First, deployment of autonomous baton-sized pressure transducers in galvanized pipe placed on the low-water crossing apron or at the base of the TxDOT flood-staff gage were attractive low-cost methods. These devices are conceptually identical to the level-loggers used in the physical model experiments. These methods place equipment in harms way. An individual logger is only hundreds of dollars and occasional equipment loss could be tolerated economically although the loss of data would be disappointing. As with laboratory devices, an independent zero or reference measurement would be needed to correct the recorded values.

A second method of stage sensing could involve non-contact radar units that are increasing being used in USGS operations in Texas. These down-looking devices require a plumbed height above the channel — unfortunately, there were no bridges where these sensors could be deployed.

---

[12]The researchers recently become aware of reasonably-priced forward-looking infrared cameras (FLIR). Such cameras were cost prohibitive at the time of the study.

2.8.3. Surface Velocity

Surface velocity could be estimated from the video images, but could also be collected independently. Surface velocity radar units are an emerging technology for non-contact streamflow monitoring; they share the same physical limitations as identified in the radar-stage devices, that is the need to look down from a considerable distance to image the water surface. At the time of project execution, a "flume-verified" instrument was not available in Texas. Side-looking and down-looking ultrasonic are alternatives that are proven technologies, but have many technical considerations and require contact with the liquid (thus exposing the instrument to damage in the bed mobility situation).

3. RESULTS

The purpose of this chapter is to present results from the variety of tasks undertaken as part of this research project.

3.1. Review of MMIS Records

Through a review of TxDOT Maintenance Management Information System (MMIS) records, the costs associated with repairs and replacement of low-water crossings in Edwards, Kimble, and Real Counties were estimated. Over a four-year period, from 1998–2002[1], total repair expenditures in the three counties were about $672K. The annual breakdown of costs are listed in Table 3.1.

Table 3.1: Results from analysis of TxDOT maintenance records.

Year	Dollar Maintenance Cost
1998	193,844
2000	80,174
2001	200,225
2002	197,445

During the course of the cost review, it became clear that the MMIS system does not serve the needs of TxDOT to determine the *long-term* costs associated with bedload mobility. Details of task costs are lost after three years, limiting the ability to review historical flood damages. Furthermore, because of the breakdown of tasks, it is possible that each event may have some costs associated with flood-damage repairs that are not accounted for.

The spatial extent of bed-mobility problems extends to at least 11 other counties, and perhaps as many as 17 counties or more. By extrapolation from the economic data from three counties, the four-year cost associated with bed-mobility is at least $2.4M (assuming an 11 county spatial extent) for the period 1998–2002 (sans 1999, as noted previously). If the geographic extent exceeds the 11-county area, then the expected cost is greater yet.

---

[1]Note that 1999 was missing from available records.

3.2. Hydrology

Historical information of flood occurrence in the study area is useful to establish context of recent low-water crossing maintenance operations by TxDOT. Two long-term stations were selected as *index* streamflow-gaging stations for flood occurrence: 08150000 Llano River at Junction, Texas and 08190000 Nueces River near Laguna, Texas. The measure of flood occurrence is the nonexceedance probability of the annual peak streamflows.

Asquith (2001) provides regional regression equations to estimate the L-moments of annual peak streamflow applicable for the stations using drainage area, basin shape factor, and main channel slope as predictor variables. Asquith and Slade (1997) lists these basin characteristics for the stations. The L-moments (mean, L-scale, L-skew, and L-kurtosis) were estimated, and for each station a four-parameter kappa distribution fit to the L-moments. The kappa distribution provides a continuous function representing the "flood-frequency curve" for the stations. Subsequently, the annual peak streamflows were successively substituted into the distribution, and the nonexceedance probability for each year at each station was calculated. To simplify analysis, the mean of the two estimated nonexceedance probabilities for each year was compute. This means is a more reliable flood occurrence measure. (Station 08150000 does not have corresponding record for each year of record at Station 08190000.) The kappa distribution is not restricted to positive values of peak streamflow for the smallest annual peak streamflow values, a nonexceedance probability could not be completed. When a negative value occurs, a nonexceedance probability of zero was assumed for plotting purposes only. The time series of the estimated nonexceedance probability by water year is shown in Figure 3.1. The symbols on the plot distinguish between years having both stations in operation and years having one station in operation. The nonexceedance probability associated with the 10-year recurrence interval event is shown. Also, the total dollars for each water year are superimposed on Figure 3.1.

Several important observations about flood occurrence information depicted in Figure 3.1 are made. First, a wide range in nonexceedance probability is evident, which is expected from hydrologic statistical theory. Second, there is a curious lack of 0.60 nonexceedance probability values from about 1930 to the present. Third, there appears to be two clusters of events having large nonexceedance probabilities spanning a half decade or more: 1930s and late 1990s to early 2000s. The clustering of historically significant flood events in the 1930s in the study area is widely known, and it is known that from about 1997 to at least the present (2004) that substantial floods have occurred throughout the study area. Fourth, TxDOT does not report significant damage repair costs in 1999 and 2000. These are years lacking significant flooding (at least on the upper Nueces and Llano River watersheds). Finally, the substantial 2003 damage costs are not associated with large nonexceedance probability; this is illustrative of the limited spatial representation of the two index stations. A logical conclusion from the data depicted in the figure could be that TxDOT has experienced historically unusually large flood damage costs in recent years because of historically unusual, but not unprecedented floods.
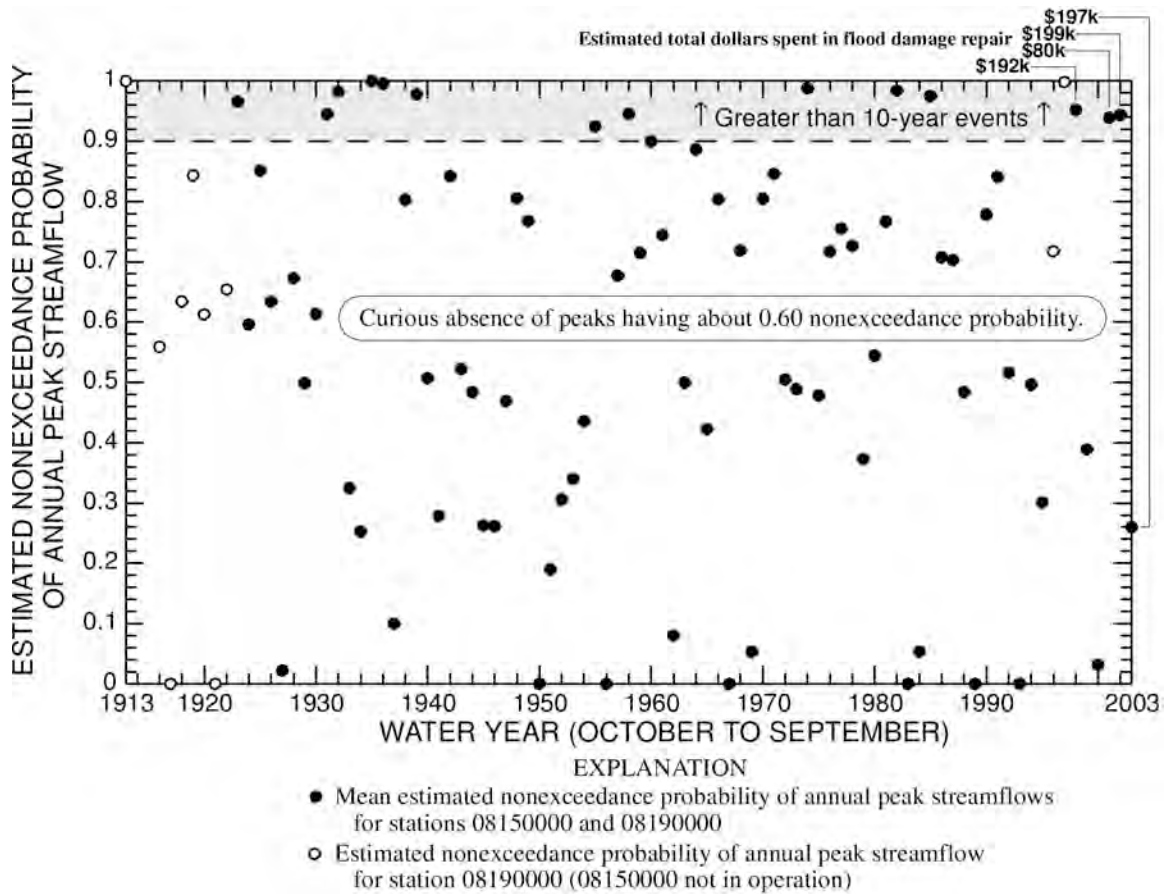
Figure 3.1: Time series of estimated nonexceedance probability of annual peak streamflow values for two selected U.S. Geological Survey streamflow-gaging stations in the study area.

3.3. Field Investigations

Two sets of field studies were conducted. A set of site visits and associated field work was conducted during the initial phase of the project. Many crossing were visited and four were selected for additional field work. After the interim report (Thompson, 2004), additional field work was undertaken by USGS researchers. Dr. Frank Heitmuller spent significant time in the study area collecting data. The results of his study were published in Heitmuller and Asquith (2008). Results from the two sets of field studies are presented in subsequent sections of this report.

3.3.1. Reconnaissance Field Work

During the first phase of the research project, four field sites were visited, three on Johnson Fork Creek and one of the Nueces River. The three Johnson Fork Creek sites are referred to as Paks,

Guzman, and Lowlands by local engineers and the Nueces River site referred to as the Ben Williams crossing. Site locations are displayed on Figure 3.5.

Three methods were used to measure particle-size distributions. The gravelometer method, the tape method, and the volumetric (or sieve) method. Particle-size distributions for bed sediments at the Guzman crossing of Johnson Fork Creek are shown on Figure 3.2. As reported by Fang and others (2006), the tape method and the gravelometer method produce results sufficiently similar that either method is acceptable. Furthermore, downstream d_{50} is greater than upstream d_{50}. That is, a greater fraction of the smaller particles were measured upstream from the crossing.

Figure 3.2: Particle-size distributions for bed sediments at the Guzman crossing of Johnson Fork Creek near Junction, Texas.

Particle-size distributions from the three Johnson Fork Creek crossings are displayed on Figure 3.3. It was observed that particle sizes upstream from a low-water crossing were larger (in general) than those downstream from the crossing. Some large particles were upstream from the Paks crossing, but this did not occur for either the Guzman or Lowlands crossings.

Grading of particles at the crossings can be interpreted in a couple of ways. Stream power of stream flows upstream from the crossing might be reduced if the crossing acts as a weir, reducing the flow velocity. Therefore, smaller particles are present in the bed sediments because the greater velocity downstream from the crossing results in the evacuation of smaller particles from the bed (natural
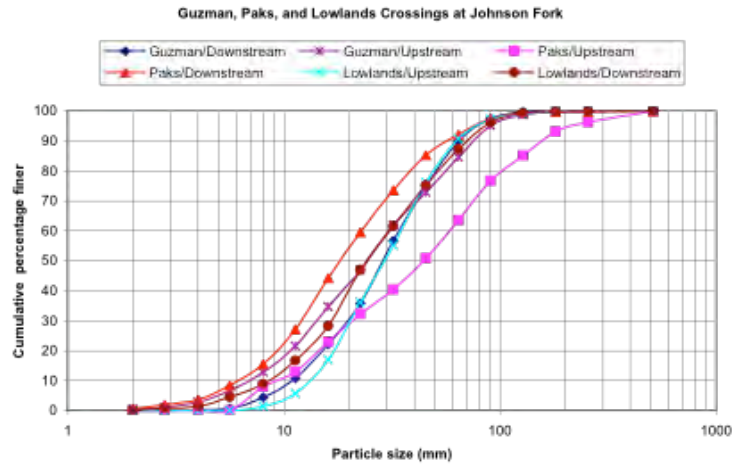
Figure 3.3: Particle-size distributions for the Paks, Guzman, and Lowlands crossings of Johnson Fork Creek.

armoring).

Samples were also collected at the surface and below grade for comparison of particle-size distributions. Results from particle-size distribution analyses of the four field sites is shown on Figure 3.4. In Figure 3.4a the median particle diameter is greater upstream of the crossing, and the surface samples are greater than respective subsurface samples. The median size at the Guzman site is about 20 mm. In Figure 3.4b the median particle diameter is difficult to interpret. Excluding the upstream surface sample, the median size at the Paks site is about 10 mm. In Figure 3.4c the surface sample's median diameter is greater upstream of the crossing, whereas the opposite is displayed for the subsurface sample. At the Lowlands location the median particle size is difficult to establish, but 15 mm is probably a reasonable estimate. Figure 3.4d is the particle-size distribution for samples from the Ben Williams site. Unlike the other sites, an excavator was available for use in sampling at Ben Williams. Apparent in Figure 3.4d is less variability both upstream and downstream and with regards to depth. The median size at Ben Williams is about 20 mm, but several large stones were uncovered during the field trip, one measuring more than a meter on the long dimension and weighing 140 pounds.

From these initial characterizations the authors conclude that the general median particle diameter is in the 20 mm range (about 1 inch). However, a number of particles are present at the study sites considerably larger than this size. In terms of existing literature, these sizes are on the larger end of the scale of prior work.

42
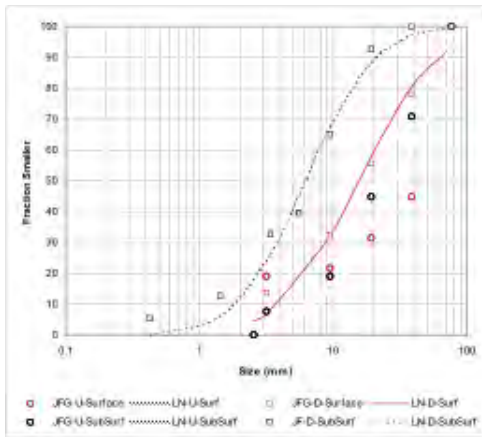
(a) Guzman Crossing.
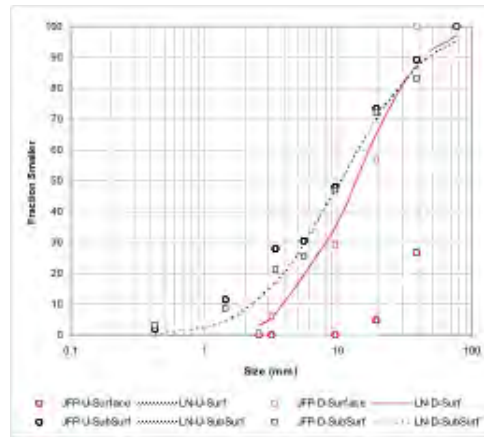
(b) Paks Crossing.
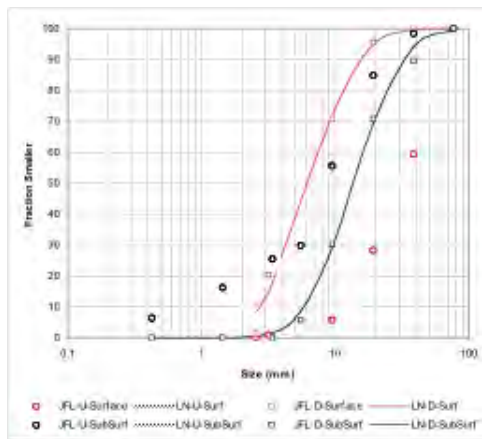
(c) Lowlands Crossing.
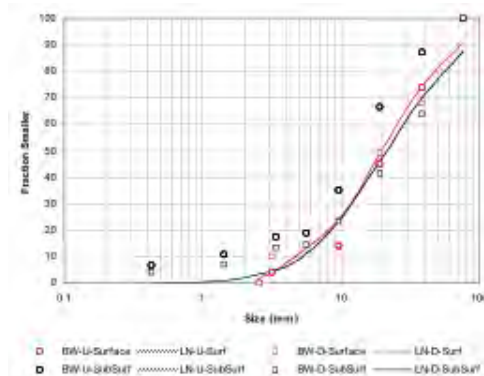
(d) Ben Williams Crossing.

Figure 3.4: Particle-size distributions from the four field-study sites with both surface and sub-surface analyses.

3.3.2. Geomorphologic Studies

USGS personnel, in collaboration with Texas Tech University, Lamar University, and the University of Houston personnel, investigated the potential for bed-material entrainment in selected streams of the Edwards Plateau. Bed-material entrainment refers to the initial, partial, or complete mobility of cobble- and gravel-sized bed material during moderate flows or large floods. The investigation of bed-material entrainment in the study area (Figure 3.5) required GIS analyses, flood-frequency analyses, field reconnaissance, field work, and numerical computations. Readers are directed to TxDOT Report 0–4695–4 (Heitmuller and Asquith, 2008) for a detailed presentation of the findings. A summary of results is provided below.

The study area contains a number of streams appropriate for bed-material entrainment research,

0   10   20   30 KILOMETERS

0   10   20   30 MILES

Edwards
Plateau
(Griffith and
others, 2004)

TEXAS

Study
area

LOCATION MAP

EXPLANATION

— **Boundary of study area**

— **Boundary of Edwards Plateau**

▲ **3** **Detailed study site and site number**

△ **17** **Low-water crossing study site and site number**

▲ **21** **Lower Colorado River Authority streamflow-gaging station and site number**

▲ **22** **U.S. Geological Survey streamflow-gaging station and site number**

▲ **2** **Detailed study site at U.S. Geological Survey streamflow-gaging station and site number**

Site number (table 1)	Site name
1	North Llano River near Roosevelt
2	08148500 North Llano River near Junction
3	South Llano River at Baker Ranch
4	South Llano River at U.S. Highway 377 near Rocksprings
5	South Llano River at 700 Springs Ranch
6	South Llano River at First Crossing
7	South Llano River at South Llano River State Park
8	South Llano River at Texas Tech University–Junction
9	South Llano River at Flatrock Crossing
10	Johnson Fork at Guzman Crossing
11	Johnson Fork at Paks Crossing
12	Johnson Fork at Lowlands Crossing
13	08150000 Llano River near Junction

Site number (table 1)	Site name
14	Llano River near Ivy Chapel
15	Llano River at Yates Crossing
16	Nueces River at Ben Williams Crossing
17	Nueces River at Vance Crossing
18	Cedar Creek at Ranch Road 336
19	Frio River at Upper Ranch Road 1120 Crossing
20	Johnson Fork near Junction
21	James River near Mason
22	08150700 Llano River near Mason
23	08190500 West Nueces River near Brackettville
24	08190000 Nueces River at Laguna
25	08196000 Dry Frio River near Reagan Wells
26	08195000 Frio River at Concan

Figure 3.5: Location of study area — Edwards, Kimble, and Real Counties, Texas, and vicinity, adapted from Heitmuller and Asquith (2008).

including the Llano River, Frio River, Nueces River, and tributaries. The streams originate in relatively western and southern parts of the Edwards Plateau, which is an elevated lower-Cretaceous limestone and dolomite tableland. The streams in the study area are incised into the plateau, resulting in removal of considerable amounts of lower-Cretaceous carbonate rock. Climatic fluctuations during the last 20,000 years have resulted in periods of variable streamflow and associated sediment transport rates. In 2007, much of the alluvial material occurred as valley fill and bed material in the streams of the plateau.

The study sites primarily were chosen to characterize downstream changes in channel geometry and bed-material entrainment potential. For this reason, all detailed study sites are in the Llano River Basin, chosen because (1) most of the problematic LWCs identified by TxDOT personnel are located there, and (2) it was desirable to analyze systematic downstream trends in bed-material entrainment potential without introducing drainage-basin variability.

Study sites range from ephemeral, bedrock, upper headwater channels to relatively wide, perennial channels occurring within Pleistocene and Holocene alluvial terraces and active floodplains. Other sites in the Frio and Nueces River Basins were visited and qualitatively examined for problems related to bed-material entrainment.

A variety of methods were used to obtain data necessary for computation of bed-material entrainment potential and included:

- GIS mapping software was used to delineate watersheds, determine drainage areas, and model watershed and channel slopes,

- Partial-duration flood-frequency analyses were done to determine the return periods of floods for USGS and Lower Colorado River Authority gaging stations in the study area. Regional regression equations were used to estimate flood frequency at ungaged study sites,

- Site reconnaissance was done with assistance from TxDOT personnel knowledgeable about the locations of sites with extreme bed-material mobility and damage to transportation infrastructure, and

- Field surveys were designed to obtain the parameters needed to apply equations to compute bed-material entrainment potential. Field surveys included measurements of channel geometry, LWC geometry, and bed-material particle sizes.

The bed-material entrainment problem for TxDOT LWCs occurs at two spatial scales — watershed scale and channel-reach scale.

First, the relative supply and abundance of cobble- and gravel-sized bed material at a site can be attributed to watershed characteristics, specifically watershed slope. The relative supply and abundance of bed material along a given channel reach becomes greater with increasingly steeper watershed slopes, based on analyses of digital elevation models and qualitative observations made during field-reconnaissance trips to the study area.

Second, the shear stresses needed to mobilize bed material at a site can be attributed to reach-scale hydraulic factors. The propensity for initial and complete entrainment of bed material depends on cross-sectional geometry and particle size. Flood-frequency analyses are associated with computations of bed-material entrainment to estimate the frequency of bed-material entrainment. In general, the frequency of entrainment increases with downstream distance, as a result of decreasing particle size and increased flood magnitudes. An average of 1 year occurs between flows that initially entrain bed material as large as the median particle size (d_{50} [diameter at which 50 percent of the sample is finer]), and an average of 1.5 years occurs between flows that completely entrain bed material up to the median particle size (d_{50}). The Froude numbers associated with initial and complete entrainment of bed material as large as the median particle size (d_{50}) are about 0.40 and 0.45, respectively.

3.4. Screening Model

Researchers at Lamar University developed a screening model to estimate the order of magnitude of gravel transport in gravel-bedded streams, and the model helps transportation planners to determine potential problem locations with and without low-water crossing. The model `SurGTAM`, Surface-based Gravel Transport Assessment Model, is a spreadsheet-based model constructed using Microsoft Excel and uses Visual Basic for Applications (VBA) as programming language. Necessary model testing was performed and it was applied for several case studies to estimate gravel transport rates at three low-water stream crossings in Texas. Basic information about the model is summarized below, and details are given by Qui (2008).

`SurGTAM` uses surface-based gravel transport equation developed by Parker (1990, 2008), as presented in Section 2.4.2. The Parker method is based on the effectiveness of selective sorting and is able to characterize the bedload material compositions (different particle size groups) of the study area. Surface-based transport models are used primarily to predict transient conditions of bed armoring, scour, or aggradation (Duan and others, 2006). `SurGTAM` can be applied to complex natural channel cross sections because several subroutines were developed to compute hydraulic parameters in complex cross sections.

Users of `SurGTAM` can use three organized Excel worksheets (details given in Appendix A) to provide necessary input data for the model. The first part of input data is the channel geometry,

- Total number of stations (or pairs of coordinates) used to describe the cross section geometry (N),

- Coordinates (x, y) or (station, elevation) in m or ft for the cross section,

- Bank stations for the main channel used to delineate left floodplain and right floodplain, and

- Manning's coefficients n for floodplains.

The second part of the input data is grain-size distribution for surface layer of the study river reach, which is represented with a series of grain sizes and associated percent finer values either by weight

(or volume) or by accounting number of particles. It is suggested that grain sizes be provided in a half-ψ interval or a one-ψ interval; and the ϕ values for grain size 2, 4, 8, 16, 64, and 128 mm are -1, -2, -3, -4, -5, and 6, respectively. The distribution can be determined by various methods through field measurements on surface sediment particles. The methods to determine particle size distribution were summarized by Shrestha (2005). The third part of the input data are the flow parameters used to estimate gravel transport. The `SurGTAM` model can be used to compute gravel transport rate for single discharge and a series of discharges within a given discharge range inputting minimum discharge, the maximum discharge, and number of discharge intervals. The model also requires input of the average channel slope (physically as slope for energy grade line, and presumably, the slope of floodplain takes the same value as the main channel). Each worksheet contains instructions and a unit conversion utility to input necessary data.

After the model execution completes, a new workbook will be created with two separate spreadsheets for the output data. The Worksheet `Sheet1` contains model results, including statistics of grain size distribution and computed channel hydraulic and gravel transport parameters). The computed channel hydraulic and gravel transport parameters include Channel Discharge (CD, m^3/s or ft^3/s), Total Gravel Transport Rate (TGRR, kg/min), Cross-section Flow Area (A, m^2 or ft^2), Wetted Perimeter (WP, m or ft), Channel Width at the water surface (CW, m or ft), Maximum Water Depth (MWD, m or ft), Shear Velocity (SV, m/s or ft/s), Hydraulic Radius (HR, m or ft), Flow Area for Left and Right Overbank (floodplain) (LA and RA, m^2 or ft^2), and Wetted Perimeters of Left and Right Overbank (LWP and RWP, m or ft). The worksheet `Sheet2` contains channel discharge (CD, m^3/s or ft^3/s) and gravel transport rates (TGRR, kg/min) at each gravel size group under single discharge or different discharges. Users can plot the total gravel transport rate, TGRR, or transport rate for different gravel size groups, versus the channel discharge as the basic model output.

`SurGTAM` was tested against two models for simple channel geometry (Qui, 2008). The model was applied to estimate gravel transport rates under historical discharge range (100 ft^3/s–85,000 ft^3/s) at three stream crossings (Guzman, Paks, and Lowlands) of Johnson Fork Creek in Kimble County, Texas.

Example results for the Guzman crossing are displayed in Figure 3.6. The estimated transport rate of natural ground surface without the low-water crossing is greater than that with road surface cross section. The transport rates are about 0.87E+07 kg/hr and 1.21E+07 kg/hr with and without road crossing when channel discharge is 85,000 ft^3/s. Based on model results, for the modeled discharge range, the presence of the roadway impacts sediment transport. The roadway-in-place model results in less gravel transport than the natural section. Therefore, it is likely that gravel will accumulate at the crossing.

3.5. Physical Modeling

Physical modeling of bed sediments and stream crossings was conducted in two phases, similar to the division of tasks for the other components of the project. During the initial phase of the project, a qualitative physical model was constructed in the University of Houston hydraulic flume.
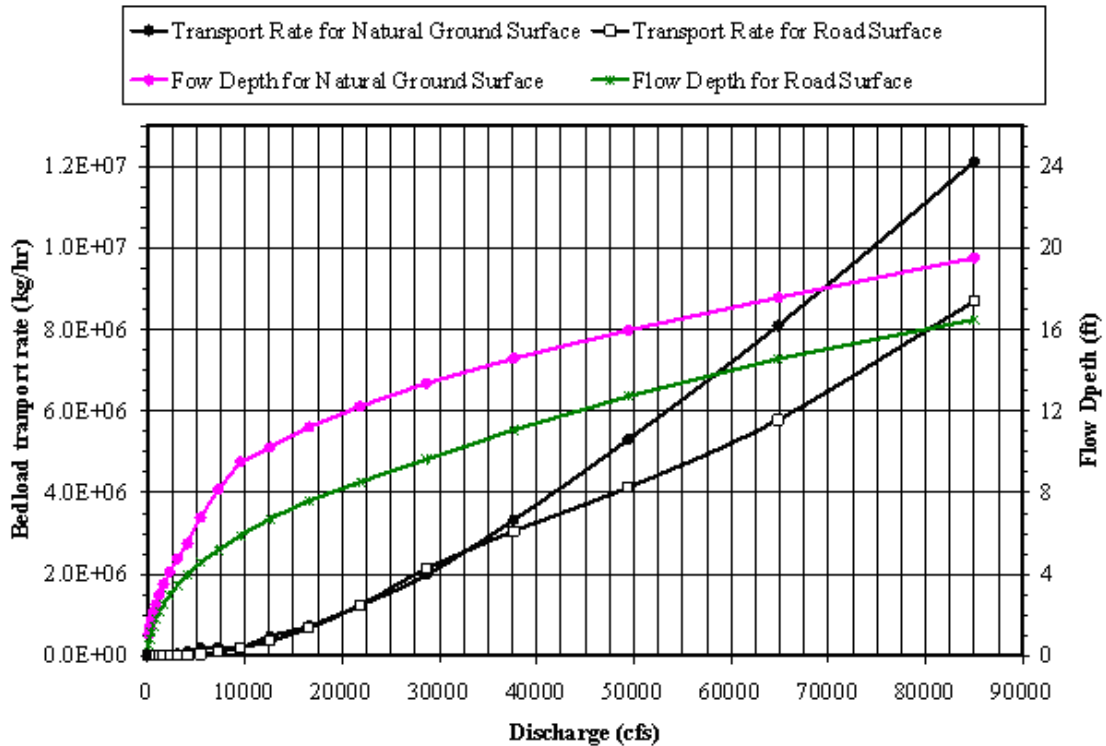
Figure 3.6: Estimates of transport rate from the screening model without stream crossing for the Guzman crossing of Johnson Fork.

Materials collected at the field-study sites were used in the flume to represent bed materials. Cinder blocks were used to simulate the crossing. The objective was to determine whether a simple physical model could generate effects considered plausible given field observations and measurements.

After the interim report was presented to TxDOT, a second set of experiments using a larger-scale model were constructed, again at the University of Houston laboratory facility. The objective of the second part of the physical modeling was to attempt to reproduce appropriately-scaled behavior and to place scale models of potential design approaches into the flume for determination of the applicability of the ideas. This following sections of the report are intended to document physical-modeling results.

3.5.1. Initial Qualitative Modeling

A single physical model experiment was conducted late in August 2004. The purpose of this experiment was to demonstrate that the laboratory flume could be operated in a fashion to simulate flash-flooding and consequent bed mobility without damaging the flume and pumping system. Cinder blocks were used as models for a box culvert and road bed. Samples from the July 2004

field trip were used as the bed material. The experiment was set up by placing the "culvert" first, then adding the bed material by spreading the field-sampled material on the upstream side of the culvert. The following series of images are documentation of the experiment. In discussions between research team members, we assumed that "interesting" behavior would occur when flows in the flume (and the field) were at critical and super-critical velocities. Whereas that indeed was true, we discovered that visible bed motion occurred even with relatively stable sub-critical flows.

Figure 3.7a is an image of the model during a simulated flooding event. In this image the upstream and downstream Froude numbers were about 0.30. In the laboratory, smaller particles can be observed to be moving, although most of the bed appeared stable. In Figures 3.7a and 3.7b, the water depth above the gravel bed was about 0.72 feet. The measured discharge was 0.94 cfs. The calculated section velocity was 1.3 ft/sec. Prior to this image the model was run for about an hour with the depth of flow below the invert elevation of the model box (that is the road bed was not flooded).

Figure 3.7b is an image during the same flow regime. The "hole" in front of the culvert is a consequence of the flow. When the experiment began, the gravel bed was essentially parallel with the culvert entry, but higher than the bottom of the culvert. The hole material deposited on the downstream side of the culvert (not pictured). The hole grew in the upstream direction (slowly) as if it were a head-cutting stream.

The next images are the result of larger flows through the test section. Forces on the bed materials were probably substantial, if not enormous. The objective of this particular set of flows was to determine if the research team could cause deposition on top of the culvert model. The flow rate and water depths in the following pictures were not measured.

The gravel bed filling the culvert is depicted on Figure 3.7c. When the culvert became full of gravel the flow was essentially vertically upward, which carried the solids materials up onto the road bed. Figure 3.7d is an image of deposition during this flow.

Figure 3.7e is an image on the downstream side of the model during high flow. The hole being formed on the downstream side is from water cascading over the structure (significant vertical flow component and visible hydraulic jump in the erosion region). In this image there is little flow through the culvert because it is completely clogged by gravel on the upstream side.

Figure 3.7f is an image of the model during receding part of the simulated flood wave. Note the gradation of the deposition (large material on the leading edge, smaller as one moves downstream). Forensic field-work should verify if such gradation occurs in natural flows.

Figure 3.8 is an image of the model after the simulated flood event. Again note the gradation moving downstream from the structure.

Bed materials moved readily when flows approached mid-culvert depths. The tendency for the culvert to clog when substantial bed-movement happened was observed. In addition, deposition of bed materials on the "roadway" was observed. Based on the observations presented above and on the judgment of the researchers, physical modeling represents a viable approach to producing reasonable behaviors of bed sediments and a potential vehicle for testing alternative designs at

(a) Upstream portion of model looking towards culvert. Entire "road bed" is submerged.

(b) Upstream of culvert. Note "hole" in gravel bed that eroded when the flow regime was changed from open flow to submerged flow.

(c) Gravel bed filling culvert.

(d) Deposition on top of culvert.

(e) Downstream side during "flash flood."

(f) Side view during "flash flood."

Figure 3.7: Sequence of images from qualitative physical model run of late August 2004.

Figure 3.8: Deposition downstream from "road bed" after flood waters receded during the qualitative physical model run of late August 2004.

modest cost.

Interpretation of Results — Drag Force Model

The initial physical modeling results suggested that some measure of when mobilization is expected can be related to physical properties of the river materials and hydraulic conditions.

The physical experiments were aimed at:

1. Identification of hydraulic conditions under which mobilization is likely to occur — in the geomorphic analysis the Froude number is the important metric that correlates with evidence of motion; in the physical model experiments critical velocities were identified. Later to be consistent these velocities were converted to Froude numbers for comparison to the geomorphic results, and

2. Identification of design elements that can accommodate the solids flow.

Simplified Mobilization Theory

A simplified mobility theory based on spherical particles rotating over a small step was used to interpret the experiments and to predict imminent mobilization. The theory assumes that the bed material is comprised of a fully submerged spherical particle on a flat bed prevented from lateral motion by a step of height h. Lift forces are neglected and flow is assumed undisturbed.

51

Figure 3.9 is a free-body diagram of the sphere and step. The particle has contact forces at a and
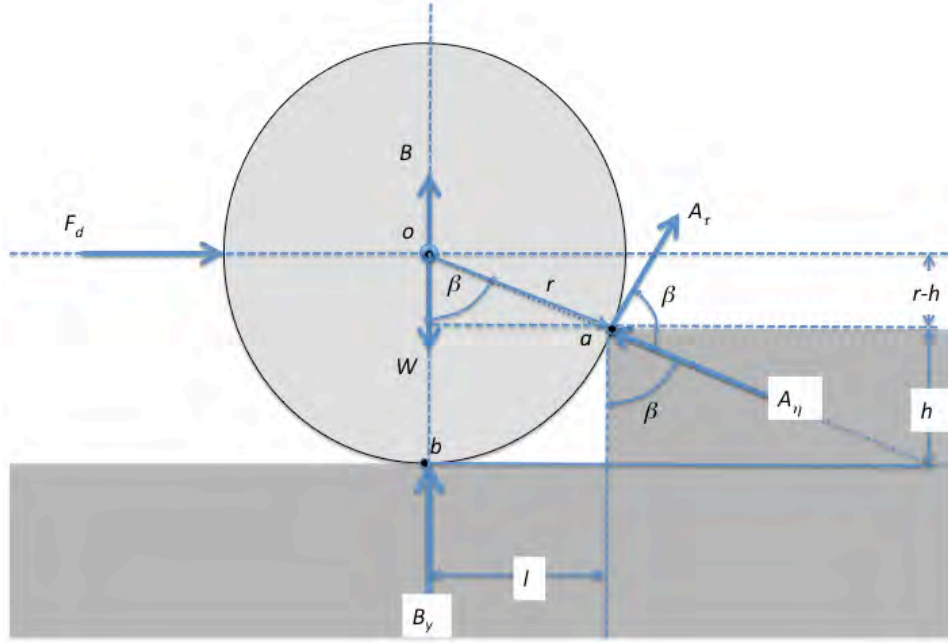
Figure 3.9: Sketch of sphere on flat bed with lateral motion restrained by a small step.

b, body forces of weight W, and buoyancy B, and a drag force caused by liquid flow past particle F_d. Neglecting friction at point b means that there is only a vertical component of normal force B_y. The contact point a produces a normal and tangential force; the tangential force is a frictional force resisting sliding, thus a is an instantaneous rotation center.

The geometry at a that relates the radius r and height h to the contact angle β is also depicted on Figure 3.9. In the context of the sketch, the following relationships are defined.

$$r - h = r \cos \beta \tag{3.1}$$

$$l = r \sin \beta \tag{3.2}$$

$$\beta = \cos^{-1} \left(\frac{r - h}{r} \right) \tag{3.3}$$

A force balance of system while the contact force at b is non-zero (but approaching zero — motion is imminent) is defined by the following relationships.

$$\sum F_x = F_d - A_\eta \sin \beta + A_\tau \cos \beta \tag{3.4}$$

$$\sum F_y = -(W - B) + B_y + A_\eta \cos \beta + A_\tau \sin \beta \tag{3.5}$$

$$\sum M_A = (W - B)l - B_y l - F_d(r - h) \tag{3.6}$$

The term $(W - B)$ is the submerged weight, W_s. Now assume that B_y vanishes (particle is just out of contact with bottom of pit), then the force balance now becomes

$$\sum F_x = F_d - A_\eta \sin\beta + A_\tau \cos\beta \tag{3.7}$$

$$\sum F_y = -W_s + A_\eta \cos\beta + A_\tau \sin\beta \tag{3.8}$$

$$\sum M_A = W_s l - F_d(r - h) \tag{3.9}$$

The moment equation provides the necessary information to determine F_d as the particle begins to rotate about the moment center. Set the moment to zero (equilibrium) and analyze.

$$W_s \frac{l}{(r - h)} = F_d \tag{3.10}$$

Substitute in geometry and the definition of submerged weight to arrive at

$$\frac{4}{3}\pi r^3 \left(\rho_s - \rho_l\right) g \ \tan\beta = F_d \tag{3.11}$$

If the analyst then assumes the drag force is proportional to momentum, a relationship of drag force and velocity is defined.

$$F_d = C_d \frac{1}{2} \ \rho_l \ V^2 \ A_p \tag{3.12}$$

The coefficient C_d is a constant of proportionality, the the velocity is some kind of average near the particle. From the fluid mechanics literature the value of C_d will probably range between 0.1 and 2.0. Setting the two expressions equal to each other and solving for velocity, produces a critical velocity, if flow is above this critical velocity the particle should begin to rotate, if below this critical velocity the particle should be "stable". The relationship of velocity to particle and fluid properties is

$$V = \sqrt{\frac{8}{3}rg\tan\beta \left(\frac{\rho_s - \rho_l}{\rho_l}\right)\left(\frac{1}{C_d}\right)} \tag{3.13}$$

Except for C_d the right hand side is entirely determined by the particle dimension r, the step height h, and the particle solids density ρ_s.

The case of shielded flow is essentially the same; a sketch is presented in Figure 3.10.

The analysis proceeds in the same fashion except the following changes are observed:

1. The projected area is reduced:

$$A_p = \pi r^2 - \beta r^2 + r^2 \sin\beta \cos\beta \tag{3.14}$$

2. The line of action of drag force changes

$$\Delta r = \frac{2r(\sin\beta \ \cos^2\beta - \sin\beta)}{3(\pi - \beta + \sin\beta \ \cos\beta)} \tag{3.15}$$

53
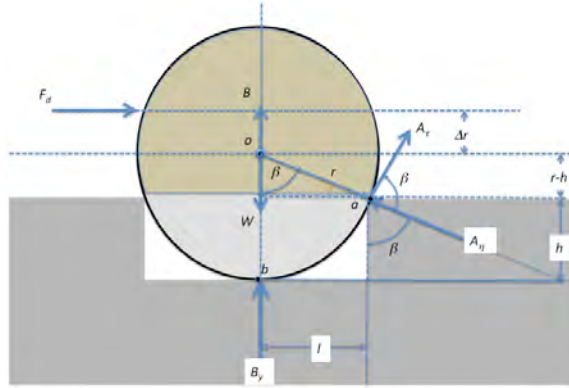
Figure 3.10: Geometry of sphere in a "pit." Flow is partially shielded by the pit.

3. Moment arm of drag force is increased

$$F_d[(r - h) + \Delta r] \tag{3.16}$$

The resulting critical velocity equation is more complex, but fundamentally the same as for the simple step case, and is,

$$V = \sqrt{\frac{\frac{8}{3}\pi r^3 \ (\rho_s - \rho_l) \ gr \sin \beta}{C_d \rho_l \left[\pi \ r^2 - \beta \ r^2 + r^2 \sin \beta \cos \beta\right] \left[r \cos \beta + \frac{2r(\sin \beta \cos^2 \beta - \sin \beta)}{3(\pi - \beta + \sin \beta \cos \beta)}\right]}}. \tag{3.17}$$

Equation 3.17 provides a tool to interpret experimental results and to predict potential motion. Although C_d is still unknown, it should range between $\approx 0.5 - 2.0$. In this development it is expressed as a velocity, however if flow geometry is well known, the Froude number should provide the same kind of information.

Experimental Bed Sizes

Two different size of rocks were used in the bed mobility lab experiments; small and large sizes. The materials were classified using large wooden sieves and manual shaking to pass materials through the sieves. These were the same sieves used in the field trips to classify bed materials.

The use of two sizes was to test the simple mobilization theory — sphere dimension is important in the theory, and to test the clogging potential of culvert models as a function of granular material dimension to the culvert opening dimension. The small sizes were roughly $\frac{1}{10}$ of the culvert dimension, while the large sizes were about $\frac{1}{5}$ the culvert dimension. The research team formulated a hypothesis that materials smaller than about $\frac{1}{9}$ of the culvert diameter[2] would pass easily and not clog the culvert while particles larger than this ratio would easily clog.

---

[2]This particular ratio is an "ad-hoc" estimate based on field observations and does not constitute a systematic value — despite this anecdotal guess, the experiments do have a rudimentary ability to evaluate the effect of different rock sizes.
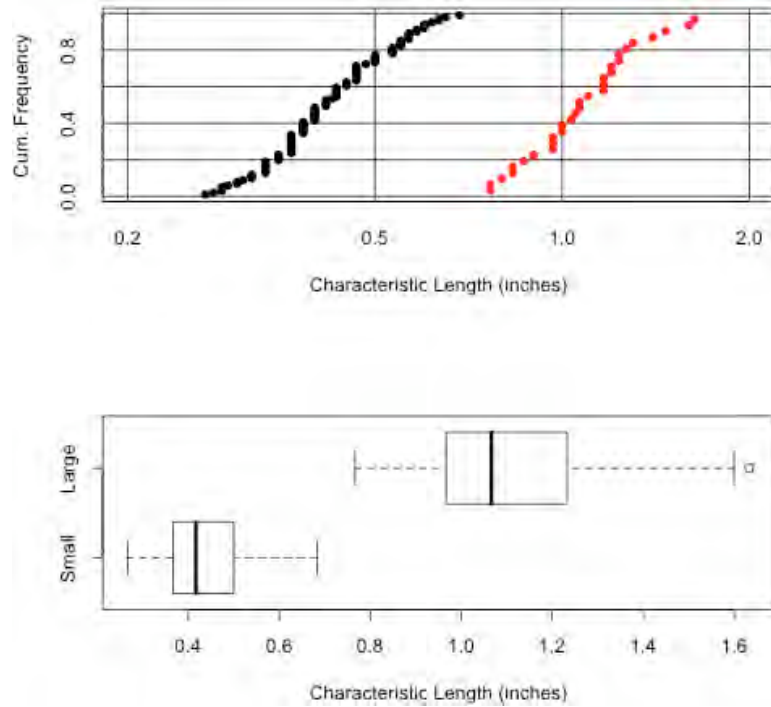
Figure 3.11: Size distributions and boxplots for experimental bed materials.

Figure 3.11 is a plot of size distributions based on the mean value of three principal dimensions, and boxplots of the same data. The researchers selected a small number of rocks from the bed and determined the size of a parallelepiped box that the rock would fit into — these dimensions are the length, width, and height as measured with a machinist caliper. The tabulated size values used to construct the figures appear in Appendix B. The figures display two important features, first that the classification tools were quite effective with nearly no overlap is size values, secondly that the sizes are different and the difference is statistically significant.

Rock Solids Density

The researchers developed the mobilization theory assuming that solids density was 2.65, which is a typical value in the literature for geologic materials. Well into the experiments, the researchers became aware that there may be a need to quantify the solids density. A displacement method was used to estimate the solids density and the researchers found that a working estimate of specific gravity is $SG_s = 2.3$ for a composite sample; meaningfully smaller that the typical value from the literature. If the sample is largely limestone (not dense flint), then the working value is even smaller. Details of the analysis and suggestions for more in-depth analysis appear in Appendix B.

3.5.2. Drag-Force Interpretation of Results

Figure 3.12 is a plot of the relationship of observed mobilization velocities and the drag-force theory for some different "exposure" ratios. This plot includes all experiments and comprises data from five different crossing models as well as values interpreted from the geomorphological studies (Heitmuller and Asquith, 2008):

1. Rectangular small width culvert,

2. Rectangular large width culvert,

3. Two-barrel circular culvert with same area as the small width rectangular culvert,

4. Four-barrel circular culvert with same area as the large width rectangular culvert, and

5. Porous structure with small width culvert.

Based on the plot, the simplified mobility theory has value in predicting impending mobilization of a solids bed over a small range of sizes. Extrapolation would not be recommended, but the "horn" shape of the curves appears to be honored by actual observations, with slightly more exposure as the rock dimension increases[3]. In larger sizes, if the interpretation is correct, greater exposure is suggested. The greater exposure is compatible with intuition (and field trips) and the geometry of the larger rocks are sufficiently different to present orientations that would tend to increase the exposure ratio ($\frac{h}{r}$). No formal attempt at curve fitting was done for this particular plot, but visual inspection indicates that a generic exposure ratio of $\frac{h}{r} = 0.32$ is a reasonable model of the behavior observed in these experiments. This ratio would be consistent with spheres in a body-centered cubic packing, although this statement requires further study (in the future). Natural packing structures anticipated would be hexagonal close packing, followed by body-centered cubic, followed by simple cubic packing.

Figure 3.13 is a plot of the observed velocity distributions for mobile and stable bed conditions. The stable bed velocities for the small size solids are close to the mobile bed velocities, while the difference is larger for the larger size solids. The differences were found to be statistically significant — barely for the small size solids; comfortably for the larger size solids. These curves are interpreted as follows:

1. The actual transition from stable to mobile would lie between the curve pair (for the given size).

2. The mobilization velocity increases with size (as anticipated) and the increase is nonlinear in diameter.

---

[3]This finding is interpretation by the authors; the size category only has two meaningful diameters!
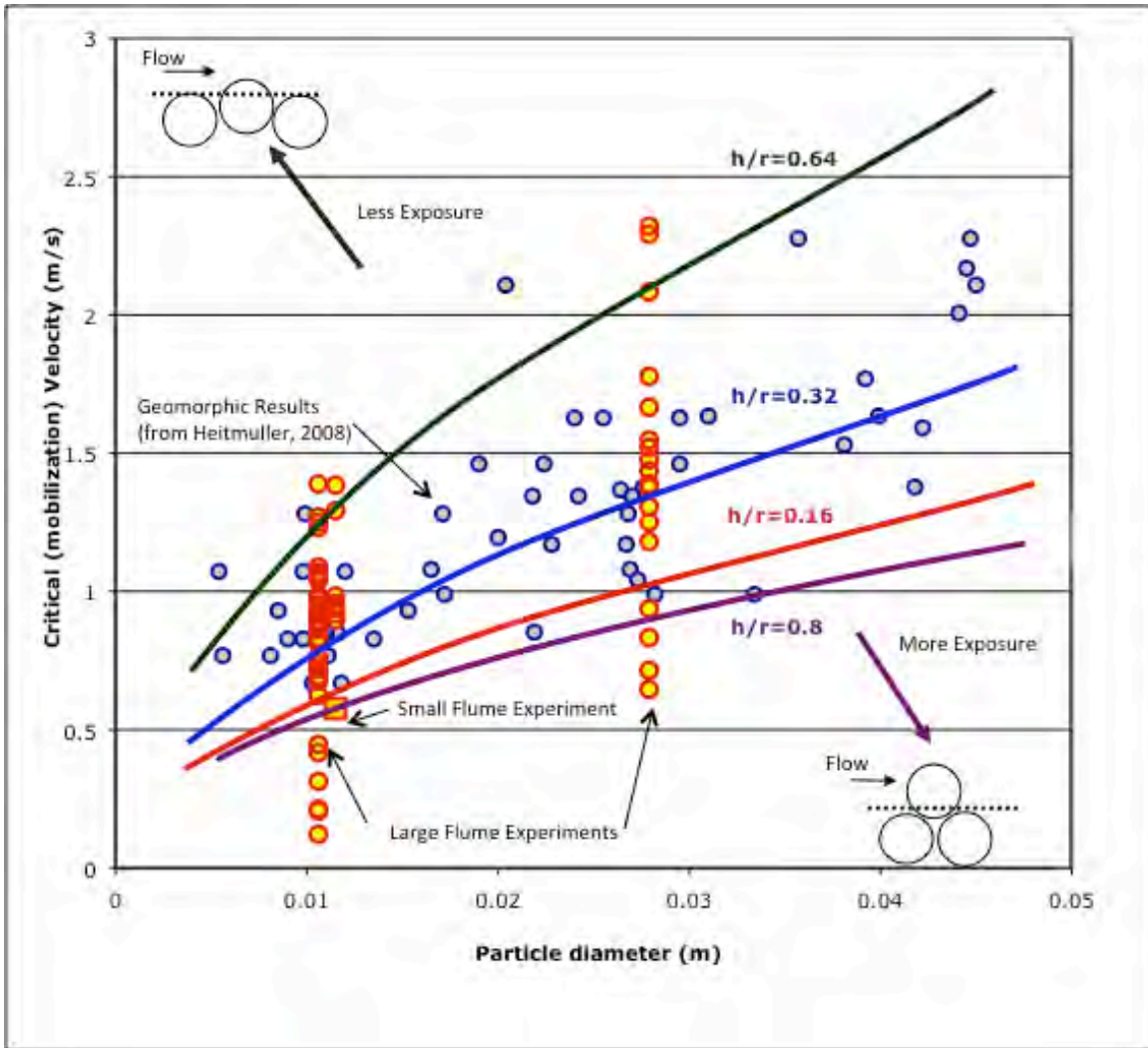
Figure 3.12: Relation between observed mobilization velocities from UH experiments and geomorphic analysis and simple mobilization model values. More "protected" spheres (in deep pits) are towards the upper right and more "exposed" spheres towards the lower left. Markers labeled "geomorphic results" are adapted from results on the USGS geomorphological studies (F.T. Heitmuller, written communication, 2008).

57
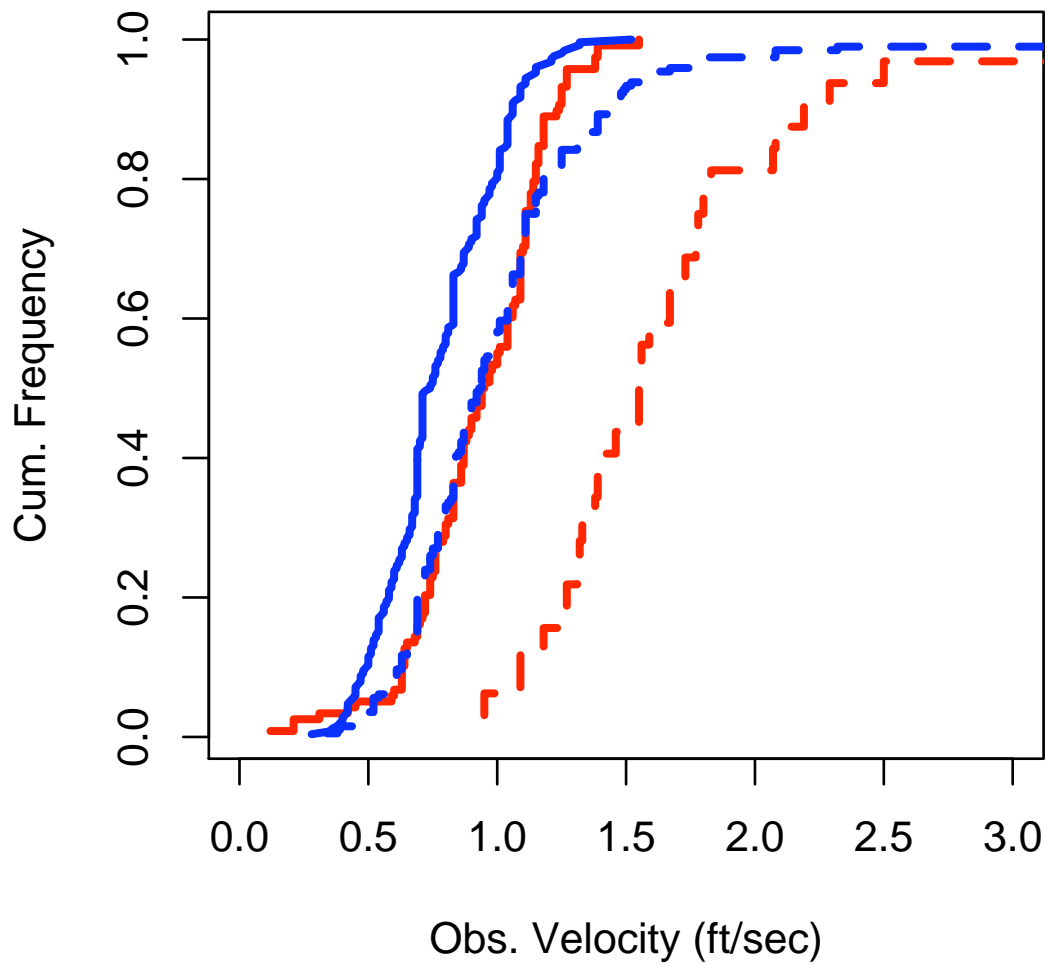
Figure 3.13: Stable (blue) and mobile (red) velocity distributions for UH experiments. Solid curves are for the small particle diameter, dashed curves for the large particle diameter.

3.5.3. Interpretation of Results

This purpose for this section of the report is to provide interpretation of the modeling results by each model crossing type. A summary of the experimental results that are used in this section appear in three parts in Appendix B.

Bed Mobility Rates

Measurements were recorded in two experiments that allowed estimation of the rate of bed propagation. In these experiments, the distance was measured from the upstream of the model to the "scour" hole formed in the bed moving towards the model and similar distances from the downstream side of the bed. An estimate of the mobilization rate from these propagation distances assuming a uniform depth of bed material is mobilized is that when the solids are moving, the rate is on the order of 1.0–2.0 pounds of solids per hour[4].

No attempt was made to scale up the estimated mass flow rate. The researchers did accelerate water to induce mass flow so the time scale in a real system over which such solids transport could occur could be much longer than in these experiments.

Culvert Clearing

In all experiments, regardless of crossing type, the solids mobilize (at sufficient discharge) and move downstream towards the crossing model. Upon arrival, solids clogged the crossing in some fashion. In some experiments, the clogged condition was a terminal condition and no further motion was observed. In most experiments, a head cut downstream from the crossing model was observed and if this head cut propagated upstream back to and through the crossing model, the crossing would "self-clear."

A general progression of the experiments is:

1. For relatively small discharges, when there is no mobilization, the system performs as expected — the culvert carries clear water as expected and the solids bed is stable. In the experiments, many such situations were produced where the bed is stable yet the crossing structure is submerged;

2. As discharge increased to the point of upstream bed mobilization, solids propagated towards the crossing structure. Generally in these cases, a downstream head cut moved towards the crossing model from the downstream side — when the experiment duration was sufficient for this cut to propagate as far as the crossing model, the model could self-clear;

3. When the bed is mobile, a dune forms just downstream from the source section where the solids are removed and this dune moves downstream. If the solids move, most of them move

---

[4]The estimates of solids mobilization are from two experiments that reported $\approx$ 5.8 lbs/5.5 hours and $\approx$ 8.2 lbs/4.3 hours; both experiments used smaller-sized solids

as part of this dune. In some experiments the dune was stopped by the crossing model and the downstream progression of the dune was greatly diminished;

4. When the dune stopped, it behaved as a weir — the solids shed were shed from the top of the dune and from the downstream side of the dune[5]; and

5. Even when stopped, dunes shed solids and in some experiments once the dune breached solids mobilization continued.

Specific features of different crossing models and their clog-clear cycle are

1. Rectangular culvert: Solids fill the culvert from the downstream towards the upstream side of the model. The filling of the culvert is reasonably uniform and the culvert clogs entirely (that is, looking from downstream to upstream the clogged culvert is as clogged as looking from the opposite direction). Researchers speculate that the solids enter the culvert and are blocked at the exit by existing downstream solids and the culvert fills in this fashion. When the downstream head cut reaches the downstream side of the model, the culvert self-clears into the cut (that is, the culvert becomes a solids source to supply the now solids-starved head cut.);

2. Two-barrel Culvert: Solids fill the culvert from the downstream, but the upstream end becomes clogged in such a matter than the downstream portion of the culverts remain relatively unfilled — hence the culvert appears partially clogged when looking from downstream to the upstream. Once the upstream portion of the culvert is occluded, the model behaves as a weir and most flow is carried across the top of the model (over the roadbed). When the downstream head cut frees materials from the downstream side of the model the culvert self-clears;

3. Four-barrel culvert: Clogs and clears in a fashion similar to the two-barrel case with the following additional observations. The middle barrels tend to clog first followed by the outer barrels. When the culvert clears, it clears from middle to the outer barrels reversing the process of clogging just described. The filling and occlusion is similar to the two-barrel case — again with upstream occlusion nearly complete whereas the downstream portion appears only partially clogged; and

4. Porous crossing: Similar to other models but with one unusual difference. Before the culvert clogs, the downstream side of the porous structure is washed away from the structure — the researchers speculate that the discharge through the structure is significant (by design it should be) and this discharge through the porous part destabilizes material enough so that when the larger flows arrive that the downstream of the model is solids deficient, thus materials that would clog, instead pass through the culvert to resupply the downstream deficit. This deficit is not maintained long, and eventually the culvert clogs. The porous models seem to self-clear more rapidly than the other models.

---

[5]The dune was undercut as if it were an earthen weir.

Solids Accommodation

Each model type clogged and cleared, and thus each is capable of conveying solids. One important question that can be answered from the limited data collected in the semi-quantitative experiments is which crossing design carries more discharge before the bed mobilizes?

A comparison of nominal discharge measurements with and without mobilized solids is depicted in Figure 3.14. The three panels represent paired models with cross sectional area is the same — thus the upper panel is a plot of the small rectangular culvert with a two-barrel circular culvert; the middle panel is a plot of the large rectangular culvert with a four-barrel circular culvert; and the bottom panel is a plot of the large rectangular culvert with a porous structure containing a rectangular culvert. The differences with and without mobilized materials is almost meaningless in these plots other than to conclude that higher discharges correspond to mobile materials in the models. There is little evidence that the multiple barrel culverts can carry a higher water discharge before mobilization than can the rectangular equivalents, and the same finding is suggested for the porous model.

A comparison of estimate Froude numbers is depicted in Figure 3.15 for the same model pairs as in Figure 3.14. Similar interpretation is indicated — there is no meaningful difference in Froude number by crossing type or by mobile/non-mobile solids in the experiments. While there is no evidence that one type of crossing performs better than another, there is a more important finding suggested by the Froude number plots — bed mobilization occurs at a Froude number well below critical Froude number and is maintained at Froude numbers below critical. The experiments mobilized materials by forcing a supercritical portion of flow to occur in the solids source region, but flow need not remain supercritical to maintain solids transport.

The second important question is which crossing design carries more solids before the crossing clogs? The experiments could not answer this question, in part because the experimental design did not properly address this question. Instead the researchers offer opinions based on the written observations in the laboratory notebook. These opinions are as follows:

- Multiple barrel culverts appear to be able to self clear "better" than single opening culverts. The presence of multiple barrels allows flow instabilities to be magnified on the downstream side of the model and keep at least one barrel clear. This finding contradicts field observations, however in the laboratory model the entire downstream side was part of the flow regime, while the multiple barrel field conditions appeared to be misaligned with respect to the downstream flow path.

- The porous model worked well — better in observation than the other crossing types. The researchers attribute this performance improvement to non-zero flow velocities through the model that destabilize the downstream side of the crossing to help the downstream head cut propagate upstream more rapidly, thereby keeping the culvert clear longer (or encourage more rapid self-clearing).

- Culvert geometry matters. Circular culverts clog on the upstream side before the downstream side is fully clogged; the rectangular culverts did not appear to clog in this fashion. Rect-

angular culverts clog more uniformly and at complete upstream occlusion, the downstream side is also nearly occluded. Circular culverts seem to self-clear better than their rectangular counterparts.
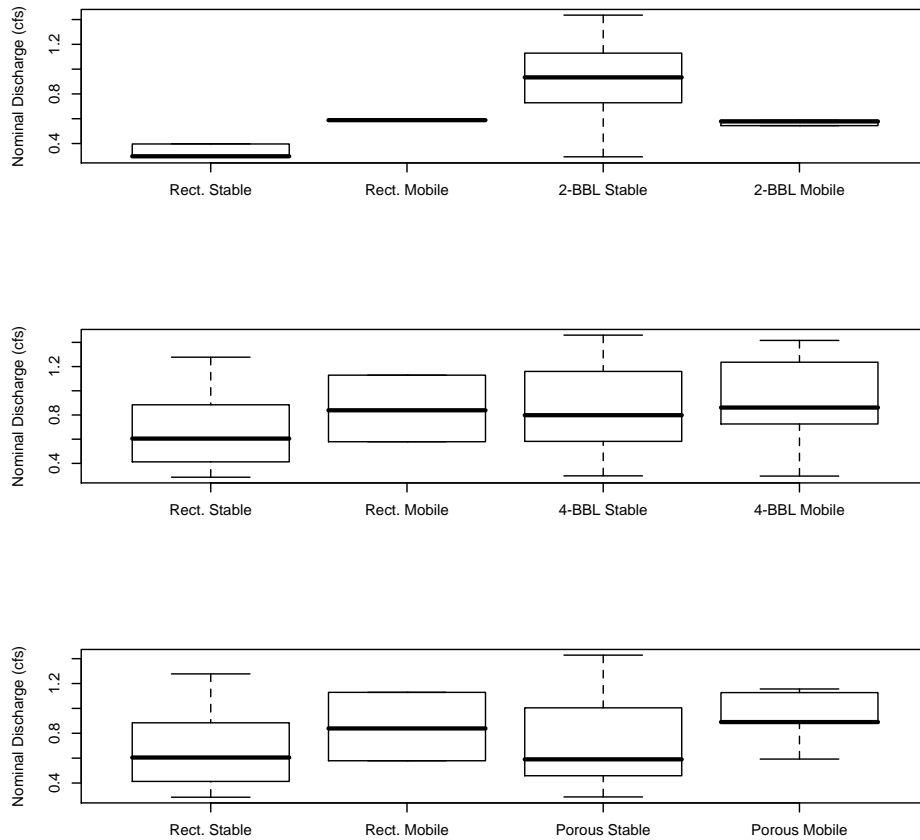
Figure 3.14: Nominal discharge for different crossing models — with and without mobilized solids.

3.6. Numerical Modeling

The purpose of this section is to present results from the University of Houston research team's numerical modeling results. The procedure used is documented in Section 2.7. A portion of the computational results are presented in that section (Section 2.7).
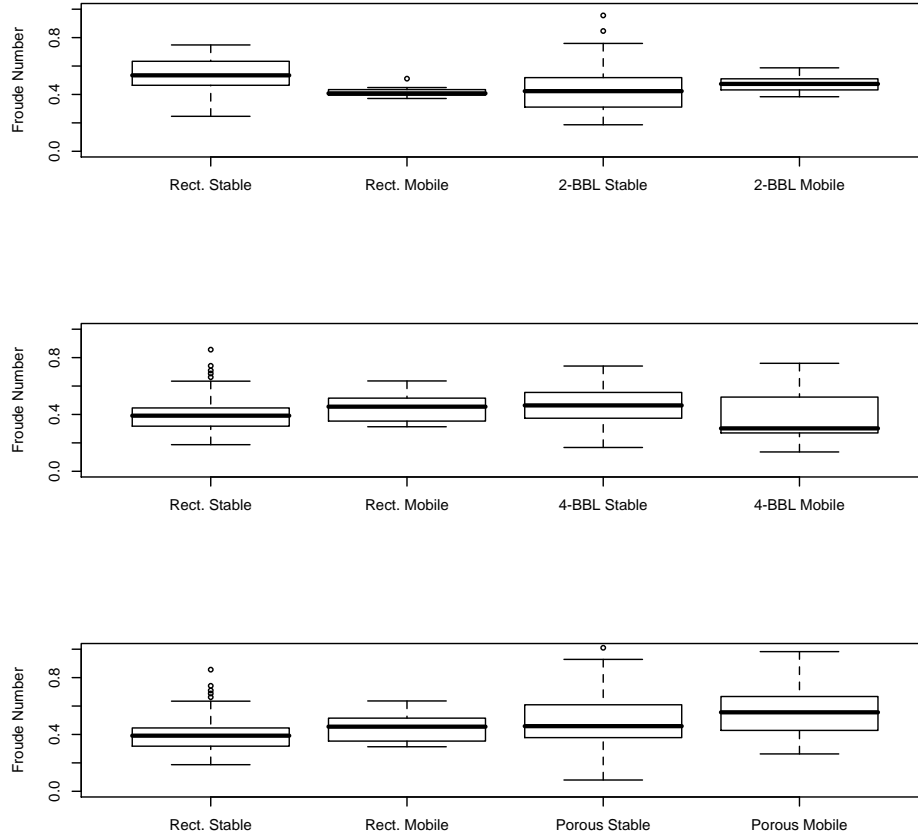
Figure 3.15: Computed Froude number (Fr) for different crossing models — with and without mobilized solids.

3.6.1. Hydrologic Modeling

`HEC-HMS` was used to model the hydrograph from the November 2, 2000 flood event. The approximate return interval of that event was 18 years. Additional details are presented in Section 2.7.3.

3.6.2. Hydraulic Modeling

`HEC-RAS` was used to model the hydrograph produced by the November 2, 2000 event, as described in Section 2.7.4. The hydraulics from the `HEC-RAS` model were used to analyze the mobilization of bed material and to model bedload transport. An average peak flow rate of 11,489 cfs was obtained and used for a steady-state hydraulic analysis.
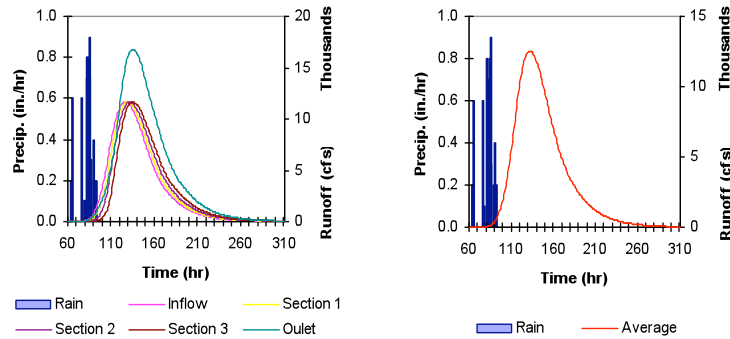
Figure 3.16: Johnson Fork Creek runoff hydrograph from the event in November 2, 2000 (Wang and Krou, 2008).

At the peak discharge for the study event, all the culverts are submerged, as shown on Figure 3.17. An unsteady flow run in `HEC-RAS` is not necessary for the computation of sediment transport; the hydrograph generated by `HEC-HMS` is sufficient. However, a second `HEC-RAS` unsteady-state model was developed to use the hydrograph depicted in Figure 3.16. The downstream boundary condition was specified as normal depth with an energy slope of 0.0027. An initial condition of 1 cms (35.3 cfs) was used to establish a starting water-surface profile.

Results from the unsteady analysis are shown on Figure 3.18a and 3.18b. Discussion of the evolution of the bed profile is presented in Section 3.6.3.

3.6.3. Bedload Transport Modeling

To have a better understanding of the performance of the Einstein, Parker, or Meyer-Peter and Müllers approaches as described above for estimating the bedload transport rate, a storm event was selected to compute the time variation of bedloads potentially transported at Guzman low water crossing, a study site of Johnson Fork. A topographic survey of the Guzman location showed that the channel was about 25 ft deep with a bottom width of 100 ft and top width of 1,500 ft (Figure 3.19a). For computation simplicity, the channel cross-section was modeled using four (4) trapezoidal sections as shown in Figure 3.19b. The channel slope S is 0.0027. Manning's roughness coefficient n calculated using the Einstein bedload determination method is about 0.01. The flow hydrograph used for calculation was recorded in November 2000. It presents a minimum of 18 cfs and maximum of 83,193 cfs on Julian days 316.89 and 318.56, respectively. The average flow over that period is 1,812 cfs (Figure 3.16).

Figure 3.20 presents bedload hydrographs calculated using the Einstein, Parker, or Meyer-Peter and Müllers approaches. For each method, surface (grid method) and subsurface (volumetric technique) sampling seem to yield results of the same order. Each graph shows the occurrence of a single surge. The peaks are observed at the time of maximum river discharge. However, only the Meyer-Peter and Müllers approach is able to capture the effect of the long recessional flow with high concentration
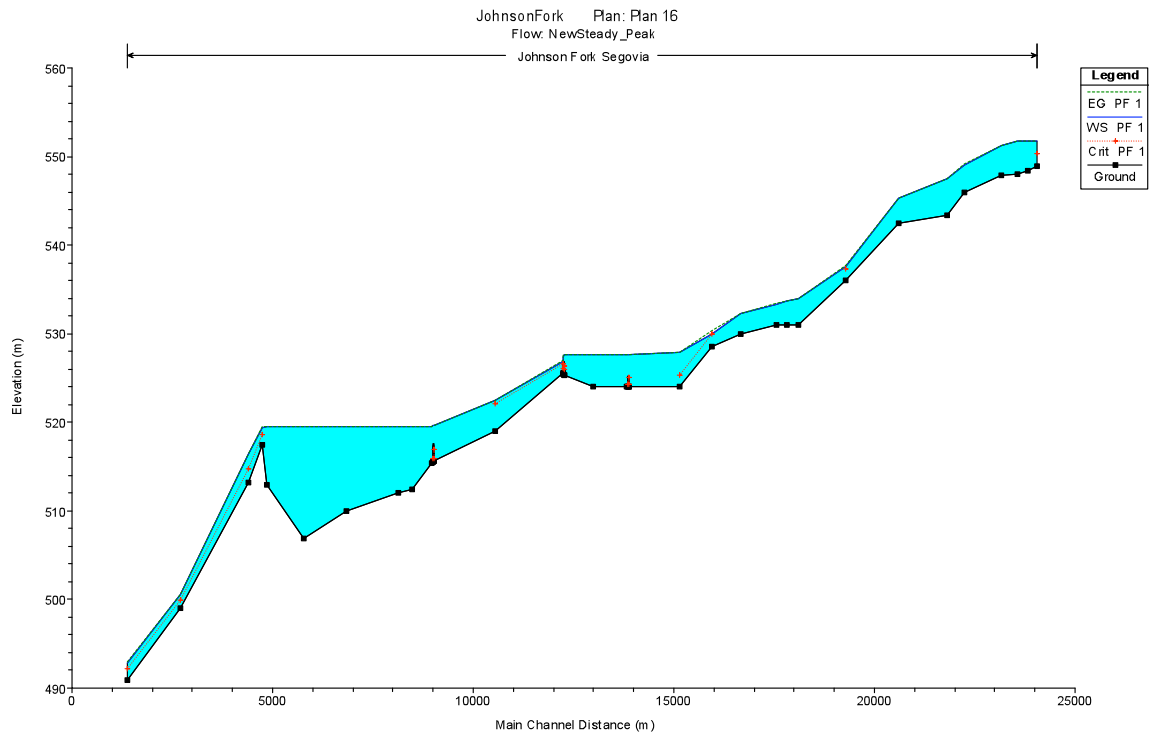
Figure 3.17: Steady water-surface profile for Johnson Fork Creek for a discharge of 11,487 cfs (Wang and Krou, 2008).
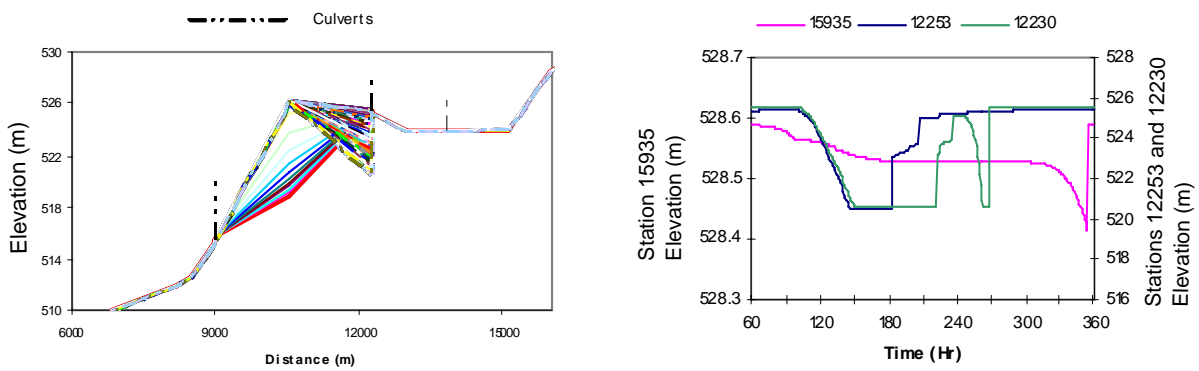
(a) Evolution of water-surface profile.

(b) Time series of bed elevation.

Figure 3.18: Water-surface profiles and time series of bed profiles for Johnson Fork Creek for the event of November 2, 2000 (Wang and Krou, 2008).

65

(a) Guzman crossing cross section.

(b) Guzman crossing cross section.
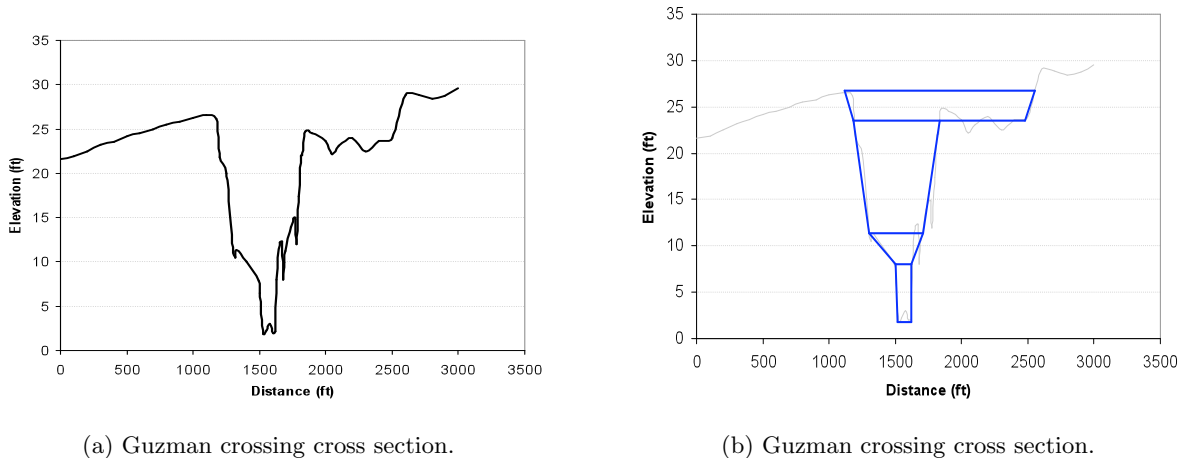
Figure 3.19: Johnson Fork Creek Guzman crossing surveyed and schematized cross sections.

of finer sediment. The difference due to the method of sampling is stressed by this technique in the smaller particle sizes (Figure 3.20c).

A close observation of Table 3.2 reveals the significance of differences in bedload quantities for identical sampling techniques when different methods are applied. For example both Parker and Meyer-Peter and Mller are widely recommended for surface sampling of gravel-bed rivers. However, for samples obtained by the grid technique, Table 3.2 shows that the volume of bedload calculated with the Meyer-peter and Mller formula is over 20 times greater than the results obtained from Parkers equal mobility approach. The Meyer-Peter and Mller bedload is about 200 times greater than that of Einstein. Einstein formula may not work well for poorly sorted and coarse bed materials because the hiding correction factor used in the determination of the transport rate via shear stress plays a very detrimental role. Variations in the results are less important when applying the same assessment method to different sampling techniques. Still, the quantities double. It can be inferred that the choice of a bedload calculation method is crucial for the design of stable structures in gravel-bed rivers.

Simons and Sentürk (1992) and Yang (2003) pointed out the quantity differences mentioned above. The key issues are finding the correct representative grain size and deriving a theoretically-based bedload transport function. Einstein (1950) used d_{35} and d_{65} as representative grain size whereas Parker and others (1982) used d_{50}, and Meyer-Peter and Müller used d_{50} and d_{90}. Uniform bed material and/or well distributed-particle size sediment are often assumed in formulae derivations, which is unfortunately rarely the case. Also, bedload transport functions are mostly based on limited experimental data, whose correlation with empirical formulae can be highly site specific. Another important source of errors in bedload estimation is the assessment of the carrying fluid. Most of the calculations performed by practicing engineers are based on clear water as transporting agent. However as it is the case for Johnson Fork Creek, the geomorphology study revealed that the river flow could contain an appreciable amount of clay and fine particles of limestone. These parameters change the density and behavior of the water and could definitely affect the transport

66
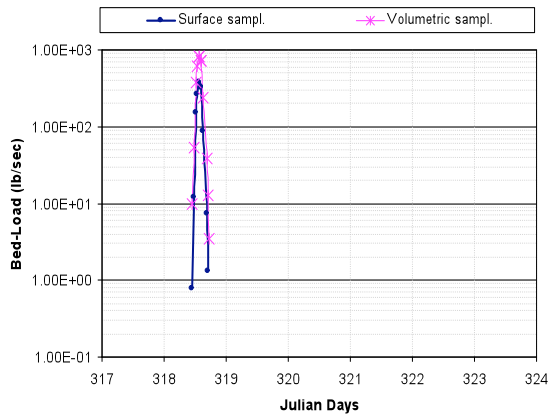
(a) Einstein's method.
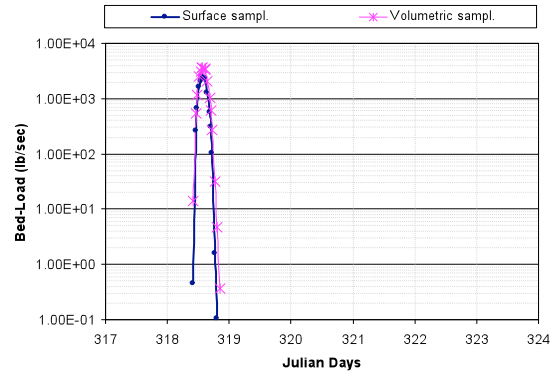
(b) Parker's method.
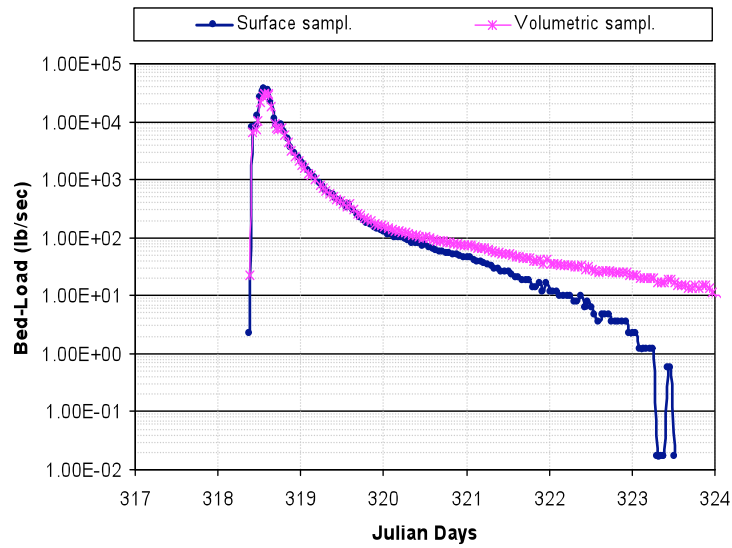
(c) Meyer-Peter and Müller's method.

Figure 3.20: Computed time variation of bedload transport rate for the November, 2000 event.

Table 3.2: Bedload transport rates estimated by University of Houston researchers for event of November, 2000, from Wang and Krou (2008). [*Grid sampling* indicates that particle distribution was developed using the grid-sampling method, *volumetric sampling* indicates that particle distribution was developed using the volumetric method, *Einstein* indicates the Einstein (1950) method for bedload transport, *Parker* indicates the Parker and others (1982) method for bedload transport, *MPM* indicate the Meyer-Peter and Müller method for bedload transport, *bedload* indicate the bedload-transport for the November, 2000 event in the indicated units.]

(a) Particle distribution from grid-sampling method.

Bedload	Einstein	Parker	MPM
ft^3	20668	194388	4388941
m^3	585.7	5508	124377
pounds	$3.41E + 06$	$3.20E + 07$	$7.25E + 08$
kilograms	$1.55E + 06$	$1.50E + 07$	$3.30E + 08$

(b) Particle distribution from volumetric-sampling method.

Bedload	Einstein	Parker	MPM
ft^3	48925	307351	3903349
m^3	1386.4	8709.5	110616
pounds	$8.10E + 06$	$5.10E + 07$	$6.45E + 08$
kilograms	$3.70E + 06$	$2.30E + 07$	$2.93E + 08$

process.

Using the Meyer-Peter and Müller (MPM) bedload transport formula, a November 2000 flood (Figure 3.16), which represents a 18-year event occurrence, generated noticeable bed material transport at three stations only, which are ID 15935, ID 12253, and ID 12230 as shown on Figure 3.21. The evolution of the water-surface profile for the study event is displayed on Figure 3.18a. The time-series of bed elevation for Stations 15935, 12253, and 12230 is displayed on Figure 3.18b. The culverts at the low water crossings of the Johnson Fork, with station ID 13857 (Guzman), 12262, and 9005, are located in the vicinity (Figure 3.18a). Figure 3.18b also shows that the river at those areas went through a cycle of aggradation and degradation during the flood event. Channel erosion and sediment deposit at those culvert sections are small. However, the significant transport capacity of those cross-sections destabilized the area. Aggradation depth as high as 7.24 m were found at Station 10547. This significant deposit if occurred at the low water crossings would cover the culverts, entirely. When maximum degradation depths were found to be infinite according to Equation 2.24, it was limited to 5 m because the elevation data of the bed rock underneath the river bed was not available. The selected maximum degradation depth was reached at Stations 12253 and 12230. The erosion is significant and can cause structural damage to the culvert to the degree that a complete failure (wash-out) might occur.

- The Llano watershed stability was assessed and bed loads in Johnson Fork creek were computed to identify the risk of heavy damages at low water crossings (LWCs) built on the stream.
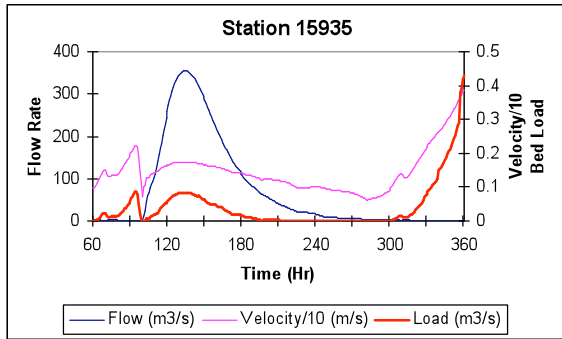
(a) Einstein (1950) and Parker and others (1982) bed-load sedigraphs for Station 15935.
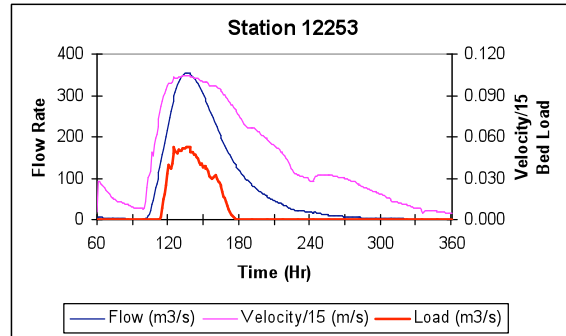
(b) Einstein (1950) and Parker and others (1982) bed-load sedigraphs for Station 12253.
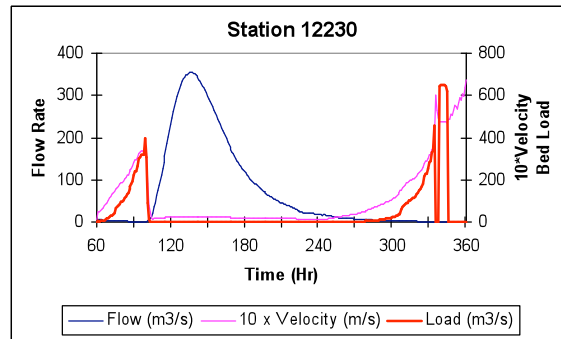
(c) Einstein (1950) and Parker and others (1982) bed-load sedigraphs for Station 12230.

Figure 3.21: Sedigraphs for Johnson Fork Creek Stations 15935, 12253, and 12230 from the Einstein (1950) and Parker and others (1982) methods for bedload transport, from Wang and Krou (2008).

An 18-year flood event, which occurred in November 2000 and was generated by a rainfall volume of 5.43 inches total during 35 hrs, was used for the studies.

- A GIS model and the MUSLE approach were applied to determine areas of the watershed which are significantly unstable. It was found that the LWCs were located in a subbasin with a high potential of sediment transport. A runoff flow hydrograph with an average peak flow rate of 11,489 cfs generated with a hydrologic model (`HEC-HMS`) was used as upstream input in a river analysis simulation (`HEC-RAS`) in order to determine time series (unsteady) hydraulic characteristics of the flow at 31 cross-sections in Johnson Fork. The MPM bed load function applied to the hydraulic characteristics obtained showed that the LWCs were located in the vicinity or in channel sections were erosions could reach 5 m and sediment settling would amount to 7 m causing the potential of structural failure, burial or wash-out of the culverts.

- The river bed size distribution at low water crossings of Johnson Fork Creek was investigated with field data collections using grid sampling and sieve (volumetric) sampling. The results indicate that the grid sampling technique yields finer size sediment than the volumetric method.

However it still presents coarser distributions than the sublayers. It should be noted that the volumetric sampling has less sediment in the upper end of the size distribution because it required that oversized particles be removed from the surface before sampling. Large pebbles with diameter of 50.8-mm and greater are found at the surface and in the subsurface as well. A significant amount of fine sediment is also present in the surface layer. This indicates poor vertical particle size segregation. According to Melis and others (1997), this deposit characteristic reflects the occurrence of a single-peak debris flow with a low recessional flow. The bulk of the debris was produced at a high flowrates. The low recessional flow with high sediment content is responsible for the significant amount of small size particles at the surface. The large stones at the surface provided a shield for the fine sediment, preventing them to be sifted. This analysis is in concordance with the channel flow hydrograph that shows a single peak (up to 83,193 cfs) followed by a long 22-hr recessional flow at an average of 3,038 cfs. Size distribution analysis of the layers of the stream bed appears to be important to inferring the general sediment transport process.

- The performance of the Einstein, Parker, or Meyer-Peter and Müller's approaches for estimating the bedload transport rate was examined. Results from bedload evaluation using Einstein's probabilistic approach, Parker's equal mobility hypothesis, and the Meyer-Peter and Müller energy slope theory differ by several orders of magnitude. For each method, surface (grid method) and subsurface (volumetric technique) sampling seem to yield results of the same order. The peaks of bedload transport rate are observed at the time of maximum river discharge. It is found that only the Meyer-Peter and Müller's approach is able to capture the effect of the long recessional flow with high concentration of finer sediment. Computed extreme bedloads of Johnson Fork Creek at Guzman suggest the importance of bed sampling techniques and selection of appropriate bedload transport models in the prediction of sediment transport rates.

- The particle size distribution from either the grid sampling method or the volumetric (sieve) sampling technique seem to yield similar prediction in bedload transport rate. Use of the simple grid sampling technique is appropriate to provide the estimation of the particle size distribution of the study area.

- Use of a GIS model and the MUSLE approach is demonstrated to be able to provide reasonable estimation of the watershed stability and the sources of sediment amount to the receiving streams. This study also provides a simple procedure by integrating the `HEC-HMS` and `HEC-RAS` models with the bedload transport model for predicting movement of bed loads. However, so far, there is no data available for the calibration of the models. Data collection and monitoring of the flow conditions and bedload movement are considerably important for the bedload transport study.

- The `HEC-RAS` hydraulic model is a one-dimensional model. Different results are found by comparing the `HEC-RAS` predictions with those from two-dimensional (2-D) flow model, especially for the unsteady flow. Adopting the 2-D flow model will enhance the predictions of the hydraulic condition for improved calculation of bedload transport rate.

70

- It is suggested to use the GIS topographical data with high resolution either to the `HEC-RAS` model or a 2-D flow code for the eventual bedload transport study. Otherwise, the flow path and movement of bed loads can not be reliably modeled.

3.7. Synthesis

The purpose of this section of the report is to tie together the results of the participating researchers and their teams. Findings are enumerated in Chapter 4.

When the project began in 2004, it was not clear what the outcome might be. At the end of the initial phase of the project, some direction was illuminated, yet it remained unclear that project goals could be achieved. However, the results from the project were (and are) important to the engineers tasked with designing low-water crossings in the hill country region of Texas. Therefore, the research team and the project management team jointly decided to press on to see what could be learned about the behavior of the bedload transported by hill county streams and how to develop designs to accommodate the heavy load of materials transported by hill country streams on an episodic basis.

The computational work accomplished by Dr. Fang and Dr. Wang demonstrated that computational tools could be used to assess the likelihood of bed-mobility problems at a particular site. In the case of Dr. Fang's approach, the computations are relatively simple, requiring only a spreadsheet program and some basic data. In the case of Dr. Wang's approach, a substantial amount of work using GIS and HEC software to develop the computations is required.

Both approach yield information about the bedload transport at the site. In the case of Dr. Fang's modeling, if the pre-crossing condition transport is greater than the post-crossing transport, then maintenance problems might occur. The crossing can be adjusted and the model reworked to assess the potential differences in crossing geometry on bedload transport.

Dr. Wang's approach is more resource intensive, but might be appropriate for the case of a significant structure, such as a primary highway crossing of a major river. The decision must be made by the designer on which approach to apply.

A conversation between Dr. Thompson and Mr. Paul Degges (then with Tennessee Department of Transportation) indicated that the TnDOT approach is to bridge problem streams. While construction of bridges might be appropriate for some Texas applications, the number of stream crossings is so numerous that bridge construction is not fiscally possible. However, use of a bridge might be appropriate for some settings.

During the term of the project, Mr. George "Rudy" Herrmann, a member of the project advisory team, sat Dr. Rosgen's stream geomporphology class[6]. A significant observation of Mr. Herrmann is that construction of the highway approaches effectively alters the stream width-depth ratio, affecting the stream power at the crossing. This simple observation is appropriate and might

---

[6]Dr. Rosgen's courses and published materials are presented at `http://www.wildlandhydrology.com/`.

explain, at least in part, why deposition often occurs on TxDOT low-water crossings.

Dr. Cleveland's physical modeling was an important component of this project. The burden of physical modeling shifted late in the project schedule because the Texas Tech facility did not come on-line as expected. Therefore, Dr. Cleveland and his crew took on responsibility for physical modeling.

The initial purpose of the physical models was to attempt to evaluate design elements to determine how to maintain a stable bed, whereas later in the physical modeling the need to accommodate solids transport became apparent. Although numerous transport theories are in the literature (enumerated in Section 2.7.5), the physical models were interpreted on a relatively simple theory because

1. The tools to measure bed shear were not available to the researchers,

2. The tools that were used were selected to have field portable equivalents, and

3. The researchers thought that "interesting" behavior would occur at Froude numbers near unity and if designs could force the critical Froude number away from the crossing there would be benefit.

The physical models did not behave entirely as expected, but some of the following observations (based on laboratory notebook comments and some supporting video) were discovered.

1. The simple mobility theory has some value in predicting bed mobilization — of some note is that the simple theory relates many of the same variables as the complex theories, providing some reassurance to the research team.

2. All culverts can self-clear if the downstream side of the crossing is "sediment-hungry," as evidenced by the clearing occurring when the downstream head cut propagates upstream to the crossing. In a real system, once clogged, this head-cut could take a long time to propagate and the crossing itself will function as a solids trap.

3. Multiple-barrel culverts seem to function better when partially-clogged than a single barrel culvert and the solids clogging pattern is different. The researchers speculate that multiple barrels introduce flow instabilities that generate eddies on the downstream side of the crossing that function is some sense as localized "sediment-hungry" portions of the bed and can draw from the culvert solids to satisfy this "hunger."

4. The porous abutment model maintains a stable bed at higher nominal discharge because it passes considerably more flow through its porous structure. It also clogs and clears — the researchers never tested a multiple barrel porous structure but would suggest it to future researchers for consideration.

5. Beds can be stable beyond what the researchers anticipate but once motion begins it is relatively easy to maintain. Both saltation and bulk motion were created in the laboratory. The

computed froude number at which motion occurs is smaller than the researchers anticipated on the order $\approx$ 0.5–0.75 being sufficient — the researchers anticipated that mobilization would occur closer to unity.

Late in the project's time frame, Mr. Herrmann developed a three-barrel design for a low-water crossing in the affected region. His analysis is presented in Appendix D. Because of the timing of this work, no physical model of the proposed design was constructed. However, in light of Mr. Herrmann's report, such a test should be conducted in the laboratory to assess the utility of Mr. Herrmann's proposed design approach.

3.8. Design Approach

The drainage systems subject to this type of mobilization are quasi-static for long durations, then incredibly dynamic for short periods of time. The design philosophy must accept that the river system will be mobile with respect to the clear water path as well as the solids transport path. The crossing must appear to the river as transparent as practical so that the natural progression of solids transport can occur. A design approach to accommodate the solids transport in regions of high bed mobility on transportation infrastructure where traffic volume cannot justify use of a bridge[7] is suggested as follows:

Geomorphic interpretation suggests that solids move relatively frequently (3-5 year return frequency). Therefore, a design philosophy should reflect that finding and a crossing should accommodate solids moving with flows expected at these return frequencies.

For new or replacement crossings, multiple-barrel culverts are favorable, and these barrels should to be aligned with the flow direction, but perfect alignment is not necessary, based on results from physical modeling. The barrels should span as much of the anticipated floodway as practical — the porous model conveys considerable discharge before flow is forced into the conventional culvert portion, by extrapolation the researchers expect that similar function could be achieved by multiple barrels that span the floodway.

Where such a span cannot be achieved, the culvert should try to accelerate water into a Froude number range exceeding 0.5 upstream and downstream from the crossing so that solids motion can be maintained through the culvert.

Bed materials might move as a dune and there will be periods of time when the gravel bed is at a greater elevation than when the crossing was constructed; at other times the bed will be at lower elevation — the engineer should accept this situation as a natural progression and not "fight" the river.

When crossings are overtopped and materials are deposited on the roadbed, these materials should be pushed to the **downstream side of the crossing**. Furthermore, when the downstream side

---

[7]The authors here assume that bridging is the most transparent approach to accommodate clear water and solids transport.

of a crossing appears to be undercut (an erosion pit in the physical model) this situation is an indication of an approaching solids "dune" or an upstream propagating head cut. If fill material is indicated to repair these "pits," fill should be extracted from the upstream side of the crossing, based on results from the physical modeling[8].

---

[8]A field visit should be made to assess if a dune is approaching. Some field surveying might be needed to locate such dunes. If there is evidence of an approaching dune, the fill material should come from the dune.

4. Summary and Conclusions

The purpose of this section of the report is to present summary material and findings. In addition, suggestions for additional work are listed because the process of research often uncovers additional questions that cannot be addressed within the given time and budgetary limits.

4.1. Summary

The objectives of Research Project 0–4695 are to answer the questions:

1. Why are some low-water stream crossings subject to significant bed-mobility events?

2. What engineering solutions are appropriate for stream crossings subject to significant bed-mobility events?

To address these questions, five tasks were undertaken:

1. To conduct a literature review;

2. To review TxDOT MMIS records and quantify maintenance costs associated with bed-mobility events;

3. To conduct field studies at three locations on Johnson Fork Creek;

4. To execute physical modeling using material recovered from field studies; and

5. To develop and execute a research program to address design and analysis issues.

After the initial research phase, a literature review (Heitmuller and others, 2005) and an interim report (Thompson, 2004) were written and delivered to TxDOT for review. The research team was directed to proceed with numerical and physical modeling to address project objectives. Details of the analysis and results are presented in Chapters 2 and 3. A broad synthesis of project progress and results is presented in Section 3.7.

It is not clear why some sites in the affected area are subject to bed-mobility issues and others are not. However, the following results are indicative:

1. From a geomorphologic perspective, the materials comprising the bedrock of the affected region, combined with watershed and channel slopes, are such that the materials can and will mobilize during episodic hydrologic events;

2. The event frequency required to mobilize bed materials is not rare, perhaps as frequent as a five-year event;

3. Bed materials mobilize when channel Froude number is approximately 0.5. This observation was counterintuitive to the project research team;

4. Physical modeling of schematic low-water crossings produces behaviors similar to those observed in the field;

5. Based on the physical modeling, the relative location of a downstream propagating "dune" of solids, the crossing, and an upstream propagating head cut impacts the behavior of mobile materials in the vicinity of a crossing. When conditions are favorable, clogged crossings can self clear; however, these conditions are always transient; and

6. Changes to the stream width-depth ratio by reducing the bank slope for the highway approaches might contribute to a reduction in stream power and exacerbate the deposition of bed-transport materials on the low-water crossing.

4.2. Conclusions

The major conclusions from Research Project 0–4695 are listed below.

1. Over a four-year period (1998–2002), maintenance costs attributable to bed-mobility problems in a four-county area of Texas was $672K. That is an average of $42K/county/year;

2. If the geographic extent of bed-mobility issues is 11 Texas counties, then the expected annual maintenance cost is $462K. If the affected area is 17 Texas counties, then the expected annual maintenance cost is $714K. These estimates should be considered lower bounds because of the difficulty in precisely determining maintenance costs associated with bed-mobility issues;

3. The TxDOT MMIS database is not adequate for tracking bed-mobility related maintenance costs.

4. A geomorphologic study (Heitmuller and Asquith, 2008) of the Llano River basin resulted in assessment of the sources and distributions of bed sediments in the affected region. A conclusion of that study is that bed sediments mobilize when the Froude number is about 0.5;

5. A screening model based on the Parker bedload transport method was developed. Although not a specific deliverable of the project, the tool demonstrates that simple tools can be used to screen sites and rough designs for changes in bedload transport;

6. Detailed numerical modeling using GIS to apply MUSLE and HEC-HMS and HEC-RAS to model the hydrology and hydraulics is feasible, if costly. Application of bedload transport equations (Einstein, Parker, and Meyer-Peters-Müller) depends on the modeling results. Application of these tools can be used to predict base level changes at points on interest;

7. Physical modeling was used to demonstrate that bed sediments mobilize when the Froude number is about 0.5, corroborating the results of Heitmuller and Asquith (2008). The physical model was used to test a few potential design approaches. If a porous foundation design can be engineered, the results of physical modeling are such that it is anticipated that bed sediments will mobilize differently than with hard approaches, potentially alleviating the problem;

8. Physical modeling also, to some extent, demonstrated that multiple barrel culverts have a potential to self-clear if the barrels are in-line with the stream flow direction. The researchers think that the barrels need to be large relative to the mean solids dimension that must pass through the system;

9. The design approach suggested by Herrmann (presented in Appendix D) is another potential solution to the problem; and

10. Both the screening model and detailed numerical model provide tools to estimate the mass of materials transported over a relatively long time frame. The estimated masses are not trivial. Based on geomorphologic investigation, the same long-term behavior is evident — non-trivial mass transport. Based on the physical modeling (using intentionally accelerated time frames), the mass moved is far larger than the research team initially anticipated. In addition, some mass always moves and consequently the amount of solids moving in a real system is probably far greater than engineers currently recognize and crossing designs should accommodate not only the clear water component, but a solids fraction component comprised of relatively large solids (too large to be carried in suspension).

4.3. Further Work

As with most research projects, the researchers involved in Research Project 0–4695 discovered questions of interest during the execution of the project. Most of the following could not be investigated during the course of this project, but may be of interest to TxDOT and other researchers for future work.

1. The physical model is probably the best approach for investigating further design solutions to bedload transport problems with TxDOT low-water crossings;

2. If an engineered porous foundation can be developed for the low-water crossing approaches to the culvert(s), then this potential solution should be further investigated using a physical model.

3. The three-barrel, offset culvert solution proposed by Herrmann (Appendix D) should be tested in a physical model;

4. The impact of cutting back the abutments at the stream bank on bedload transport should be investigated using a physical model;

5. A well calibrated computational fluid dynamics (CFD) model, that can replicate physical model results, should be used for (subsequent to the physical models) detailed parametric studies; and

6. Unattended field monitoring is crucial — TxDOT should consider monitoring several sites over a long period with occasional field visits to validate the findings suggested by the numerical modeling and physical modeling. One well documented actual crossing studied over a long period (decade) would provide substantial data for validation of the methods used in this research project. This monitoring should be a cooperative effort using a handful of trained TxDOT engineers, USGS personnel, and University personnel. Ideally the TxDOT cooperators would visit the locations frequently as part of their field activities, with scheduled visits for data recovery by USGS and University participants (alternate visits), and post-event visits for data recovery and re-instrumentation using personnel from all three participants.

The instrumentation of value would be a set of autonomous water-lever transducers in steel pipes carefully secured for post-event recovery and to defeat vandals. The instrumentation should also include an autonomous video image system in both the visible and infrared range, carefully secured to protect against vandals and oriented to capture the necessary data without compromising public privacy. The existing three-barrel staggered culvert system should be the first of these crossings so instrumented. The long-term expenses of such a monitoring activity could be controlled by the cooperative structure suggested.

Bibliography

(2006, August). National hydrographic database.

Ackerman, C. T. (2005). HEC-GeoRAS: An extension for support of HEC-RAS using ArcGIS. User's manual CPD–83, U.S. Army Corps of Engineers, Davis, California.

Asquith, W. H. (2001). Effects of regulation on L-moments of annual peak streamflow in Texas. Water-Resources Investigations Report 01–4243, U.S. Geological Survey, Austin, Texas.

Asquith, W. H. and R. M. Slade (1997). Regional equations for estimation of peak-streamflow frequency for natural basins in Texas. Water-Resources Investigation Report 96–4307, U.S. Geological Survey, Austin, Texas. (In PDF).

Bedient, P. and W. Huber (2002). *Hydrology and floodplain analysis.* Upper Saddle River, NJ 07458: Prentice Hall.

Brunner, G. W. (2008). HEC-RAS river analysis system — version 4.0. User's manual CPD–68, Hydrologic Engineering Center, Davis, California.

Bunte, K. (1992). *Dynamics of gravel-bed rivers*, Chapter Particle number grain-size composition of bedload in a mountain stream, pp. 55–72. New York: Wiley.

Casagli, N., L. Ermini, and G. Rosati (2003). Determining grain size distribution of the material composing landslide dams in the Northern Apennines: Sampling and processing methods. *Engineering geology 69*, 83–97.

Chow, V. T., D. R. Maidment, and L. W. Mays (1988). *Applied hydrology.* McGraw-Hill.

Church, M., D. McLean, and J. Wolcott (1987). *River bed gravels: Sampling and analysis.* John Wiley & Sons.

Duan, J., L. Chen, and S. Scott (2006). Appication of surface-based bed load transport equation to a desert gravel-bed stream. *Journal of hydraulic research 44*(5), 624–630.

Einstein, H. (1950). The bed-load function for sediment transportation in open channel flows. Technical Bulletin No. 1026, U.S. Department of Agriculture.

Fang, X., J. Qui, G. Shrestha, T. G. Cleveland, D. B. Thompson, and K. Wang (2006). Analysis of gravel transport over low-water stream crossings. In *Proceedings of the Texas Section American Society of Civil Engineers, spring conference, April 19–21, Beaumont, Texas*, pp. Digital publication.

Green, J. (2003). The precision of sampling grain size percentiles using the Wolman method. *Earth surface processes and landforms 28*, 979–991.

Heitmuller, F. T. and W. H. Asquith (2008). Potential for bed-material entrainment in selected streams of the Edwards Plateau — Edwards, Kimble, and Real Counties, Texas, and vicinity. Scientific Investigations Report 2008–5017, U.S. Geological Survey, Austin, Texas 78754.

Heitmuller, F. T., W. H. Asquith, X. Fang, D. B. Thompson, and K.-H. Wang (2005). Literature review for Texas Department of Transportation research project 0–4695: Guidance for design in areas of extreme bed-load mobility, edwards plateau, texas. Open-File Report 2005–1234, U.S. Geological Survey, Austin, Texas.

Herrmann, G. R. (2008a). Report of observations and recommendations: RM 335 and un-named stream. Technical report, Texas Department of Transportation, San Angelo, Texas.

Herrmann, G. R. (2008b). Supplemental report: Subsequent actions, observations, and conditions RM 335 and un-named stream. Technical report, Texas Department of Transportation, San Angelo, Texas.

Kerenyi, K., J. S. Jones, and S. Stein (2003). Bottomless culvert scour study: Phast I laboratory report. Technical Report FHWA–RD–02–078, Federal Highway Administration, McLean, Virginia 22151.

Kondolf, G. (1997). Application of the pebble count: Notes on purpose, method, and variants. *Journal of the American water resources association 33*(1), 79–87.

Melis, T., R. Webb, and P. Griffiths (1997). Debris flows in Grand Canyon national park: Peak discharges, flow transformations, and hydrographs. In *Proceedings of the 1997 1st international conference on debris-flow hazards mitigation: Mechanics, prediction, and assessment*, pp. 727–736.

Parker, G. (1990). Surface-based bedload transport relation for gravel rivers. *Journal of hydraulic research 28*(4), 417–436.

Parker, G. (2008). *Manual of Practice 110: Transport of gravel and sediment mixtures*. 1801 Alexander Bell Drive, Reston, Virginia 20191: American Society of Civil Engineers.

Parker, G., S. Dhamotharan, and H. Stefan (1982). Model experiment on mobile paved gravel bed stream. *Water Resources Research 18*(5), 1395–1407.

Parker, G., P. C. Klingeman, and D. G. McLean (1982). Bedload and size distribution in paved gravel-bed streams. *Journal of the Hydraulics Division 108*(HY4), 544–570.

Qui, J. (2008). *Gravel transport estimation and flow simulation of low-water stream crossings*. Ph. D. thesis, Lamar University, Beaumont, Texas.

Shrestha, G. (2005). Gravel transport over low-water crossings in Johnson Fork River. Master's thesis, Lamar University, Beaumont, Texas.

Simons, D. and F. Sentürk (1992). *Sediment transport technology.* Fort Collins, Colorado: Colorado State University.

Thompson, D. B. (2004). Bed load mobility: interim report. Technical Report 0–4695–2, Center for Multidisciplinary Research in Transportation, Lubbock, Texas 79409.

U.S. Army Corps of Engineers (2002). HEC-RAS river analysis system – version 3.1. User's manual CPD–68, Hydrologic Engineering Center, Davis, California.

U.S. Army Corps of Engineers (2008). Hydrologic modeling system HEC-HMS — version 3.2.0. User's manual CPD–74A, Hydrologic Engineering Center, Davis, California.

U.S. Interagency Advisory Committee on Water Data (1982). Guidelines for determining flood flow frequency. Bulletin 17-B of the Hydrology Subcommittee, U.S. Geological Survey, Office of Water Data Coordination, Reston, Virginia.

Wang, K. and J. Krou (2008). Numerical modeling for TxDOT bed-mobility project. Project report, University of Houston, Houston, Texas.

Wischmeier, W. and D. Smith (1978). Predicting rainfall erosion losses: a guide to conservation planning. Agriculture Handbook 537, Science and Education Administration, U.S. Department of Agriculture, Washington, D.C.

Yang, C. (2003). *Sediment transport: theory and practice.* Malabar, Florida: Krieger publishing company.

A. Lamar University SurGTAM

The purpose of this section is to present an example of the input and output from the SurGTAM spreadsheet.
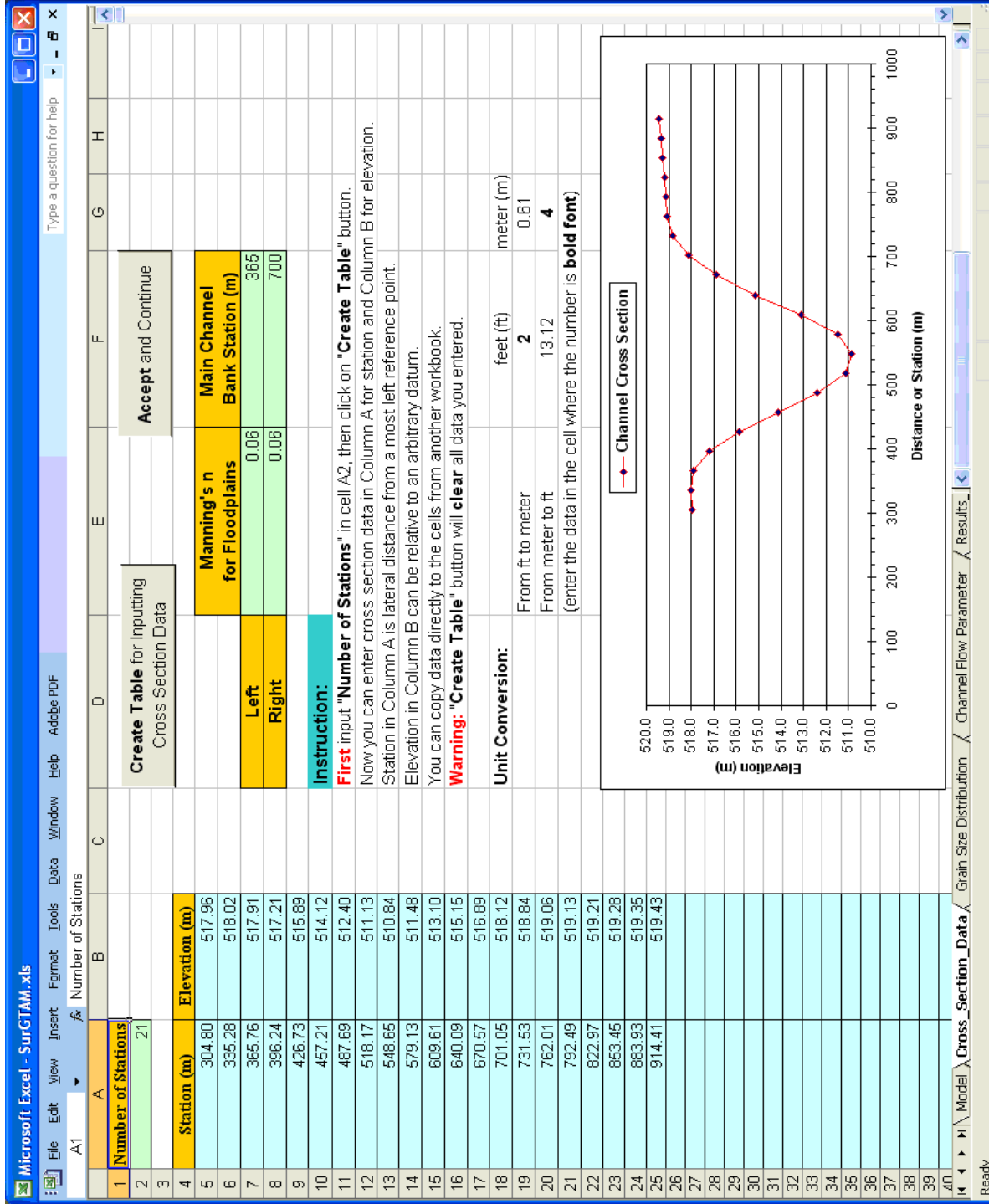
Figure A.1: Excel worksheet for the input of cross-section geometry data in SurGTAM.

Microsoft Excel - SurGTAM.xls

File | Edit | View | Insert | Format | Tools | Data | Window | Help | Adobe PDF

Type a question for help

A1   fx   Number of Size Groups

	A	B	C	D	E	F	G	H	I
1	**Number of Size Groups**			**Create Table** for		**Accept** and Continue			
2	**5**			Inputting Data					
3									
4	**Grain Sepcific Gravity**	2.65		**Instruction:**					
5				**First** input "**Number of Size Groups**" in cell A2, then click on "**Create Table**" button.					
6	**Grain Size (mm)**	**% Finer**		Click "**Accept**" button to continue upon finishing the input data.					
7	3.2	1.0		**Warning:** "**Create Table**" button will **clear** all data you entered.					
8	9.5	5.8							
9	19.1	28.2		**Information on Surface Grain Size Distribution**					
10	38.1	59.2		Based on Parker's surface-based equation, you need to provided surface layer grain size distribution					
11	76.2	100.0		in order to carry on the calculation. It is suggested that grain sizes be provided in a half-phi interval					
12				to a one-phi interval. Grain sizes in a one-phi interval are 2, 4, 8, 16, 64, and 128 mm.					
13				The percent finers associated to the finest and coarsest grain sizes must be 0 and 100, respectively.					
14									
15									
16				**Unit Conversion:**		Size (inches)	Size (mm)	φ scale	
17						From in to mm	**2**	50.80	-5.7
18						From mm to in	0.16	**4**	-2.0
19						(enter the data in the cell where the number is **bold font**)			
20									

Grain Size Distribution For Surface Layer

Percentage Finer (%) — 100.0, 80.0, 60.0, 40.0, 20.0, 0.0

Grain Size (mm) — 1.0, 10.0

Model / Cross_Section_Data / **Grain Size Distribution** / Channel Flow Parameter / Resu...

Ready

Figure A.2: Excel worksheet for the input of grain-size (particle-size) distribution data in SurGTAM.
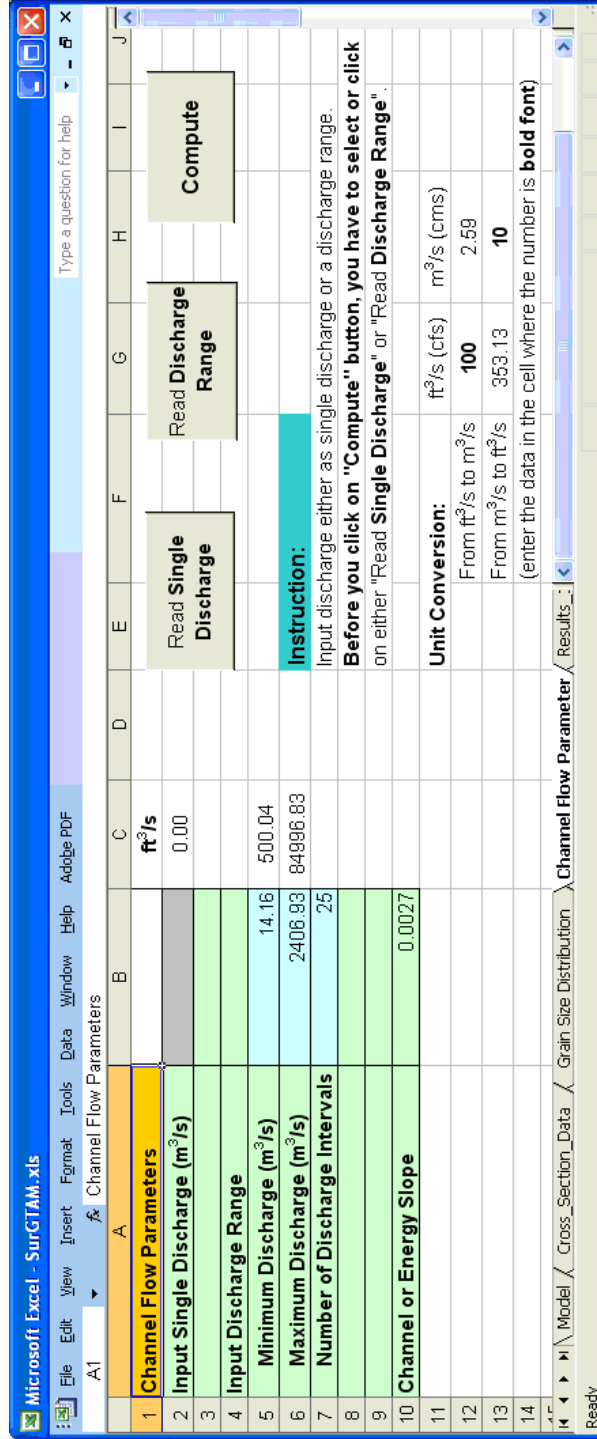
Figure A.3: Excel worksheet for the input of channel-flow data in SurGTAM.

B. University of Houston — Physical Model and Supporting Data

This appendix contains a report on the quantification of the solids density, the solids sizes used in the physical model studies and the experimental results for crossing model studies conducted in the large wooden flume.

Material Density for Samples from Ben WIlliams Crossing

The researchers developed the mobilization theory assuming that solids density was 2.65 a typical value in the literature for geologic materials. Well into the experiments, the researchers became aware that there may be a need to quantify the solids density.

Twelve (12) stones collected from the bed material at the Ben Williams low-water crossing in Real County, Texas were collected in 2005 during a field reconnoissance visit that year. The bed material was analyzed for sizing characteristics, but not for solids density or specific weight. Fortunately, the material was kept at the University for use in physical models and thus was available for a rapid analysis.

The bed material was stored in the University of Houston hydraulics laboratory, and the author simply grabbed stones that looked like they would fit into a displacement vessel (300 mL glass beaker with a reference mark). Each stone was weighed using a Mettler analytical mechanical balance. The balance was not calibrated because NIST weights were not available, however the balance correctly weighed a 25 mL volumetric bottle (an accurate volume), after establishing mechanical zero.

These weights are recorded to the precision on the instrument (+/- 0.0001 grams). The solids volumes were determined by displacement of water in a displacement vessel. The vessel is a 300mL laboratory beaker. The beaker reference mark for 200 mL corresponds to an actual volume (determined by volumetric bottles and a titration burette) of 188.2 mL. This reference volume is used to compute the solids volumes. The stone is added to the displacement beaker, water is added by titration burette until water covers the stone and the water level reaches the reference mark on the beaker. The volume added is recorded and the solids volume, Equation B.1 is the difference between the reference volume and the added volume.

$$V_\text{solids} = V_\text{reference} - V_\text{water added} \tag{B.1}$$

The solids density, Equation B.2, is the ratio of stone mass to solids volume. The specific gravity, Equation B.3, is the ratio of the solids density and water density. The laboratory is unheated and the author estimates the temperature was about 15°C, so a tabulated value for water density, $\rho_w = 0.9991 g/mL$, at 15°C was used (Mays, 2001).

$$\rho_\text{solids} = \frac{m_\text{solids}}{V_\text{solids}} \tag{B.2}$$

$$SG_\text{solids} = \frac{\rho_\text{solids}}{\rho_w} \tag{B.3}$$

Two stones were too large for the original displacement vessel, so a larger beaker (500mL) was used. A known water volume (300mL) was added and a reference mark was scored onto the beaker by the author. This vessel was used in an identical fashion for the two larger stones.

The experimental results are listed on Table B.1. The classification of the stone types is based on the appearance of the stones. The "flint" classification are stones that have sharp knife-like edges where weathering has broken the edge of the stone. The stones classified as "limestone" are more rounded and have a vuggy appearance.[1]

Table B.1: Laboratory Analysis of Bed Material.

Sample	mass (g)	V_a (mL)	V_r (mL)	V_s (mL)	ρ_s	SG_s	Class.
1	65.1514	155.8	188.2	32.4	2.011	2.013	Limestone
2	21.0866	178.8	188.2	9.4	2.243	2.245	Limestone
3	43.0177	172.5	188.2	15.7	2.740	2.742	Flint
4	26.1528	175.9	188.2	12.3	2.126	2.128	Limestone
5	50.1372	171.0	188.2	17.2	2.915	2.918	Flint
6	15.1415	184.0	188.2	4.2	3.605	3.608	Flint
7	19.0030	177.0	188.2	11.2	1.697	1.698	Limestone
8	32.0481	173.6	188.2	14.6	2.195	2.197	Limestone
9	19.1181	177.8	188.2	10.4	1.838	1.840	Limestone
10	31.1457	176.6	188.2	11.6	2.685	2.687	Flint
11	152.2	250.0	300.0	50.0	3.044	3.047	Flint
12	172.1	227.2	300.0	72.8	2.364	2.366	Limestone

The results listed in Table B.1 were enter and analyzed in the R statistics package (R Development Core Team (2005)).

---

[1]Small holes and bubbles are visible at the surface of these stones, like a sponge or closed-cell foam.

Figure B.1 is a boxplot of the results, both composite and classified by analyst determined rock-type. The boxplot suggests that the mean values of the two rock classifications are different. Subsequent analysis supports this hypothesis, and the difference is significant.
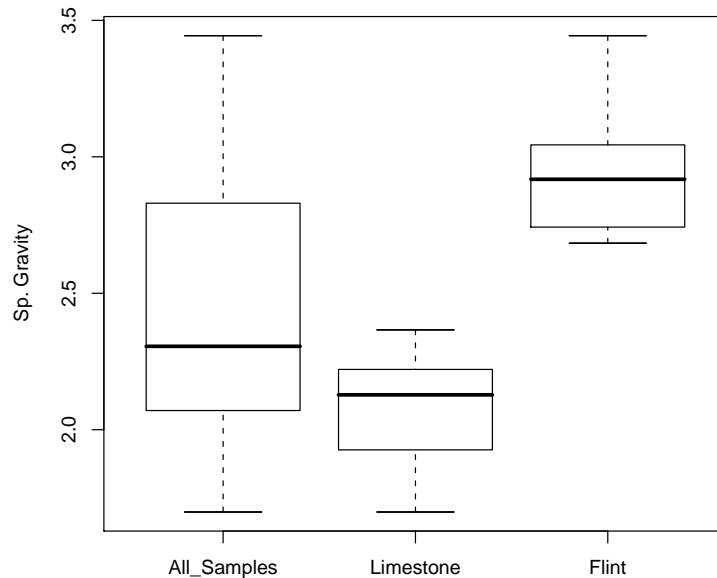
Figure B.1: Boxplot of Specific Gravity Measurements from Ben Williams Crossing

The results suggest that the composite mean or median value of specific gravity for the bed materials in the region is lower than the value typically used for generic geologic materials.[2] The results further suggest that a fraction of the bed material present is quite a bit lower than the typical value, in this case about 20% for the limestone component. The "flint" component is about 10% larger than the typical value. Unknown from this analysis is the relative proportion of the two components, and this relative proportion is important to determine the characteristic value for use in the region[3].

The rapid analysis suggests that the bed materials in the vicinity of the Ben Williams crossing have a specific gravity that on average (actually the median) are lower than the typical engineering value used for geologic materials. This lower specific gravity would support a hypothesis that the bed materials in the region are more mobile than expected (lower forces are needed to mobilize the bed).

The two different rock types as determined by the author suggest a further consideration. If there

---

[2]Typical value assumed in this report is ($\rho_s = 2.65$)

[3]It is quite possible that the proportion of the low and high SG materials is such that the typical value is appropriate.

is indeed a bimodal specific gravity distribution in the region, then one would anticipate that the lighter materials would be more mobile, and the denser materials left behind. Whether this hypothesis is feasible to test at this point of the research is unknown.

Until further density (specific gravity) measurements are performed, preferably using a more precise approach to the displacement technique, a working estimate of specific gravity is $SG_s = 2.3$ for a composite sample[4]. If the sample is largely limestone (not dense flint), then the working value is even smaller.

Solids Size Tabulations Used in Crossing Model Experiments

Two different size of rocks were used in the bed mobility lab experiments; small and large sizes. The materials were classified using large wooden sieves and manual shaking to pass materials through the sieves. These were the same sieves used in the field trips to classify bed materials.

Tables B.2 and B.3 are the actual sizes measured. The reader is advised that the count is different for the larger and smaller sizes.

Table B.2: Dimensions of bed material used in experiments — Small Stones.

[COUNT is the identification number of the sample; LENGTH is the longest dimension identified by the analyst; WIDTH is a dimension perpendicular to lenght, HEIGHT is the dimension perpendicular to both length and width; ROW_MEAN is the arithmetic mean along the row. This value is used as the nominal dimension for analysis of experimental results.

COUNT	LENGTH	WIDTH	HEIGHT	ROW_MEAN
1	0.8	0.4	0.4	0.53
2	0.4	0.5	0.25	0.38
3	0.5	0.35	0.35	0.4
4	0.5	0.35	0.3	0.38
5	0.45	0.4	0.15	0.33
6	0.9	0.55	0.5	0.65
7	0.9	0.65	0.5	0.68
8	0.6	0.5	0.4	0.5
9	0.8	0.6	0.4	0.6
10	0.85	0.5	0.45	0.6
11	0.9	0.5	0.4	0.6
12	0.8	0.65	0.4	0.61
13	1	0.5	0.4	0.63
14	0.8	0.5	0.35	0.55
15	0.8	0.65	0.3	0.58
16	0.6	0.5	0.3	0.46
17	0.5	0.6	0.15	0.41

Continued on next page

---

[4]Reasonable care was exercised in this rapid assessment, but a better way to measure displacement is to fabricate the vessel with a narrow riser tube to improve the repeatability of the displacement measurement. Because the solid volume is in the denominator, the estimates are expected to be particularly sensitive to the volume measurement for small sized rocks.

Table B.2: Dimensions of bed material used in experiments — Small Stones — Continued

COUNT	LENGTH	WIDTH	HEIGHT	ROW_MEAN
18	1.1	0.6	0.2	0.63
19	0.8	0.65	0.25	0.56
20	0.5	0.3	0.05	0.28
21	0.5	0.35	0.2	0.35
22	0.4	0.3	0.15	0.28
23	0.7	0.65	0.25	0.53
24	0.7	0.6	0.2	0.5
25	0.65	0.5	0.25	0.46
26	0.9	0.5	0.3	0.56
27	0.9	0.4	0.4	0.56
28	0.8	0.85	0.1	0.58
29	0.85	0.65	0.15	0.55
30	0.7	0.6	0.35	0.55
31	0.8	0.6	0.2	0.53
32	0.7	0.6	0.2	0.5
33	0.75	0.4	0.25	0.46
34	0.7	0.5	0.3	0.5
35	0.6	0.5	0.25	0.45
36	0.7	0.4	0.2	0.43
37	0.75	0.5	0.25	0.5
38	0.7	0.4	0.15	0.41
39	0.6	0.4	0.3	0.43
40	0.6	0.5	0.3	0.46
41	0.6	0.5	0.3	0.46
42	0.6	0.4	0.3	0.43
43	0.7	0.4	0.3	0.46
44	0.6	0.5	0.05	0.38
45	0.4	0.3	0.2	0.3
46	0.8	0.5	0.35	0.55
47	0.5	0.3	0.2	0.33
48	0.7	0.5	0.25	0.48
49	0.5	0.5	0.1	0.36
50	0.5	0.4	0.2	0.36
51	0.7	0.5	0.2	0.46
52	0.4	0.3	0.1	0.26
53	0.6	0.4	0.25	0.41
54	0.5	0.4	0.02	0.30
55	0.5	0.4	0.15	0.35
56	0.5	0.3	0.15	0.31
57	0.6	0.5	0.2	0.43
58	0.4	0.5	0.15	0.35
59	0.7	0.5	0.5	0.56
60	0.5	0.4	0.1	0.33
61	0.6	0.3	0.2	0.36
62	0.45	0.4	0.3	0.38
63	0.5	0.4	0.25	0.38
64	0.35	0.25	0.25	0.28
65	0.5	0.5	0.15	0.38
66	0.5	0.5	0.1	0.36
67	0.8	0.6	0.2	0.53

Continued on next page

Table B.2: Dimensions of bed material used in experiments — Small Stones — Continued

COUNT	LENGTH	WIDTH	HEIGHT	ROW_MEAN
68	0.7	0.3	0.25	0.41
69	0.6	0.5	0.3	0.46
70	0.6	0.3	0.2	0.36
71	0.7	0.5	0.2	0.46
72	0.6	0.4	0.1	0.36
73	0.6	0.5	0.2	0.43
74	0.6	0.4	0.2	0.4
75	0.5	0.5	0.2	0.4
76	0.5	0.3	0.3	0.36
77	0.45	0.4	0.02	0.29
78	0.6	0.5	0.1	0.4
79	0.6	0.4	0.1	0.36
80	0.5	0.4	0.1	0.33
81	0.6	0.5	0.1	0.4
82	0.5	0.5	0.2	0.4
83	0.6	0.4	0.2	0.4
84	0.7	0.35	0.25	0.43
85	0.6	0.3	0.2	0.36
86	0.5	0.5	0.35	0.45
87	0.6	0.4	0.2	0.4
88	0.55	0.3	0.1	0.31
89	0.5	0.4	0.2	0.36
90	0.7	0.4	0.25	0.45
91	0.5	0.4	0.1	0.33
92	0.5	0.45	0.05	0.33
93	0.6	0.6	0.08	0.42
94	0.5	0.3	0.2	0.33
95	0.5	0.3	0.25	0.35
96	0.5	0.5	0.15	0.38
97	0.5	0.3	0.1	0.3
98	0.4	0.4	0.025	0.27
99	0.5	0.4	0.2	0.36
100	0.5	0.3	0.15	0.31
Mean:	0.62	0.45	0.22	0.43

Table B.3: Dimensions of bed material used in experiments — Large Stones.

[COUNT is the identification number of the sample; LENGTH is the longest dimension identified by the analyst; WIDTH is a dimension perpendicular to lenght, HEIGHT is the dimension perpendicular to both length and width; ROW_MEAN is the arithmetic mean along the row. This value is used as the nomonal dimension for analysis of experimental results..

COUNT	LENGTH	WIDTH	HEIGHT	ROW_MEAN
1	2	2	0.9	1.63
2	2	1.9	0.9	1.6
3	1	1.2	1	1.06
4	1.9	0.8	0.6	1.1

Continued on next page

Table B.3: Dimensions of bed material used in experiments — Large Stones. — Continued

COUNT	LENGTH	WIDTH	HEIGHT	ROW_MEAN
5	2	1	0.8	1.26
6	2	1.6	0.6	1.4
7	1.7	1.3	0.9	1.3
8	1.5	0.7	0.7	0.96
9	1.3	1.4	0.8	1.16
10	1.8	1	0.9	1.23
11	1.8	1.1	0.6	1.16
12	1	0.9	0.6	0.83
13	1.25	1	0.9	1.05
14	1.3	0.8	0.2	0.76
15	1.2	0.9	0.3	0.8
16	1.2	0.8	0.7	0.9
17	1.3	0.8	0.2	0.76
18	1.6	1.4	0.2	1.06
19	1.3	1.3	0.5	1.03
20	1.7	1.2	0.8	1.23
21	1.2	0.9	0.8	0.96
22	1.6	0.8	0.6	1
23	1.5	0.8	0.7	1
24	2.3	1.4	0.7	1.46
25	1	0.7	0.9	0.86
26	2.1	1.3	0.2	1.2
27	1	0.7	0.8	0.83
28	1.8	0.8	0.9	1.16
29	1.7	1.2	0.7	1.2
30	1.3	0.9	0.7	0.96
Mean	1.3	0.9	0.7	0.96

Wood Flume Experimental Results Summary (3 Tables)

Table B.4: Solids Mobilization Experimental Data — Large Flume Study — Part 1.

[EXP is experiment number; MODEL is the crossing model description; THR is binary variable indicating whether discharge is accelerated into the model; PUM is number of pumps operating; VAL is number of vales open; DEP is depth in head tank; Q is a computed discharge (in $\frac{ft^3}{sec}$ from PUM, VAL, DEP combinations as determined from time-to-drain curves The precision reflected in the table is a result of arithmetic and exceeds measurement precision; DATA TYPE is an indicator of whether data is from a tracer test or a computed mean values.

EXP	MODEL	THRT	PUM	VAL	DEP	Q	DATA TYPE
1	Single, Rectangular,Small	YES	2	1	3.16	.296	TRACER
1	Single, Rectangular,Small	YES	2	1	3.16	.296	TRACER
1	Single, Rectangular,Small	YES	2	1	3.16	.296	TRACER
1	Single, Rectangular,Small	YES	2	1	3.16	.296	TRACER
1	Single, Rectangular,Small	YES	2	1	3.16	.296	TRACER

Continued on next page

92

Table B.4: Solids Mobilization Experimental Data — Large Flume Study — Part 1. — Continued

EXP	MODEL	THRT	PUM	VAL	DEP	Q	DATA TYPE
1	Single, Rectangular,Small	YES	2	1	3.16	.296	TRACER
1	Single, Rectangular,Small	YES	2	1	3.16	.296	COMPUTED_MEANS
2	Single, Rectangular,Small	YES	2	1	3.22	.298	TRACER
2	Single, Rectangular,Small	YES	2	1	3.22	.298	TRACER
2	Single, Rectangular,Small	YES	2	1	3.22	.298	TRACER
2	Single, Rectangular,Small	YES	2	1	3.22	.298	TRACER
2	Single, Rectangular,Small	YES	2	1	3.22	.298	TRACER
2	Single, Rectangular,Small	YES	2	1	3.22	.298	TRACER
2	Single, Rectangular,Small	YES	2	1	3.22	.298	COMPUTED_MEANS
3-A	Single, Rectangular,Small	YES	2	1	3.11	.293	TRACER
3-A	Single, Rectangular,Small	YES	2	1	3.11	.293	TRACER
3-A	Single, Rectangular,Small	YES	2	1	3.11	.293	TRACER
3-A	Single, Rectangular,Small	YES	2	1	3.11	.293	TRACER
3-A	Single, Rectangular,Small	YES	2	1	3.11	.293	TRACER
3-A	Single, Rectangular,Small	YES	2	1	3.11	.293	TRACER
3-A	Single, Rectangular,Small	YES	2	1	3.11	.293	COMPUTED_MEANS
3-B	Single, Rectangular,Small	YES	2	1	3.03	.29	TRACER
3-B	Single, Rectangular,Small	YES	2	1	3.03	.29	TRACER
3-B	Single, Rectangular,Small	YES	2	1	3.03	.29	TRACER
3-B	Single, Rectangular,Small	YES	2	1	3.03	.29	TRACER
3-B	Single, Rectangular,Small	YES	2	1	3.03	.29	TRACER
3-B	Single, Rectangular,Small	YES	2	1	3.03	.29	TRACER
3-B	Single, Rectangular,Small	YES	2	1	3.03	.29	COMPUTED_MEANS
4-A	Single, Rectangular,Small	YES	2	2	1.43	.398	TRACER
4-A	Single, Rectangular,Small	YES	2	2	1.43	.398	TRACER
4-A	Single, Rectangular,Small	YES	2	2	1.43	.398	TRACER
4-A	Single, Rectangular,Small	YES	2	2	1.43	.398	TRACER
4-A	Single, Rectangular,Small	YES	2	2	1.43	.398	TRACER
4-A	Single, Rectangular,Small	YES	2	2	1.43	.398	TRACER
4-A	Single, Rectangular,Small	YES	2	2	1.43	.398	COMPUTED_MEANS
4-B	Single, Rectangular,Small	YES	2	2	1.42	.396	TRACER
4-B	Single, Rectangular,Small	YES	2	2	1.42	.396	TRACER
4-B	Single, Rectangular,Small	YES	2	2	1.42	.396	TRACER
4-B	Single, Rectangular,Small	YES	2	2	1.42	.396	TRACER
4-B	Single, Rectangular,Small	YES	2	2	1.42	.396	TRACER
4-B	Single, Rectangular,Small	YES	2	2	1.42	.396	TRACER
4-B	Single, Rectangular,Small	YES	2	2	1.42	.396	COMPUTED_MEANS
5	Single, Rectangular,Small	YES	3	2	3.13	.589	TRACER
5	Single, Rectangular,Small	YES	3	2	3.13	.589	TRACER
5	Single, Rectangular,Small	YES	3	2	3.13	.589	TRACER
5	Single, Rectangular,Small	YES	3	2	3.13	.589	TRACER
5	Single, Rectangular,Small	YES	3	2	3.13	.589	TRACER
5	Single, Rectangular,Small	YES	3	2	3.13	.589	TRACER
5	Single, Rectangular,Small	YES	3	2	3.13	.589	COMPUTED_MEANS
6-A	Single, Rectangular, Large	YES	3	2	3.03	.579	TRACER
6-A	Single, Rectangular, Large	YES	3	2	3.03	.579	TRACER
6-A	Single, Rectangular, Large	YES	3	2	3.03	.579	TRACER
6-A	Single, Rectangular, Large	YES	3	2	3.03	.579	TRACER
6-A	Single, Rectangular, Large	YES	3	2	3.03	.579	TRACER

Continued on next page

Table B.4: Solids Mobilization Experimental Data — Large Flume Study — Part 1. — Continued

EXP	MODEL	THRT	PUM	VAL	DEP	Q	DATA TYPE
6-A	Single, Rectangular, Large	YES	3	2	3.03	.579	TRACER
6-A	Single, Rectangular, Large	YES	3	2	3.03	.579	COMPUTED_MEANS
6-B	Single, Rectangular, Large	YES	3	2	3.03	.579	TRACER
6-B	Single, Rectangular, Large	YES	3	2	3.03	.579	TRACER
6-B	Single, Rectangular, Large	YES	3	2	3.03	.579	TRACER
6-B	Single, Rectangular, Large	YES	3	2	3.03	.579	TRACER
6-B	Single, Rectangular, Large	YES	3	2	3.03	.579	TRACER
6-B	Single, Rectangular, Large	YES	3	2	3.03	.579	COMPUTED_MEANS
7	2-Barrel, Circular Conduit	YES	3	2	3.02	.578	TRACER
7	2-Barrel, Circular Conduit	YES	3	2	3.02	.578	TRACER
7	2-Barrel, Circular Conduit	YES	3	2	3.02	.578	TRACER
7	2-Barrel, Circular Conduit	YES	3	2	3.02	.578	TRACER
7	2-Barrel, Circular Conduit	YES	3	2	3.02	.578	TRACER
7	2-Barrel, Circular Conduit	YES	3	2	3.02	.578	TRACER
7	2-Barrel, Circular Conduit	YES	3	2	3.02	.578	TRACER
7	2-Barrel, Circular Conduit	YES	3	2	3.02	.578	COMPUTED_MEANS
8	2-Barrel, Circular Conduit	NO	2	1	3.1	.293	TRACER
8	2-Barrel, Circular Conduit	NO	2	1	3.1	.293	TRACER
8	2-Barrel, Circular Conduit	NO	2	1	3.1	.293	TRACER
8	2-Barrel, Circular Conduit	NO	2	1	3.1	.293	TRACER
8	2-Barrel, Circular Conduit	NO	2	1	3.1	.293	TRACER
8	2-Barrel, Circular Conduit	NO	2	1	3.1	.293	TRACER
8	2-Barrel, Circular Conduit	NO	2	1	3.1	.293	COMPUTED_MEANS
9	2-Barrel, Circular Conduit	NO	2	2	1.57	.417	TRACER
9	2-Barrel, Circular Conduit	NO	2	2	1.57	.417	TRACER
9	2-Barrel, Circular Conduit	NO	2	2	1.57	.417	TRACER
9	2-Barrel, Circular Conduit	NO	2	2	1.57	.417	TRACER
9	2-Barrel, Circular Conduit	NO	2	2	1.57	.417	TRACER
9	2-Barrel, Circular Conduit	NO	2	2	1.57	.417	TRACER
9	2-Barrel, Circular Conduit	NO	2	2	1.57	.417	COMPUTED_MEANS
10	2-Barrel, Circular Conduit	NO	3	2	3.12	.588	TRACER
10	2-Barrel, Circular Conduit	NO	3	2	3.12	.588	TRACER
10	2-Barrel, Circular Conduit	NO	3	2	3.12	.588	TRACER
10	2-Barrel, Circular Conduit	NO	3	2	3.12	.588	TRACER
10	2-Barrel, Circular Conduit	NO	3	2	3.12	.588	TRACER
10	2-Barrel, Circular Conduit	NO	3	2	3.12	.588	TRACER
10	2-Barrel, Circular Conduit	NO	3	2	3.12	.588	COMPUTED_MEANS
11	2-Barrel, Circular Conduit	NO	3	3	1.19	.544	TRACER
11	2-Barrel, Circular Conduit	NO	3	3	1.19	.544	TRACER
11	2-Barrel, Circular Conduit	NO	3	3	1.19	.544	TRACER
11	2-Barrel, Circular Conduit	NO	3	3	1.19	.544	TRACER
11	2-Barrel, Circular Conduit	NO	3	3	1.19	.544	TRACER
11	2-Barrel, Circular Conduit	NO	3	3	1.19	.544	TRACER
11	2-Barrel, Circular Conduit	NO	3	3	1.19	.544	COMPUTED_MEANS
12	2-Barrel, Circular Conduit	NO	4	3	2.93	.854	TRACER
12	2-Barrel, Circular Conduit	NO	4	3	2.93	.854	TRACER
12	2-Barrel, Circular Conduit	NO	4	3	2.93	.854	TRACER
12	2-Barrel, Circular Conduit	NO	4	3	2.93	.854	TRACER
12	2-Barrel, Circular Conduit	NO	4	3	2.93	.854	TRACER

Continued on next page

94

Table B.4: Solids Mobilization Experimental Data — Large Flume Study — Part 1. — Continued

EXP	MODEL	THRT	PUM	VAL	DEP	Q	DATA TYPE
12	2-Barrel, Circular Conduit	NO	4	3	2.93	.854	TRACER
12	2-Barrel, Circular Conduit	NO	4	3	2.93	.854	TRACER
12	2-Barrel, Circular Conduit	NO	4	3	2.93	.854	COMPUTED_MEANS
13	2-Barrel, Circular Conduit	NO	4	3	2.95	.857	TRACER
13	2-Barrel, Circular Conduit	NO	4	3	2.95	.857	TRACER
13	2-Barrel, Circular Conduit	NO	4	3	2.95	.857	TRACER
13	2-Barrel, Circular Conduit	NO	4	3	2.95	.857	TRACER
13	2-Barrel, Circular Conduit	NO	4	3	2.95	.857	TRACER
13	2-Barrel, Circular Conduit	NO	4	3	2.95	.857	TRACER
13	2-Barrel, Circular Conduit	NO	4	3	2.95	.857	COMPUTED_MEANS
14	2-Barrel, Circular Conduit	NO	4	4	1.2	.729	TRACER
14	2-Barrel, Circular Conduit	NO	4	4	1.2	.729	TRACER
14	2-Barrel, Circular Conduit	NO	4	4	1.2	.729	TRACER
14	2-Barrel, Circular Conduit	NO	4	4	1.2	.729	TRACER
14	2-Barrel, Circular Conduit	NO	4	4	1.2	.729	TRACER
14	2-Barrel, Circular Conduit	NO	4	4	1.2	.729	TRACER
14	2-Barrel, Circular Conduit	NO	4	4	1.2	.729	COMPUTED_MEANS
15	2-Barrel, Circular Conduit	NO	5	4	2.88	1.129	TRACER
15	2-Barrel, Circular Conduit	NO	5	4	2.88	1.129	TRACER
15	2-Barrel, Circular Conduit	NO	5	4	2.88	1.129	TRACER
15	2-Barrel, Circular Conduit	NO	5	4	2.88	1.129	TRACER
15	2-Barrel, Circular Conduit	NO	5	4	2.88	1.129	TRACER
15	2-Barrel, Circular Conduit	NO	5	4	2.88	1.129	TRACER
15	2-Barrel, Circular Conduit	NO	5	4	2.88	1.129	COMPUTED_MEANS
16	2-Barrel, Circular Conduit	NO	5	5	1.26	.933	TRACER
16	2-Barrel, Circular Conduit	NO	5	5	1.26	.933	TRACER
16	2-Barrel, Circular Conduit	NO	5	5	1.26	.933	TRACER
16	2-Barrel, Circular Conduit	NO	5	5	1.26	.933	TRACER
16	2-Barrel, Circular Conduit	NO	5	5	1.26	.933	TRACER
16	2-Barrel, Circular Conduit	NO	5	5	1.26	.933	TRACER
16	2-Barrel, Circular Conduit	NO	5	5	1.26	.933	COMPUTED_MEANS
17	2-Barrel, Circular Conduit	NO	5	5	1.74	1.097	TRACER
17	2-Barrel, Circular Conduit	NO	5	5	1.74	1.097	TRACER
17	2-Barrel, Circular Conduit	NO	5	5	1.74	1.097	TRACER
17	2-Barrel, Circular Conduit	NO	5	5	1.74	1.097	TRACER
17	2-Barrel, Circular Conduit	NO	5	5	1.74	1.097	TRACER
17	2-Barrel, Circular Conduit	NO	5	5	1.74	1.097	TRACER
17	2-Barrel, Circular Conduit	NO	5	5	1.74	1.097	TRACER
17	2-Barrel, Circular Conduit	NO	6	5	1.74	1.097	COMPUTED_MEANS
18	2-Barrel, Circular Conduit	NO	6	5	2.98	1.436	TRACER
18	2-Barrel, Circular Conduit	NO	6	5	2.98	1.436	TRACER
18	2-Barrel, Circular Conduit	NO	6	5	2.98	1.436	TRACER
18	2-Barrel, Circular Conduit	NO	6	5	2.98	1.436	TRACER
18	2-Barrel, Circular Conduit	NO	6	5	2.98	1.436	TRACER
18	2-Barrel, Circular Conduit	NO	6	5	2.98	1.436	TRACER
18	2-Barrel, Circular Conduit	NO	6	5	2.98	1.436	TRACER
18	2-Barrel, Circular Conduit	NO	6	5	2.98	1.436	COMPUTED_MEANS
19	2-Barrel, Circular Conduit	NO	6	6	1.62	1.27	TRACER
19	2-Barrel, Circular Conduit	NO	6	6	1.62	1.27	TRACER

Continued on next page

95

Table B.4: Solids Mobilization Experimental Data — Large Flume Study — Part 1. — Continued

EXP	MODEL	THRT	PUM	VAL	DEP	Q	DATA TYPE
19	2-Barrel, Circular Conduit	NO	6	6	1.62	1.27	TRACER
19	2-Barrel, Circular Conduit	NO	6	6	1.62	1.27	TRACER
19	2-Barrel, Circular Conduit	NO	6	6	1.62	1.27	TRACER
19	2-Barrel, Circular Conduit	NO	6	6	1.62	1.27	TRACER
19	2-Barrel, Circular Conduit	NO	6	6	1.62	1.27	COMPUTED_MEANS
20	4-Barrel, Circular Conduit	NO	4	4	1.4	.787	TRACER
20	4-Barrel, Circular Conduit	NO	4	4	1.4	.787	TRACER
20	4-Barrel, Circular Conduit	NO	4	4	1.4	.787	TRACER
20	4-Barrel, Circular Conduit	NO	4	4	1.4	.787	TRACER
20	4-Barrel, Circular Conduit	NO	4	4	1.4	.787	TRACER
20	4-Barrel, Circular Conduit	NO	4	4	1.4	.787	TRACER
20	4-Barrel, Circular Conduit	NO	4	4	1.4	.787	COMPUTED_MEANS
21	4-Barrel, Circular Conduit	NO	5	4	3.04	1.16	TRACER
21	4-Barrel, Circular Conduit	NO	5	4	3.04	1.16	TRACER
21	4-Barrel, Circular Conduit	NO	5	4	3.04	1.16	TRACER
21	4-Barrel, Circular Conduit	NO	5	4	3.04	1.16	TRACER
21	4-Barrel, Circular Conduit	NO	5	4	3.04	1.16	TRACER
21	4-Barrel, Circular Conduit	NO	5	4	3.04	1.16	TRACER
21	4-Barrel, Circular Conduit	NO	5	4	3.04	1.16	COMPUTED_MEANS
22	4-Barrel, Circular Conduit	NO	5	5	1.76	1.103	TRACER
22	4-Barrel, Circular Conduit	NO	5	5	1.76	1.103	TRACER
22	4-Barrel, Circular Conduit	NO	5	5	1.76	1.103	TRACER
22	4-Barrel, Circular Conduit	NO	5	5	1.76	1.103	TRACER
22	4-Barrel, Circular Conduit	NO	5	5	1.76	1.103	TRACER
22	4-Barrel, Circular Conduit	NO	5	5	1.76	1.103	TRACER
22	4-Barrel, Circular Conduit	NO	5	5	1.76	1.103	COMPUTED_MEANS
23	4-Barrel, Circular Conduit	NO	6	5	2.9	1.416	TRACER
23	4-Barrel, Circular Conduit	NO	6	5	2.9	1.416	TRACER
23	4-Barrel, Circular Conduit	NO	6	5	2.9	1.416	TRACER
23	4-Barrel, Circular Conduit	NO	6	5	2.9	1.416	TRACER
23	4-Barrel, Circular Conduit	NO	6	5	2.9	1.416	TRACER
23	4-Barrel, Circular Conduit	NO	6	5	2.9	1.416	TRACER
23	4-Barrel, Circular Conduit	NO	6	5	2.9	1.416	COMPUTED_MEANS
24	4-Barrel, Circular Conduit	NO	6	6	2.14	1.46	TRACER
24	4-Barrel, Circular Conduit	NO	6	6	2.14	1.46	TRACER
24	4-Barrel, Circular Conduit	NO	6	6	2.14	1.46	TRACER
24	4-Barrel, Circular Conduit	NO	6	6	2.14	1.46	TRACER
24	4-Barrel, Circular Conduit	NO	6	6	2.14	1.46	TRACER
24	4-Barrel, Circular Conduit	NO	6	6	2.14	1.46	TRACER
24	4-Barrel, Circular Conduit	NO	6	6	2.14	1.46	COMPUTED_MEANS
25	4-Barrel, Circular Conduit	YES	2	1	3.15	.295	TRACER
25	4-Barrel, Circular Conduit	YES	2	1	3.15	.295	TRACER
25	4-Barrel, Circular Conduit	YES	2	1	3.15	.295	TRACER
25	4-Barrel, Circular Conduit	YES	2	1	3.15	.295	COMPUTED_MEANS
26	4-Barrel, Circular Conduit	YES	2	2	1.	.333	TRACER
26	4-Barrel, Circular Conduit	YES	2	2	1.	.333	TRACER
26	4-Barrel, Circular Conduit	YES	2	2	1.	.333	TRACER
26	4-Barrel, Circular Conduit	YES	2	2	1.	.333	TRACER
26	4-Barrel, Circular Conduit	YES	2	2	1.	.333	TRACER

Continued on next page

96

Table B.4: Solids Mobilization Experimental Data — Large Flume Study — Part 1. — Continued

EXP	MODEL	THRT	PUM	VAL	DEP	Q	DATA TYPE
26	4-Barrel, Circular Conduit	YES	2	2	1.	.333	TRACER
26	4-Barrel, Circular Conduit	YES	2	2	1.	.333	COMPUTED_MEANS
27	4-Barrel, Circular Conduit	YES	3	2	3.07	.583	TRACER
27	4-Barrel, Circular Conduit	YES	3	2	3.07	.583	TRACER
27	4-Barrel, Circular Conduit	YES	3	2	3.07	.583	TRACER
27	4-Barrel, Circular Conduit	YES	3	2	3.07	.583	TRACER
27	4-Barrel, Circular Conduit	YES	3	2	3.07	.583	TRACER
27	4-Barrel, Circular Conduit	YES	3	2	3.07	.583	TRACER
27	4-Barrel, Circular Conduit	YES	3	2	3.07	.583	COMPUTED_MEANS
28	4-Barrel, Circular Conduit	YES	3	3	1.7	.651	TRACER
28	4-Barrel, Circular Conduit	YES	3	3	1.7	.651	TRACER
28	4-Barrel, Circular Conduit	YES	3	3	1.7	.651	TRACER
28	4-Barrel, Circular Conduit	YES	3	3	1.7	.651	TRACER
28	4-Barrel, Circular Conduit	YES	3	3	1.7	.651	TRACER
28	4-Barrel, Circular Conduit	YES	3	3	1.7	.651	TRACER
28	4-Barrel, Circular Conduit	YES	3	3	1.7	.651	COMPUTED_MEANS
29	4-Barrel, Circular Conduit	YES	4	3	2.98	.861	TRACER
29	4-Barrel, Circular Conduit	YES	4	3	2.98	.861	TRACER
29	4-Barrel, Circular Conduit	YES	4	3	2.98	.861	TRACER
29	4-Barrel, Circular Conduit	YES	4	3	2.98	.861	TRACER
29	4-Barrel, Circular Conduit	YES	4	3	2.98	.861	TRACER
29	4-Barrel, Circular Conduit	YES	4	3	2.98	.861	TRACER
29	4-Barrel, Circular Conduit	YES	4	3	2.98	.861	COMPUTED_MEANS
30	4-Barrel, Circular Conduit	YES	4	4	1.19	.726	TRACER
30	4-Barrel, Circular Conduit	YES	4	4	1.19	.726	TRACER
30	4-Barrel, Circular Conduit	YES	4	4	1.19	.726	TRACER
30	4-Barrel, Circular Conduit	YES	4	4	1.19	.726	TRACER
30	4-Barrel, Circular Conduit	YES	4	4	1.19	.726	TRACER
30	4-Barrel, Circular Conduit	YES	4	4	1.19	.726	TRACER
30	4-Barrel, Circular Conduit	YES	4	4	1.19	.726	COMPUTED_MEANS
31	4-Barrel, Circular Conduit	YES	5	5	1.85	1.131	TRACER
31	4-Barrel, Circular Conduit	YES	5	5	1.85	1.131	TRACER
31	4-Barrel, Circular Conduit	YES	5	5	1.85	1.131	ROCK_AS_TRACER
31	4-Barrel, Circular Conduit	YES	5	5	1.85	1.131	COMPUTED_MEANS
32	4-Barrel, Circular Conduit	YES	6	6	1.89	1.372	TRACER
33	Porous, Rectangular, Small	YES	2	1	3.	.288	TRACER
33	Porous, Rectangular, Small	YES	2	1	3.	.288	TRACER
33	Porous, Rectangular, Small	YES	2	1	3.	.288	TRACER
33	Porous, Rectangular, Small	YES	2	1	3.	.288	TRACER
33	Porous, Rectangular, Small	YES	2	1	3.	.288	TRACER
33	Porous, Rectangular, Small	YES	2	1	3.	.288	TRACER
33	Porous, Rectangular, Small	YES	2	1	3.	.288	TRACER
33	Porous, Rectangular, Small	YES	2	1	3.	.288	COMPUTED_MEANS
34	Porous, Rectangular, Small	YES	2	2	1.9	.459	TRACER
34	Porous, Rectangular, Small	YES	2	2	1.9	.459	TRACER
34	Porous, Rectangular, Small	YES	2	2	1.9	.459	TRACER
34	Porous, Rectangular, Small	YES	2	2	1.9	.459	TRACER
34	Porous, Rectangular, Small	YES	2	2	1.9	.459	TRACER
34	Porous, Rectangular, Small	YES	2	2	1.9	.459	TRACER

Continued on next page

Table B.4: Solids Mobilization Experimental Data — Large Flume Study — Part 1. — Continued

EXP	MODEL	THRT	PUM	VAL	DEP	Q	DATA TYPE
34	Porous, Rectangular, Small	YES	2	2	1.9	.459	COMPUTED_MEANS
35	Porous, Rectangular, Small	YES	2	1	3.07	.291	TRACER
35	Porous, Rectangular, Small	YES	2	1	3.07	.291	TRACER
35	Porous, Rectangular, Small	YES	2	1	3.07	.291	TRACER
35	Porous, Rectangular, Small	YES	2	1	3.07	.291	TRACER
35	Porous, Rectangular, Small	YES	2	1	3.07	.291	TRACER
35	Porous, Rectangular, Small	YES	2	1	3.07	.291	COMPUTED_MEANS
36	Porous, Rectangular, Small	YES	2	2	1.86	.454	TRACER
36	Porous, Rectangular, Small	YES	2	2	1.86	.454	TRACER
36	Porous, Rectangular, Small	YES	2	2	1.86	.454	TRACER
36	Porous, Rectangular, Small	YES	2	2	1.86	.454	TRACER
36	Porous, Rectangular, Small	YES	2	2	1.86	.454	COMPUTED_MEANS
37	Porous, Rectangular, Small	YES	3	2	3.08	.584	TRACER
37	Porous, Rectangular, Small	YES	3	2	3.08	.584	TRACER
37	Porous, Rectangular, Small	YES	3	2	3.08	.584	TRACER
37	Porous, Rectangular, Small	YES	3	2	3.08	.584	TRACER
37	Porous, Rectangular, Small	YES	3	2	3.08	.584	TRACER
37	Porous, Rectangular, Small	YES	3	2	3.08	.584	TRACER
37	Porous, Rectangular, Small	YES	3	2	3.08	.584	COMPUTED_MEANS
38	Porous, Rectangular, Small	YES	3	3	1.41	.592	TRACER
38	Porous, Rectangular, Small	YES	3	3	1.41	.592	TRACER
38	Porous, Rectangular, Small	YES	3	3	1.41	.592	TRACER
38	Porous, Rectangular, Small	YES	3	3	1.41	.592	TRACER
38	Porous, Rectangular, Small	YES	3	3	1.41	.592	TRACER
38	Porous, Rectangular, Small	YES	3	3	1.41	.592	TRACER
38	Porous, Rectangular, Small	YES	3	3	1.41	.592	COMPUTED_MEANS
39	Porous, Rectangular, Small	YES	4	3	3.16	.887	TRACER
39	Porous, Rectangular, Small	YES	4	3	3.16	.887	TRACER
39	Porous, Rectangular, Small	YES	4	3	3.16	.887	TRACER
39	Porous, Rectangular, Small	YES	4	3	3.16	.887	TRACER
39	Porous, Rectangular, Small	YES	4	3	3.16	.887	COMPUTED_MEANS
40	Porous, Rectangular, Small	YES	4	4	1.79	.89	TRACER
40	Porous, Rectangular, Small	YES	4	4	1.79	.89	TRACER
40	Porous, Rectangular, Small	YES	4	4	1.79	.89	TRACER
40	Porous, Rectangular, Small	YES	4	4	1.79	.89	TRACER
40	Porous, Rectangular, Small	YES	4	4	1.79	.89	COMPUTED_MEANS
41	Porous, Rectangular, Small	YES	5	5	1.4	.984	TRACER
41	Porous, Rectangular, Small	YES	5	5	1.4	.984	TRACER
41	Porous, Rectangular, Small	YES	5	5	1.4	.984	TRACER
41	Porous, Rectangular, Small	YES	5	5	1.4	.984	COMPUTED_MEANS
42	Porous, Rectangular, Small	YES	5	4	3.02	1.156	TRACER
42	Porous, Rectangular, Small	YES	5	4	3.02	1.156	TRACER
42	Porous, Rectangular, Small	YES	5	4	3.02	1.156	TRACER
42	Porous, Rectangular, Small	YES	5	4	3.02	1.156	COMPUTED_MEANS
43	Porous, Rectangular, Small	YES	4	4	2.3	1.009	TRACER
43	Porous, Rectangular, Small	YES	4	4	2.3	1.009	TRACER
43	Porous, Rectangular, Small	YES	4	4	2.3	1.009	TRACER
43	Porous, Rectangular, Small	YES	4	4	2.3	1.009	TRACER
43	Porous, Rectangular, Small	YES	4	4	2.3	1.009	TRACER

Continued on next page

98

Table B.4: Solids Mobilization Experimental Data — Large Flume Study — Part 1. — Continued

EXP	MODEL	THRT	PUM	VAL	DEP	Q	DATA TYPE
43	Porous, Rectangular, Small	YES	4	4	2.3	1.009	TRACER
43	Porous, Rectangular, Small	YES	4	4	2.3	1.009	COMPUTED_MEANS
44	Porous, Rectangular, Small	NO	2	2	1.9	.459	TRACER
44	Porous, Rectangular, Small	NO	2	2	1.9	.459	TRACER
44	Porous, Rectangular, Small	NO	2	2	1.9	.459	TRACER
44	Porous, Rectangular, Small	NO	2	2	1.9	.459	TRACER
44	Porous, Rectangular, Small	NO	2	2	1.9	.459	TRACER
44	Porous, Rectangular, Small	NO	2	2	1.9	.459	TRACER
44	Porous, Rectangular, Small	NO	2	2	1.9	.459	COMPUTED_MEANS
45	Porous, Rectangular, Small	NO	3	2	3.	.576	TRACER
45	Porous, Rectangular, Small	NO	3	2	3.	.576	TRACER
45	Porous, Rectangular, Small	NO	3	2	3.	.576	TRACER
45	Porous, Rectangular, Small	NO	3	2	3.	.576	TRACER
45	Porous, Rectangular, Small	NO	3	2	3.	.576	TRACER
45	Porous, Rectangular, Small	NO	3	2	3.	.576	TRACER
45	Porous, Rectangular, Small	NO	3	2	3.	.576	COMPUTED_MEANS
46	Porous, Rectangular, Small	NO	3	3	1.4	.59	TRACER
46	Porous, Rectangular, Small	NO	3	3	1.4	.59	TRACER
46	Porous, Rectangular, Small	NO	3	3	1.4	.59	TRACER
46	Porous, Rectangular, Small	NO	3	3	1.4	.59	TRACER
46	Porous, Rectangular, Small	NO	3	3	1.4	.59	TRACER
46	Porous, Rectangular, Small	NO	3	3	1.4	.59	TRACER
46	Porous, Rectangular, Small	NO	3	3	1.4	.59	COMPUTED_MEANS
47	Porous, Rectangular, Small	NO	4	3	3.	.864	TRACER
47	Porous, Rectangular, Small	NO	4	3	3.	.864	TRACER
47	Porous, Rectangular, Small	NO	4	3	3.	.864	TRACER
47	Porous, Rectangular, Small	NO	4	3	3.	.864	TRACER
47	Porous, Rectangular, Small	NO	4	3	3.	.864	TRACER
47	Porous, Rectangular, Small	NO	4	3	3.	.864	TRACER
47	Porous, Rectangular, Small	NO	4	3	3.	.864	COMPUTED_MEANS
48	Porous, Rectangular, Small	NO	4	4	2.3	1.009	TRACER
48	Porous, Rectangular, Small	NO	4	4	2.3	1.009	TRACER
48	Porous, Rectangular, Small	NO	4	4	2.3	1.009	TRACER
48	Porous, Rectangular, Small	NO	4	4	2.3	1.009	TRACER
48	Porous, Rectangular, Small	NO	4	4	2.3	1.009	TRACER
48	Porous, Rectangular, Small	NO	4	4	2.3	1.009	TRACER
48	Porous, Rectangular, Small	NO	4	4	2.3	1.009	COMPUTED_MEANS
49	Porous, Rectangular, Small	YES	4	4	2.28	1.005	TRACER
49	Porous, Rectangular, Small	YES	4	4	2.28	1.005	TRACER
49	Porous, Rectangular, Small	YES	4	4	2.28	1.005	TRACER
49	Porous, Rectangular, Small	YES	4	4	2.28	1.005	TRACER
49	Porous, Rectangular, Small	YES	4	4	2.28	1.005	TRACER
49	Porous, Rectangular, Small	YES	4	4	2.28	1.005	COMPUTED_MEANS
50	Porous, Rectangular, Small	YES	5	4	2.87	1.127	TRACER
50	Porous, Rectangular, Small	YES	5	4	2.87	1.127	TRACER
50	Porous, Rectangular, Small	YES	5	4	2.87	1.127	TRACER
50	Porous, Rectangular, Small	YES	5	4	2.87	1.127	TRACER
50	Porous, Rectangular, Small	YES	5	4	2.87	1.127	TRACER
50	Porous, Rectangular, Small	YES	5	4	2.87	1.127	TRACER

Continued on next page

99

Table B.4: Solids Mobilization Experimental Data — Large Flume Study — Part 1. — Continued

EXP	MODEL	THRT	PUM	VAL	DEP	Q	DATA TYPE
50	Porous, Rectangular, Small	YES	5	4	2.87	1.127	COMPUTED_MEANS
51	Porous, Rectangular, Small	YES	5	5	1.97	1.167	TRACER
51	Porous, Rectangular, Small	YES	5	5	1.97	1.167	TRACER
51	Porous, Rectangular, Small	YES	5	5	1.97	1.167	TRACER
51	Porous, Rectangular, Small	YES	5	5	1.97	1.167	TRACER
51	Porous, Rectangular, Small	YES	5	5	1.97	1.167	TRACER
51	Porous, Rectangular, Small	YES	5	5	1.97	1.167	TRACER
51	Porous, Rectangular, Small	YES	5	5	1.97	1.167	COMPUTED_MEANS
52	Porous, Rectangular, Small	YES	6	5	2.95	1.428	TRACER
52	Porous, Rectangular, Small	YES	6	5	2.95	1.428	TRACER
52	Porous, Rectangular, Small	YES	6	5	2.95	1.428	TRACER
52	Porous, Rectangular, Small	YES	6	5	2.95	1.428	TRACER
52	Porous, Rectangular, Small	YES	6	5	2.95	1.428	TRACER
52	Porous, Rectangular, Small	YES	6	5	2.95	1.428	TRACER
52	Porous, Rectangular, Small	YES	6	5	2.95	1.428	COMPUTED_MEANS
53	Porous, Rectangular, Small	YES	6	6	1.84	1.354	TRACER
53	Porous, Rectangular, Small	YES	6	6	1.84	1.354	TRACER
53	Porous, Rectangular, Small	YES	6	6	1.84	1.354	TRACER
53	Porous, Rectangular, Small	YES	6	6	1.84	1.354	TRACER
53	Porous, Rectangular, Small	YES	6	6	1.84	1.354	TRACER
53	Porous, Rectangular, Small	YES	6	6	1.84	1.354	TRACER
53	Porous, Rectangular, Small	YES	6	6	1.84	1.354	COMPUTED_MEANS
54	Single, Rectangular, Large	YES	2	1	3.25	.3	TRACER
54	Single, Rectangular, Large	YES	2	1	3.25	.3	TRACER
54	Single, Rectangular, Large	YES	2	1	3.25	.3	TRACER
54	Single, Rectangular, Large	YES	2	1	3.25	.3	TRACER
54	Single, Rectangular, Large	YES	2	1	3.25	.3	TRACER
54	Single, Rectangular, Large	YES	2	1	3.25	.3	COMPUTED_MEANS
55	Single, Rectangular, Large	YES	2	2	1.54	.413	TRACER
55	Single, Rectangular, Large	YES	2	2	1.54	.413	TRACER
55	Single, Rectangular, Large	YES	2	2	1.54	.413	TRACER
55	Single, Rectangular, Large	YES	2	2	1.54	.413	TRACER
55	Single, Rectangular, Large	YES	2	2	1.54	.413	TRACER
55	Single, Rectangular, Large	YES	2	2	1.54	.413	COMPUTED_MEANS
56	Single, Rectangular, Large	YES	3	2	3.14	.589	TRACER
56	Single, Rectangular, Large	YES	3	2	3.14	.589	TRACER
56	Single, Rectangular, Large	YES	3	2	3.14	.589	TRACER
56	Single, Rectangular, Large	YES	3	2	3.14	.589	TRACER
56	Single, Rectangular, Large	YES	3	2	3.14	.589	TRACER
56	Single, Rectangular, Large	YES	3	2	3.14	.589	COMPUTED_MEANS
57	Single, Rectangular, Large	YES	3	3	1.47	.605	TRACER
57	Single, Rectangular, Large	YES	3	3	1.47	.605	TRACER
57	Single, Rectangular, Large	YES	3	3	1.47	.605	TRACER
57	Single, Rectangular, Large	YES	3	3	1.47	.605	TRACER
57	Single, Rectangular, Large	YES	3	3	1.47	.605	TRACER
57	Single, Rectangular, Large	YES	3	3	1.47	.605	COMPUTED_MEANS
58	Single, Rectangular, Large	YES	4	3	3.14	.884	TRACER
58	Single, Rectangular, Large	YES	4	3	3.14	.884	TRACER
58	Single, Rectangular, Large	YES	4	3	3.14	.884	TRACER

Continued on next page

Table B.4: Solids Mobilization Experimental Data — Large Flume Study — Part 1. — Continued

EXP	MODEL	THRT	PUM	VAL	DEP	Q	DATA TYPE
58	Single, Rectangular, Large	YES	4	3	3.14	.884	TRACER
58	Single, Rectangular, Large	YES	4	3	3.14	.884	TRACER
58	Single, Rectangular, Large	YES	4	3	3.14	.884	COMPUTED_MEANS
59	Single, Rectangular, Large	YES	4	4	1.59	.839	TRACER
59	Single, Rectangular, Large	YES	4	4	1.59	.839	TRACER
59	Single, Rectangular, Large	YES	4	4	1.59	.839	TRACER
59	Single, Rectangular, Large	YES	4	4	1.59	.839	TRACER
59	Single, Rectangular, Large	YES	4	4	1.59	.839	TRACER
59	Single, Rectangular, Large	YES	4	4	1.59	.839	COMPUTED_MEANS
60	Single, Rectangular, Large	YES	5	5	1.6	1.052	TRACER
60	Single, Rectangular, Large	YES	5	5	1.6	1.052	TRACER
60	Single, Rectangular, Large	YES	5	5	1.6	1.052	TRACER
60	Single, Rectangular, Large	YES	5	5	1.6	1.052	TRACER
60	Single, Rectangular, Large	YES	5	5	1.6	1.052	TRACER
60	Single, Rectangular, Large	YES	5	5	1.6	1.052	COMPUTED_MEANS
61	Single, Rectangular, Large	YES	6	6	1.28	1.129	TRACER
61	Single, Rectangular, Large	YES	6	6	1.28	1.129	TRACER
61	Single, Rectangular, Large	YES	6	6	1.28	1.129	TRACER
61	Single, Rectangular, Large	YES	6	6	1.28	1.129	TRACER
61	Single, Rectangular, Large	YES	6	6	1.28	1.129	TRACER
61	Single, Rectangular, Large	YES	6	6	1.28	1.129	TRACER
61	Single, Rectangular, Large	YES	6	6	1.28	1.129	TRACER
61	Single, Rectangular, Large	YES	6	6	1.28	1.129	TRACER
61	Single, Rectangular, Large	YES	6	6	1.28	1.129	COMPUTED_MEANS
62	Single, Rectangular, Large	NO	2	1	2.95	.286	TRACER
62	Single, Rectangular, Large	NO	2	1	2.95	.286	TRACER
62	Single, Rectangular, Large	NO	2	1	2.95	.286	TRACER
62	Single, Rectangular, Large	NO	2	1	2.95	.286	TRACER
62	Single, Rectangular, Large	NO	2	1	2.95	.286	TRACER
62	Single, Rectangular, Large	NO	2	1	2.95	.286	COMPUTED_MEANS
63	Single, Rectangular, Large	NO	2	2	1.1	.349	TRACER
63	Single, Rectangular, Large	NO	2	2	1.1	.349	TRACER
63	Single, Rectangular, Large	NO	2	2	1.1	.349	TRACER
63	Single, Rectangular, Large	NO	2	2	1.1	.349	TRACER
63	Single, Rectangular, Large	NO	2	2	1.1	.349	TRACER
63	Single, Rectangular, Large	NO	2	2	1.1	.349	COMPUTED_MEANS
64	Single, Rectangular, Large	NO	3	2	2.96	.572	TRACER
64	Single, Rectangular, Large	NO	3	2	2.96	.572	TRACER
64	Single, Rectangular, Large	NO	3	2	2.96	.572	TRACER
64	Single, Rectangular, Large	NO	3	2	2.96	.572	TRACER
64	Single, Rectangular, Large	NO	3	2	2.96	.572	TRACER
64	Single, Rectangular, Large	NO	3	2	2.96	.572	COMPUTED_MEANS
65	Single, Rectangular, Large	NO	3	3	1.12	.528	TRACER
65	Single, Rectangular, Large	NO	3	3	1.12	.528	TRACER
65	Single, Rectangular, Large	NO	3	3	1.12	.528	TRACER
65	Single, Rectangular, Large	NO	3	3	1.12	.528	TRACER
65	Single, Rectangular, Large	NO	3	3	1.12	.528	TRACER
65	Single, Rectangular, Large	NO	3	3	1.12	.528	COMPUTED_MEANS
66	Single, Rectangular, Large	NO	4	3	2.95	.857	TRACER

Continued on next page

101

Table B.4: Solids Mobilization Experimental Data — Large Flume Study — Part 1. — Continued

EXP	MODEL	THRT	PUM	VAL	DEP	Q	DATA TYPE
66	Single, Rectangular, Large	NO	4	3	2.95	.857	TRACER
66	Single, Rectangular, Large	NO	4	3	2.95	.857	TRACER
66	Single, Rectangular, Large	NO	4	3	2.95	.857	TRACER
66	Single, Rectangular, Large	NO	4	3	2.95	.857	TRACER
66	Single, Rectangular, Large	NO	4	3	2.95	.857	COMPUTED_MEANS
67	Single, Rectangular, Large	NO	4	4	1.3	.759	TRACER
67	Single, Rectangular, Large	NO	4	4	1.3	.759	TRACER
67	Single, Rectangular, Large	NO	4	4	1.3	.759	TRACER
67	Single, Rectangular, Large	NO	4	4	1.3	.759	TRACER
67	Single, Rectangular, Large	NO	4	4	1.3	.759	TRACER
67	Single, Rectangular, Large	NO	4	4	1.3	.759	COMPUTED_MEANS
68	Single, Rectangular, Large	NO	5	4	2.71	1.095	TRACER
68	Single, Rectangular, Large	NO	5	4	2.71	1.095	TRACER
68	Single, Rectangular, Large	NO	5	4	2.71	1.095	TRACER
68	Single, Rectangular, Large	NO	5	4	2.71	1.095	TRACER
68	Single, Rectangular, Large	NO	5	4	2.71	1.095	TRACER
68	Single, Rectangular, Large	NO	5	4	2.71	1.095	COMPUTED_MEANS
69	Single, Rectangular, Large	NO	5	5	.79	.739	TRACER
69	Single, Rectangular, Large	NO	5	5	.79	.739	TRACER
69	Single, Rectangular, Large	NO	5	5	.79	.739	TRACER
69	Single, Rectangular, Large	NO	5	5	.79	.739	TRACER
69	Single, Rectangular, Large	NO	5	5	.79	.739	TRACER
69	Single, Rectangular, Large	NO	5	5	.79	.739	COMPUTED_MEANS
70	Single, Rectangular, Large	NO	6	5	2.36	1.278	TRACER
70	Single, Rectangular, Large	NO	6	5	2.36	1.278	TRACER
70	Single, Rectangular, Large	NO	6	5	2.36	1.278	TRACER
70	Single, Rectangular, Large	NO	6	5	2.36	1.278	TRACER
70	Single, Rectangular, Large	NO	6	5	2.36	1.278	TRACER
70	Single, Rectangular, Large	NO	6	5	2.36	1.278	COMPUTED_MEANS
71	Single, Rectangular, Large	NO	6	6	.81	.898	TRACER
71	Single, Rectangular, Large	NO	6	6	.81	.898	TRACER
71	Single, Rectangular, Large	NO	6	6	.81	.898	TRACER
71	Single, Rectangular, Large	NO	6	6	.81	.898	TRACER
71	Single, Rectangular, Large	NO	6	6	.81	.898	TRACER
71	Single, Rectangular, Large	NO	6	6	.81	.898	COMPUTED_MEANS
72	4-Barrell, Circular Conduit	YES	2	1	3.19	.297	TRACER
72	4-Barrell, Circular Conduit	YES	2	1	3.19	.297	TRACER
72	4-Barrell, Circular Conduit	YES	2	1	3.19	.297	TRACER
72	4-Barrell, Circular Conduit	YES	2	1	3.19	.297	TRACER
72	4-Barrell, Circular Conduit	YES	2	1	3.19	.297	TRACER
72	4-Barrell, Circular Conduit	YES	2	1	3.19	.297	COMPUTED_MEANS
73	4-Barrell, Circular Conduit	YES	2	2	1.54	.413	TRACER
73	4-Barrell, Circular Conduit	YES	2	2	1.54	.413	TRACER
73	4-Barrell, Circular Conduit	YES	2	2	1.54	.413	TRACER
73	4-Barrell, Circular Conduit	YES	2	2	1.54	.413	TRACER
73	4-Barrell, Circular Conduit	YES	2	2	1.54	.413	TRACER
73	4-Barrell, Circular Conduit	YES	2	2	1.54	.413	COMPUTED_MEANS
74	4-Barrell, Circular Conduit	YES	3	2	3.21	.596	TRACER
74	4-Barrell, Circular Conduit	YES	3	2	3.21	.596	TRACER

Continued on next page

Table B.4: Solids Mobilization Experimental Data — Large Flume Study — Part 1. — Continued

EXP	MODEL	THRT	PUM	VAL	DEP	Q	DATA TYPE
74	4-Barrell, Circular Conduit	YES	3	2	3.21	.596	TRACER
74	4-Barrell, Circular Conduit	YES	3	2	3.21	.596	TRACER
74	4-Barrell, Circular Conduit	YES	3	2	3.21	.596	COMPUTED_MEANS
75	4-Barrell, Circular Conduit	YES	3	3	1.36	.582	TRACER
75	4-Barrell, Circular Conduit	YES	3	3	1.36	.582	TRACER
75	4-Barrell, Circular Conduit	YES	3	3	1.36	.582	TRACER
75	4-Barrell, Circular Conduit	YES	3	3	1.36	.582	TRACER
75	4-Barrell, Circular Conduit	YES	3	3	1.36	.582	TRACER
75	4-Barrell, Circular Conduit	YES	3	3	1.36	.582	COMPUTED_MEANS
76	4-Barrell, Circular Conduit	YES	4	3	3.09	.877	TRACER
76	4-Barrell, Circular Conduit	YES	4	3	3.09	.877	TRACER
76	4-Barrell, Circular Conduit	YES	4	3	3.09	.877	TRACER
76	4-Barrell, Circular Conduit	YES	4	3	3.09	.877	TRACER
76	4-Barrell, Circular Conduit	YES	4	3	3.09	.877	TRACER
76	4-Barrell, Circular Conduit	YES	4	3	3.09	.877	COMPUTED_MEANS
77	4-Barrell, Circular Conduit	YES	4	4	1.48	.809	TRACER
77	4-Barrell, Circular Conduit	YES	4	4	1.48	.809	TRACER
77	4-Barrell, Circular Conduit	YES	4	4	1.48	.809	TRACER
77	4-Barrell, Circular Conduit	YES	4	4	1.48	.809	TRACER
77	4-Barrell, Circular Conduit	YES	4	4	1.48	.809	TRACER
77	4-Barrell, Circular Conduit	YES	4	4	1.48	.809	TRACER
77	4-Barrell, Circular Conduit	YES	4	4	1.48	.809	COMPUTED_MEANS
78	4-Barrell, Circular Conduit	YES	5	4	3.07	1.166	TRACER
78	4-Barrell, Circular Conduit	YES	5	4	3.07	1.166	TRACER
78	4-Barrell, Circular Conduit	YES	5	4	3.07	1.166	TRACER
78	4-Barrell, Circular Conduit	YES	5	4	3.07	1.166	TRACER
78	4-Barrell, Circular Conduit	YES	5	4	3.07	1.166	TRACER
78	4-Barrell, Circular Conduit	YES	5	4	3.07	1.166	TRACER
78	4-Barrell, Circular Conduit	YES	5	4	3.07	1.166	COMPUTED_MEANS
79	4-Barrell, Circular Conduit	YES	5	5	1.51	1.022	TRACER
79	4-Barrell, Circular Conduit	YES	5	5	1.51	1.022	TRACER
79	4-Barrell, Circular Conduit	YES	5	5	1.51	1.022	TRACER
79	4-Barrell, Circular Conduit	YES	5	5	1.51	1.022	TRACER
79	4-Barrell, Circular Conduit	YES	5	5	1.51	1.022	TRACER
79	4-Barrell, Circular Conduit	YES	5	5	1.51	1.022	COMPUTED_MEANS
80	4-Barrell, Circular Conduit	YES	6	5	2.6	1.341	TRACER
80	4-Barrell, Circular Conduit	YES	6	5	2.6	1.341	TRACER
80	4-Barrell, Circular Conduit	YES	6	5	2.6	1.341	TRACER
80	4-Barrell, Circular Conduit	YES	6	5	2.6	1.341	COMPUTED_MEANS
81	4-Barrell, Circular Conduit	YES	6	6	1.46	1.206	TRACER
81	4-Barrell, Circular Conduit	YES	6	6	1.46	1.206	TRACER
81	4-Barrell, Circular Conduit	YES	6	6	1.46	1.206	TRACER
81	4-Barrell, Circular Conduit	YES	6	6	1.46	1.206	COMPUTED_MEANS
82	Porous, Rectangular, Small	YES	2	1	3.08	.292	TRACER
82	Porous, Rectangular, Small	YES	2	1	3.08	.292	TRACER
82	Porous, Rectangular, Small	YES	2	1	3.08	.292	TRACER
82	Porous, Rectangular, Small	YES	2	1	3.08	.292	TRACER
82	Porous, Rectangular, Small	YES	2	1	3.08	.292	TRACER
82	Porous, Rectangular, Small	YES	2	1	3.08	.292	COMPUTED_MEANS

Continued on next page

Table B.4: Solids Mobilization Experimental Data — Large Flume Study — Part 1. — Continued

EXP	MODEL	THRT	PUM	VAL	DEP	Q	DATA TYPE
83	Porous, Rectangular, Small	YES	2	2	1.29	.378	TRACER
83	Porous, Rectangular, Small	YES	2	2	1.29	.378	TRACER
83	Porous, Rectangular, Small	YES	2	2	1.29	.378	TRACER
83	Porous, Rectangular, Small	YES	2	2	1.29	.378	TRACER
83	Porous, Rectangular, Small	YES	2	2	1.29	.378	TRACER
83	Porous, Rectangular, Small	YES	2	2	1.29	.378	COMPUTED_MEANS
84	Porous, Rectangular, Small	YES	3	2	3.09	.585	TRACER
84	Porous, Rectangular, Small	YES	3	2	3.09	.585	TRACER
84	Porous, Rectangular, Small	YES	3	2	3.09	.585	TRACER
84	Porous, Rectangular, Small	YES	3	2	3.09	.585	TRACER
84	Porous, Rectangular, Small	YES	3	2	3.09	.585	TRACER
84	Porous, Rectangular, Small	YES	3	2	3.09	.585	COMPUTED_MEANS
85	Porous, Rectangular, Small	YES	3	3	1.08	.519	TRACER
85	Porous, Rectangular, Small	YES	3	3	1.08	.519	TRACER
85	Porous, Rectangular, Small	YES	3	3	1.08	.519	TRACER
85	Porous, Rectangular, Small	YES	3	3	1.08	.519	TRACER
85	Porous, Rectangular, Small	YES	3	3	1.08	.519	TRACER
85	Porous, Rectangular, Small	YES	3	3	1.08	.519	TRACER
85	Porous, Rectangular, Small	YES	3	3	1.08	.519	COMPUTED_MEANS
86	Porous, Rectangular, Small	YES	4	3	2.94	.856	TRACER
86	Porous, Rectangular, Small	YES	4	3	2.94	.856	TRACER
86	Porous, Rectangular, Small	YES	4	3	2.94	.856	TRACER
86	Porous, Rectangular, Small	YES	4	3	2.94	.856	TRACER
86	Porous, Rectangular, Small	YES	4	3	2.94	.856	TRACER
86	Porous, Rectangular, Small	YES	4	3	2.94	.856	TRACER
86	Porous, Rectangular, Small	YES	4	3	2.94	.856	COMPUTED_MEANS
87	Porous, Rectangular, Small	YES	4	4	1.34	.77	TRACER
87	Porous, Rectangular, Small	YES	4	4	1.34	.77	TRACER
87	Porous, Rectangular, Small	YES	4	4	1.34	.77	TRACER
87	Porous, Rectangular, Small	YES	4	4	1.34	.77	TRACER
87	Porous, Rectangular, Small	YES	4	4	1.34	.77	TRACER
87	Porous, Rectangular, Small	YES	4	4	1.34	.77	TRACER
87	Porous, Rectangular, Small	YES	4	4	1.34	.77	COMPUTED_MEANS
88	Porous, Rectangular, Small	YES	5	4	2.85	1.123	TRACER
88	Porous, Rectangular, Small	YES	5	4	2.85	1.123	TRACER
88	Porous, Rectangular, Small	YES	5	4	2.85	1.123	TRACER
88	Porous, Rectangular, Small	YES	5	4	2.85	1.123	TRACER
88	Porous, Rectangular, Small	YES	5	4	2.85	1.123	TRACER
88	Porous, Rectangular, Small	YES	5	4	2.85	1.123	COMPUTED_MEANS
89	Porous, Rectangular, Small	YES	5	5	1.35	.966	TRACER
89	Porous, Rectangular, Small	YES	5	5	1.35	.966	TRACER
89	Porous, Rectangular, Small	YES	5	5	1.35	.966	TRACER
89	Porous, Rectangular, Small	YES	5	5	1.35	.966	TRACER
89	Porous, Rectangular, Small	YES	5	5	1.35	.966	TRACER
89	Porous, Rectangular, Small	YES	5	5	1.35	.966	TRACER
89	Porous, Rectangular, Small	YES	5	5	1.35	.966	COMPUTED_MEANS
90	Porous, Rectangular, Small	YES	6	5	2.89	1.414	TRACER
90	Porous, Rectangular, Small	YES	6	5	2.89	1.414	TRACER
90	Porous, Rectangular, Small	YES	6	5	2.89	1.414	TRACER

Continued on next page

104

Table B.4: Solids Mobilization Experimental Data — Large Flume Study — Part 1. — Continued

EXP	MODEL	THRT	PUM	VAL	DEP	Q	DATA TYPE
90	Porous, Rectangular, Small	YES	6	5	2.89	1.414	TRACER
90	Porous, Rectangular, Small	YES	6	5	2.89	1.414	TRACER
90	Porous, Rectangular, Small	YES	6	5	2.89	1.414	TRACER
90	Porous, Rectangular, Small	YES	6	5	2.89	1.414	COMPUTED_MEANS
91	Porous, Rectangular, Small	YES	6	6	1.59	1.258	TRACER
91	Porous, Rectangular, Small	YES	6	6	1.59	1.258	TRACER
91	Porous, Rectangular, Small	YES	6	6	1.59	1.258	TRACER
91	Porous, Rectangular, Small	YES	6	6	1.59	1.258	TRACER
91	Porous, Rectangular, Small	YES	6	6	1.59	1.258	TRACER
91	Porous, Rectangular, Small	YES	6	6	1.59	1.258	COMPUTED_MEANS

Table B.5: Solids Mobilization Experimental Data — Large Flume Study — Part 2.

[EXP is the experiment number; D_UP is the approach depth above the mobile bed (datalogger and/or imagery) in inches; FRMS is the number of $\frac{1}{30}$ second image frames; DIST is the tracer distance traveled, in inches; V_1 is velocity from image analysis in feet per second ;V_2 is velocity from laboratory notebook, in feet per second;$\bar{V}$ is the average of the two tracer-type velocities, in feet per second; $V_{computed}$ is a velocity computed from the nominal discharge, in feet per second.

EXP	D_UP	FRMS	DIST	V_1	V_2	$\bar{V}$	$V_{computed}$
1	.42	18	4.0	.56	.56	.56	.68
1	.42	27	6.0	.56	.56	.56	.68
1	.42	17	5.0	.69	.74	.71	.68
1	.42	32	6.0	.5	.47	.48	.68
1	.42	17	6.0	1.	.88	.94	.68
1	.42	15	5.0	.83	.83	.83	.68
1	.42		.0	.69	.67	.68	.68
2	.51	13	4.0	.56	.77	.66	.66
2	.51	17	5.0	.69	.74	.71	.66
2	.51	16	4.0	.56	.63	.59	.66
2	.51	14	4.0	.67	.71	.69	.66
2	.51	18	5.0	.69	.69	.69	.66
2	.51	21	5.0	.6	.6	.6	.66
2	.51		.0	.63	.69	.66	.66
3-A	.46	28	5.0	.46	.45	.45	.56
3-A	.46	30	6.0	.5	.5	.5	.56
3-A	.46	19	7.0	.97	.92	.95	.56
3-A	.46	32	7.0	.53	.55	.54	.56
3-A	.46	25	5.0	.52	.5	.51	.56
3-A	.46	30	5.0	.42	.42	.42	.56
3-A	.46		.0	.57	.56	.56	.56
3-B	.4	26	5.0	.46	.48	.47	.55
3-B	.4	35	6.0	.42	.43	.42	.55
3-B	.4	30	7.0	.65	.58	.62	.55
3-B	.4	19	7.0	.97	.92	.95	.55
3-B	.4	28	5.0	.42	.45	.43	.55
3-B	.4	33	5.0	.38	.38	.38	.55
3-B	.4		.0	.55	.54	.54	.55
4-A	.65	18	6.0	.83	.83	.83	.95
4-A	.65	6	3.0	1.25	1.25	1.25	.95
4-A	.65	10	4.0	.83	1.	.92	.95
4-A	.65	13	4.0	.83	.77	.8	.95
4-A	.65	11	4.0	1.11	.91	1.01	.95
4-A	.65	11	4.0	1.67	.91	1.29	.95
4-A	.65		.0	.97	.95	.96	.95
4-B	.61	12	5.0	1.04	1.04	1.04	.99
4-B	.61	16	5.0	.6	.78	.69	.99
4-B	.61	9	4.0	1.11	1.11	1.11	.99
4-B	.61	13	5.0	1.04	.96	1.	.99
4-B	.61	11	5.0	1.04	1.14	1.09	.99
4-B	.61	11	6.0	1.67	1.36	1.52	.99
4-B	.61		.0	.97	1.01	.99	.99
5	.73	7	4.0	1.67	1.43	1.55	1.15

Continued on next page

Table B.5: Solids Mobilization Experimental Data — Large Flume Study — Part 2. — Continued

EXP	D_UP	FRMS	DIST	V_1	V_2	$\bar{V}$	$V_{computed}$
5	.73	12	6.0	1.	1.25	1.13	1.15
5	.73	6	3.0	.63	1.25	.94	1.15
5	.73	7	4.0	.83	1.43	1.13	1.15
5	.73	9	4.0	1.11	1.11	1.11	1.15
5	.73	8	4.0	.83	1.25	1.04	1.15
5	.73		.0	1.01	1.29	1.15	1.15
6-A	.69	13	5.0	1.04	.96	1.	1.1
6-A	.69	13	5.0	1.04	.96	1.	1.1
6-A	.69	11	7.0	1.17	1.59	1.38	1.1
6-A	.69	11	4.0	.83	.91	.87	1.1
6-A	.69	9	4.0	1.11	1.11	1.11	1.1
6-A	.69	7	5.0	.69	1.79	1.24	1.1
6-A	.69		.0	.98	1.22	1.1	1.1
6-B	.69	11	5.0	1.04	1.14	1.09	1.01
6-B	.69	11	5.0	1.04	1.14	1.09	1.01
6-B	.69	12	5.0	.83	1.04	.94	1.01
6-B	.69	16	6.0	.83	.94	.89	1.01
6-B	.69	8	4.0	.83	1.25	1.04	1.01
6-B	.69		.0	.92	1.1	1.01	1.01
7	.61	9	4.0	1.11	1.11	1.11	1.15
7	.61	6	4.0	1.11	1.67	1.39	1.15
7	.61	9	4.0	1.11	1.11	1.11	1.15
7	.61	9	4.0	1.11	1.11	1.11	1.15
7	.61	10	4.0	1.11	1.	1.06	1.15
7	.61	8	4.0	1.11	1.25	1.18	1.15
7	.61	9	4.0	.83	1.11	.97	1.15
7	.61		.0	1.11	1.19	1.15	1.15
8	.38	20	4.0	.48	.5	.49	.49
8	.38	22	4.0	.42	.45	.44	.49
8	.38	22	4.0	.37	.45	.41	.49
8	.38	24	4.0	.42	.42	.42	.49
8	.38	19	4.0	.48	.53	.5	.49
8	.38	27	4.0	.33	.37	.35	.49
8	.38		.0	.43	.47	.45	.49
9	.43	14	4.0	.67	.71	.69	.71
9	.43	12	4.0	.67	.83	.75	.71
9	.43	15	4.0	.67	.67	.67	.71
9	.43	14	4.0	.67	.71	.69	.71
9	.43	15	4.0	.67	.67	.67	.71
9	.43	12	4.0	.67	.83	.75	.71
9	.43		.0	.67	.74	.7	.71
10	.44	13	4.0	.67	.77	.72	.76
10	.44	12	4.0	.83	.83	.83	.76
10	.44	16	4.0	.56	.63	.59	.76
10	.44	14	4.0	.67	.71	.69	.76
10	.44	11	4.0	.83	.91	.87	.76
10	.44	11	4.0	.83	.91	.87	.76
10	.44		.0	.73	.79	.76	.76
11	.39	14	4.0	.83	.71	.77	.8
11	.39	13	4.0	.83	.77	.8	.8

Continued on next page

Table B.5: Solids Mobilization Experimental Data — Large Flume Study — Part 2. — Continued

EXP	D_UP	FRMS	DIST	V_1	V_2	V	$V_{computed}$
11	.39	12	4.0	.67	.83	.75	.8
11	.39	11	4.0	.83	.91	.87	.8
11	.39	12	4.0	.83	.83	.83	.8
11	.39	11	4.0	.67	.91	.79	.8
11	.39		.0	.78	.83	.8	.8
12	.39	10	4.0	.83	1.	.92	.89
12	.39	10	4.0	1.11	1.	1.06	.89
12	.39	12	4.0	.83	.83	.83	.89
12	.39	12	4.0	.83	.83	.83	.89
12	.39	11	4.0	.83	.91	.87	.89
12	.39	10	4.0	.83	1.	.92	.89
12	.39	11	4.0	.83	.91	.87	.89
12	.39		.0	.83	.93	.88	.89
13	.38	10	4.0	1.11	1.	1.06	.89
13	.38	12	4.0	.83	.83	.83	.89
13	.38	12	4.0	.83	.83	.83	.89
13	.38	10	4.0	.83	1.	.92	.89
13	.38	9	4.0	.83	1.11	.97	.89
13	.38	11	4.0	.83	.91	.87	.89
13	.38		.0	.83	.95	.89	.89
14	.38	11	4.0	1.11	.91	1.01	.97
14	.38	10	4.0	1.11	1.	1.06	.97
14	.38	12	4.0	.83	.83	.83	.97
14	.38	12	4.0	.83	.83	.83	.97
14	.38	11	4.0	1.11	.91	1.01	.97
14	.38	11	4.0	.83	.91	.87	.97
14	.38		.0	.97	.9	.94	.97
15	.41	8	4.0	1.11	1.25	1.18	1.07
15	.41	9	4.0	.83	1.11	.97	1.07
15	.41	10	4.0	1.11	1.	1.06	1.07
15	.41	12	4.0	1.11	.83	.97	1.07
15	.41	9	4.0	1.11	1.11	1.11	1.07
15	.41	11	4.0	1.11	.91	1.01	1.07
15	.41		.0	1.11	1.04	1.07	1.07
16	.43	10	4.0	.83	1.	.92	.93
16	.43	10	4.0	1.11	1.	1.06	.93
16	.43	12	4.0	.83	.83	.83	.93
16	.43	11	4.0	1.11	.91	1.01	.93
16	.43	11	4.0	1.11	.91	1.01	.93
16	.43	12	4.0	.83	.83	.83	.93
16	.43		.0	.97	.91	.94	.94
17	.62	16	4.0	.67	.63	.65	.71
17	.62	14	4.0	.67	.71	.69	.71
17	.62	14	4.0	.67	.71	.69	.71
17	.62	12	4.0	.83	.83	.83	.71
17	.62	14	4.0	.67	.71	.69	.71
17	.62	15	4.0	.67	.67	.67	.71
17	.62	14	4.0	.83	.71	.77	.71
17	.62		.0	.71	.71	.71	.71
18	.52	11	4.0	.67	.91	.79	1.91

Continued on next page

Table B.5: Solids Mobilization Experimental Data — Large Flume Study — Part 2. — Continued

EXP	D_UP	FRMS	DIST	V_1	V_2	$\bar{V}$	$V_{computed}$
18	.52	11	4.0	1.11	.91	1.01	1.91
18	.52	11	4.0	1.11	.91	1.01	1.91
18	.52	11	4.0	.83	.91	.87	1.91
18	.52	12	4.0	.83	.83	.83	1.91
18	.52	10	4.0	.83	1.	.92	1.91
18	.52	12	4.0	.83	.83	.83	1.91
18	.52		.0	.89	.9	.89	1.91
19	.61	13	4.0	.83	.77	.8	.78
19	.61	12	4.0	.83	.83	.83	.78
19	.61	14	4.0	.67	.71	.69	.78
19	.61	13	4.0	.83	.77	.8	.78
19	.61	12	4.0	.83	.83	.83	.78
19	.61	13	4.0	.83	.77	.8	.78
19	.61		.0	.81	.78	.79	.78
20	.5	19	5.0	.69	.66	.68	.73
20	.5	15	5.0	.6	.83	.71	.73
20	.5	17	5.0	.52	.74	.63	.73
20	.5	17	5.0	.69	.74	.71	.73
20	.5	15	5.0	.69	.83	.76	.73
20	.5	16	5.0	.6	.78	.69	.73
20	.5		.0	.63	.76	.7	.73
21	.52	17	5.0	.69	.74	.71	.77
21	.52	18	5.0	.69	.69	.69	.77
21	.52	17	5.0	.6	.74	.67	.77
21	.52	17	5.0	.6	.74	.67	.77
21	.52	18	5.0	.69	.69	.69	.77
21	.52	15	5.0	.69	.83	.76	.77
21	.52		.0	.66	.74	.7	.77
22	.53	13	5.0	.83	.96	.9	.85
22	.53	11	5.0	.83	1.14	.98	.85
22	.53	15	5.0	.69	.83	.76	.85
22	.53	14	5.0	.83	.89	.86	.85
22	.53	18	5.0	.69	.69	.69	.85
22	.53	19	5.0	.69	.66	.68	.85
22	.53		.0	.76	.86	.81	.85
23	.53	12	5.0	1.04	1.04	1.04	.84
23	.53	15	5.0	.83	.83	.83	.84
23	.53	16	5.0	.69	.78	.74	.84
23	.53	16	5.0	.69	.78	.74	.84
23	.53	14	5.0	.83	.89	.86	.84
23	.53	16	5.0	.69	.78	.74	.84
23	.53		.0	.8	.85	.83	.84
24	.53	9	5.0	.69	1.39	1.04	.82
24	.53	14	5.0	.83	.89	.86	.82
24	.53	15	5.0	.83	.83	.83	.82
24	.53	16	5.0	.69	.78	.74	.82
24	.53	15	5.0	.83	.83	.83	.82
24	.53	17	5.0	.83	.74	.78	.82
24	.53		.0	.79	.91	.85	.82
25	.31	57	5.0	.21	.22	.21	.25

Continued on next page

109

Table B.5: Solids Mobilization Experimental Data — Large Flume Study — Part 2. — Continued

EXP	D_UP	FRMS	DIST	V_1	V_2	$\bar{V}$	$V_{computed}$
25	.31	38	5.0	.3	.33	.31	.25
25	.31	56	5.0	.19	.22	.21	.25
25	.31		.0	.12	.13	.12	.25
26	.38	11	5.0	1.04	1.14	1.09	.92
26	.38	12	5.0	1.04	1.04	1.04	.92
26	.38	11	5.0	.83	1.14	.98	.92
26	.38	33	5.0	.42	.38	.4	.92
26	.38	9	5.0	1.04	1.39	1.22	.92
26	.38	13	5.0	.83	.96	.9	.92
26	.38		.0	.87	1.01	.94	.92
27	.47	10	5.0	.83	1.25	1.04	1.04
27	.47	12	5.0	.83	1.04	.94	1.04
27	.47	10	5.0	1.04	1.25	1.15	1.04
27	.47	12	5.0	1.04	1.04	1.04	1.04
27	.47	11	5.0	.83	1.14	.98	1.04
27	.47	10	5.0	.83	1.25	1.04	1.04
27	.47		.0	.9	1.16	1.03	1.04
28	.76	11	5.0	1.04	1.14	1.09	.92
28	.76	13	5.0	.83	.96	.9	.92
28	.76	15	5.0	.69	.83	.76	.92
28	.76	13	5.0	.69	.96	.83	.92
28	.76	14	5.0	.83	.89	.86	.92
28	.76	11	5.0	1.04	1.14	1.09	.92
28	.76		.0	.86	.99	.92	.92
29	.79	21	4.0	.42	.48	.45	.73
29	.79	10	2.0	.33	.5	.42	.73
29	.79	7	3.0	.83	1.07	.95	.73
29	.79	10	4.0	1.11	1.	1.06	.73
29	.79	9	4.0	.83	1.11	.97	.73
29	.79	8	3.0	.5	.94	.72	.73
29	.79		.0	.67	.85	.76	.73
30	.85	7	4.0	1.11	1.43	1.27	1.24
30	.85	6	4.0	1.11	1.67	1.39	1.24
30	.85	6	3.0	1.25	1.25	1.25	1.24
30	.85	6	3.0	.63	1.25	.94	1.24
30	.85	7	4.0	1.11	1.43	1.27	1.24
30	.85	7	4.0	1.11	1.43	1.27	1.24
30	.85		.0	1.05	1.41	1.23	1.24
31	.91	10	4.0	.83	1.	.92	1.23
31	.91	11	5.0	1.04	1.14	1.09	1.23
31	.91	12	3.0	.63	.63	.63	1.23
31	.91		.0	.83	.92	.88	1.23
32	1.1	18	7.0	1.17	.97	1.07	1.08
33	1.1	18	5.0	.69	.69	.69	.06
33	1.1	16	5.0	.6	.78	.69	.06
33	1.1	13	5.0	1.04	.96	1.	.06
33	1.1	14	5.0	.83	.89	.86	.06
33	1.1	19	5.0	.69	.66	.68	.06
33	1.1	18	5.0	.69	.69	.69	.06
33	1.1	20	5.0	.69	.63	.66	.06

Continued on next page

Table B.5: Solids Mobilization Experimental Data — Large Flume Study — Part 2. — Continued

EXP	D_UP	FRMS	DIST	V_1	V_2	$\bar{V}$	$V_{computed}$
33	1.1		.0	.76	.78	.77	.06
34	1.5	14	7.0	1.17	1.25	1.21	.07
34	1.5	10	4.0	.83	1.	.92	.07
34	1.5	12	5.0	1.04	1.04	1.04	.07
34	1.5	13	5.0	1.04	.96	1.	.07
34	1.5	12	5.0	1.04	1.04	1.04	.07
34	1.5	11	5.0	1.04	1.14	1.09	.07
34	1.5		.0	1.03	1.07	1.05	.07
35	.42	26	5.0	.42	.48	.45	.52
35	.42	20	4.0	.56	.5	.53	.52
35	.42	16	4.0	.56	.63	.59	.52
35	.42	21	4.0	.48	.48	.48	.52
35	.42	18	4.0	.48	.56	.52	.52
35	.42		.0	.5	.53	.51	.52
36	.55	10	5.0	1.39	1.25	1.32	1.13
36	.55	11	5.0	1.39	1.14	1.26	1.13
36	.55	16	5.0	.83	.78	.81	1.13
36	.55	9	4.0	1.11	1.11	1.11	1.13
36	.55		.0	1.18	1.07	1.13	1.13
37	.58	11	5.0	1.04	1.14	1.09	1.16
37	.58	14	7.0	1.17	1.25	1.21	1.16
37	.58	10	5.0	1.39	1.25	1.32	1.16
37	.58	11	5.0	1.04	1.14	1.09	1.16
37	.58	10	5.0	1.04	1.25	1.15	1.16
37	.58	12	5.0	1.04	1.04	1.04	1.16
37	.58		.0	1.12	1.18	1.15	1.16
38	.69	12	5.0	1.04	1.04	1.04	1.15
38	.69	10	5.0	1.04	1.25	1.15	1.15
38	.69	12	6.0	1.	1.25	1.13	1.15
38	.69	12	6.0	1.25	1.25	1.25	1.15
38	.69	12	6.0	1.25	1.25	1.25	1.15
38	.69	14	6.0	1.	1.07	1.04	1.15
38	.69		.0	1.1	1.19	1.14	1.15
39	.91	12	4.0	.83	.83	.83	.69
39	.91	13	4.0	.67	.77	.72	.69
39	.91	17	4.0	.67	.59	.63	.69
39	.91	14	4.0	.56	.71	.63	.69
39	.91		.0	.68	.73	.7	.69
40	.81	11	5.0	1.04	1.14	1.09	1.17
40	.81	8	4.0	1.11	1.25	1.18	1.17
40	.81	8	4.0	1.11	1.25	1.18	1.17
40	.81	8	4.0	1.11	1.25	1.18	1.17
40	.81		.0	1.09	1.22	1.16	1.17
41	.79	10	6.0	1.25	1.5	1.38	1.19
41	.79	11	5.0	1.04	1.14	1.09	1.19
41	.79	11	5.0	1.04	1.14	1.09	1.19
41	.79		.0	1.11	1.26	1.18	1.19
42	.85	7	3.0	1.25	1.07	1.16	1.16
42	.85	9	5.0	.83	1.39	1.11	1.16
42	.85	14	6.0	1.25	1.07	1.16	1.16

Table B.5: Solids Mobilization Experimental Data — Large Flume Study — Part 2. — Continued

EXP	D_UP	FRMS	DIST	V_1	V_2	$\bar{V}$	$V_{computed}$
42	.85		.0	1.11	1.18	1.14	1.16
43	.51	26	5.0	.46	.48	.47	.4
43	.51	24	4.0	.42	.42	.42	.4
43	.51	31	5.0	.38	.4	.39	.4
43	.51	32	4.0	.24	.31	.28	.4
43	.51	27	5.0	.46	.46	.46	.4
43	.51	26	4.0	.33	.38	.36	.4
43	.51		.0	.38	.41	.4	.4
44	.55	23	5.0	.46	.54	.5	.51
44	.55	24	5.0	.42	.52	.47	.51
44	.55	19	5.0	.52	.66	.59	.51
44	.55	24	5.0	.52	.52	.52	.51
44	.55	28	5.0	.46	.45	.45	.51
44	.55	26	5.0	.52	.48	.5	.51
44	.55		.0	.48	.53	.51	.51
45	.53	22	5.0	.6	.57	.58	.53
45	.53	23	5.0	.52	.54	.53	.53
45	.53	22	5.0	.52	.57	.54	.53
45	.53	22	5.0	.52	.57	.54	.53
45	.53	24	5.0	.52	.52	.52	.53
45	.53	23	5.0	.6	.54	.57	.53
45	.53		.0	.55	.55	.55	.53
46	.53	19	5.0	.6	.66	.63	.6
46	.53	19	4.0	.56	.53	.54	.6
46	.53	22	5.0	.6	.57	.58	.6
46	.53	19	5.0	.69	.66	.68	.6
46	.53	21	5.0	.6	.6	.6	.6
46	.53	22	5.0	.6	.57	.58	.6
46	.53		.0	.61	.6	.6	.6
47	.5	20	5.0	.6	.63	.61	.62
47	.5	22	5.0	.52	.57	.54	.62
47	.5	22	5.0	.6	.57	.58	.62
47	.5	17	5.0	.83	.74	.78	.62
47	.5	21	5.0	.6	.6	.6	.62
47	.5	20	5.0	.6	.63	.61	.62
47	.5		.0	.62	.62	.62	.62
48	.5	18	5.0	.69	.69	.69	.71
48	.5	17	5.0	.69	.74	.71	.71
48	.5	15	5.0	.83	.83	.83	.71
48	.5	17	5.0	.69	.74	.71	.71
48	.5	18	5.0	.6	.69	.64	.71
48	.5	19	5.0	.69	.66	.68	.71
48	.5		.0	.7	.73	.71	.71
49	.39	23	5.0	.6	.54	.57	.65
49	.39	19	5.0	.6	.66	.63	.65
49	.39	19	5.0	.6	.66	.63	.65
49	.39	17	5.0	.69	.74	.71	.65
49	.39	18	5.0	.69	.69	.69	.65
49	.39		.0	.63	.66	.65	.65
50	.41	17	5.0	.69	.74	.71	.65

Continued on next page

Table B.5: Solids Mobilization Experimental Data — Large Flume Study — Part 2. — Continued

EXP	D_UP	FRMS	DIST	V_1	V_2	$\bar{V}$	$V_{computed}$
50	.41	19	5.0	.6	.66	.63	.65
50	.41	18	5.0	.6	.69	.64	.65
50	.41	21	5.0	.6	.6	.6	.65
50	.41	18	5.0	.6	.69	.64	.65
50	.41	18	5.0	.6	.69	.64	.65
50	.41		.0	.61	.68	.65	.65
51	.4	18	5.0	.6	.69	.64	.75
51	.4	17	5.0	.83	.74	.78	.75
51	.4	13	5.0	.83	.96	.9	.75
51	.4	16	5.0	.69	.78	.74	.75
51	.4	17	5.0	.69	.74	.71	.75
51	.4	17	5.0	.69	.74	.71	.75
51	.4		.0	.72	.77	.75	.75
52	.37	15	5.0	.69	.83	.76	.81
52	.37	17	5.0	.69	.74	.71	.81
52	.37	12	5.0	1.04	1.04	1.04	.81
52	.37	15	5.0	.83	.83	.83	.81
52	.37	15	5.0	.69	.83	.76	.81
52	.37	17	5.0	.69	.74	.71	.81
52	.37		.0	.78	.84	.81	.81
53	.42	17	5.0	.69	.74	.71	.71
53	.42	16	5.0	.83	.78	.81	.71
53	.42	17	5.0	.69	.74	.71	.71
53	.42	19	5.0	.69	.66	.68	.71
53	.42	17	5.0	.69	.74	.71	.71
53	.42	18	5.0	.69	.69	.69	.7
53	.42		.0	.72	.72	.72	.71
54	.41	24	5.0	.52	.52	.52	.54
54	.41	17	5.0	.69	.74	.71	.54
54	.41	24	5.0	.52	.52	.52	.54
54	.41	33	5.0	.38	.38	.38	.54
54	.41	22	5.0	.6	.57	.58	.54
54	.41		.0	.54	.54	.54	.54
55	.51	13	5.0	1.04	.96	1.	.85
55	.51	16	5.0	.69	.78	.74	.85
55	.51	16	5.0	.69	.78	.74	.85
55	.51	18	5.0	.69	.69	.69	.85
55	.51	12	5.0	1.04	1.04	1.04	.85
55	.51		.0	.83	.85	.84	.85
56	.54	13	5.0	1.04	.96	1.	.99
56	.54	13	5.0	1.04	.96	1.	.99
56	.54	12	5.0	.83	1.04	.94	.99
56	.54	12	5.0	1.04	1.04	1.04	.99
56	.54	12	5.0	.83	1.04	.94	.99
56	.54		.0	.96	1.01	.99	.99
57	.58	10	4.0	.83	1.	.92	.85
57	.58	13	4.0	.67	.77	.72	.85
57	.58	13	5.0	.83	.96	.9	.85
57	.58	18	5.0	.69	.69	.69	.85
57	.58	7	3.0	.83	1.07	.95	.85

Continued on next page

Table B.5: Solids Mobilization Experimental Data — Large Flume Study — Part 2. — Continued

EXP	D_UP	FRMS	DIST	V_1	V_2	V	$V_{computed}$
57	.58		.0	.77	.9	.84	.85
58	.87	8	5.0	1.39	1.56	1.48	1.1
58	.87	12	5.0	1.04	1.04	1.04	1.1
58	.87	9	5.0	1.04	1.39	1.22	1.1
58	.87	11	4.0	.83	.91	.87	1.1
58	.87	11	4.0	.83	.91	.87	1.1
58	.87		.0	1.03	1.16	1.1	1.1
59	.82	8	4.0	1.11	1.25	1.18	1.16
59	.82	4	2.0	.83	1.25	1.04	1.16
59	.82	12	6.0	1.25	1.25	1.25	1.16
59	.82	9	5.0	1.39	1.39	1.39	1.16
59	.82	9	4.0	1.11	1.11	1.11	1.16
59	.82		.0	1.14	1.16	1.15	1.16
60	.74	5	4.0	1.11	2.	1.56	1.51
60	.74	9	4.0	1.11	1.11	1.11	1.51
60	.74	9	5.0	1.39	1.39	1.39	1.51
60	.74	8	6.0	1.67	1.88	1.77	1.51
60	.74	3	2.0	1.67	1.67	1.67	1.51
60	.74		.0	1.39	1.61	1.5	1.51
61	.73	7	3.0	.83	1.07	.95	1.73
61	.73	4	3.0	2.5	1.88	2.19	1.73
61	.73	5	4.0	1.11	2.	1.56	1.73
61	.73	8	7.0	1.94	2.19	2.07	1.73
61	.73	7	5.0	1.39	1.79	1.59	1.73
61	.73	3	4.0	1.67	3.33	2.5	1.73
61	.73	5	4.0	1.67	2.	1.83	1.73
61	.73	8	4.0	1.11	1.25	1.18	1.73
61	.73		.0	1.53	1.94	1.73	1.73
62	.32	17	4.0	.56	.59	.57	.63
62	.32	16	4.0	.67	.63	.65	.63
62	.32	17	4.0	.67	.59	.63	.63
62	.32	16	4.0	.56	.63	.59	.63
62	.32	14	4.0	.67	.71	.69	.63
62	.32		.0	.62	.63	.63	.63
63	.34	15	4.0	.83	.67	.75	.7
63	.34	15	4.0	.67	.67	.67	.7
63	.34	15	4.0	.67	.67	.67	.7
63	.34	14	4.0	.67	.71	.69	.7
63	.34	16	5.0	.69	.78	.74	.7
63	.34		.0	.71	.7	.7	.7
64	.65	14	4.0	.67	.71	.69	.77
64	.65	13	4.0	.83	.77	.8	.77
64	.65	14	4.0	.83	.71	.77	.77
64	.65	11	4.0	.83	.91	.87	.77
64	.65	14	4.0	.67	.71	.69	.77
64	.65		.0	.77	.76	.77	.77
65	1.1	14	5.0	.83	.89	.86	.82
65	1.1	18	5.0	.69	.69	.69	.82
65	1.1	13	4.0	.83	.77	.8	.82
65	1.1	15	5.0	.83	.83	.83	.82

Continued on next page

Table B.5: Solids Mobilization Experimental Data — Large Flume Study — Part 2. — Continued

EXP	D_UP	FRMS	DIST	V_1	V_2	$\bar{V}$	$V_{computed}$
65	1.1	16	6.0	.83	.94	.89	.82
65	1.1		.0	.81	.83	.82	.82
66	1.35	13	4.0	.83	.77	.8	.8
66	1.35	14	4.0	.67	.71	.69	.8
66	1.35	17	6.0	.83	.88	.86	.8
66	1.35	13	4.0	.67	.77	.72	.8
66	1.35	13	4.0	.83	.77	.8	.8
66	1.35		.0	.77	.78	.77	.8
67	1.35	11	4.0	1.11	.91	1.01	.89
67	1.35	22	8.0	.95	.91	.93	.89
67	1.35	13	4.0	.83	.77	.8	.89
67	1.35	9	4.0	.83	1.11	.97	.89
67	1.35	13	4.0	.67	.77	.72	.89
67	1.35		.0	.88	.89	.89	.89
68	1.98	13	6.0	1.25	1.15	1.2	.95
68	1.98	15	4.0	.67	.67	.67	.95
68	1.98	16	5.0	.69	.78	.74	.95
68	1.98	12	5.0	1.04	1.04	1.04	.95
68	1.98	9	4.0	1.11	1.11	1.11	.95
68	1.98		.0	.95	.95	.95	.95
69	2.1	13	5.0	1.04	.96	1.	.91
69	2.1	10	4.0	.83	1.	.92	.91
69	2.1	11	4.0	.83	.91	.87	.91
69	2.1	17	6.0	.83	.88	.86	.91
69	2.1	12	4.0	.83	.83	.83	.91
69	2.1		.0	.88	.92	.9	.91
70	2.2	12	5.0	.83	1.04	.94	.97
70	2.2	11	4.0	.83	.91	.87	.97
70	2.2	12	4.0	.83	.83	.83	.97
70	2.2	11	5.0	1.04	1.14	1.09	.97
70	2.2	10	4.0	1.11	1.	1.06	.97
70	2.2		.0	.93	.98	.96	.97
71	2.21	12	4.0	.83	.83	.83	.96
71	2.21	11	4.0	1.11	.91	1.01	.96
71	2.21	11	4.0	1.11	.91	1.01	.96
71	2.21	12	4.0	.83	.83	.83	.96
71	2.21	12	5.0	1.04	1.04	1.04	.96
71	2.21		.0	.99	.91	.95	.96
72	.44	19	5.0	.6	.66	.63	.47
72	.44	29	4.0	.33	.34	.34	.47
72	.44	24	4.0	.37	.42	.39	.47
72	.44	24	5.0	.52	.52	.52	.47
72	.44	24	5.0	.46	.52	.49	.47
72	.44		.0	.46	.49	.47	.47
73	1.2	19	5.0	1.04	.66	.85	.6
73	1.2	29	5.0	.52	.43	.48	.6
73	1.2	24	5.0	.52	.52	.52	.6
73	1.2	24	5.0	.46	.52	.49	.6
73	1.2	24	5.0	.69	.52	.61	.6
73	1.2		.0	.65	.53	.59	.6

Continued on next page

115

Table B.5: Solids Mobilization Experimental Data — Large Flume Study — Part 2. — Continued

EXP	D_UP	FRMS	DIST	V_1	V_2	V	$V_{computed}$
74	1.34	12	5.0	1.04	1.04	1.04	.82
74	1.34	13	5.0	1.04	.96	1.	.82
74	1.34	10	4.0	.83	1.	.92	.82
74	1.34	13	4.0	.83	.77	.8	.82
74	1.34		.0	.75	.88	.81	.82
75	1.61	21	5.0	.6	.6	.6	.94
75	1.61	11	5.0	1.04	1.14	1.09	.94
75	1.61	9	4.0	1.11	1.11	1.11	.94
75	1.61	10	4.0	1.11	1.	1.06	.94
75	1.61	15	5.0	.83	.83	.83	.94
75	1.61		.0	.94	.94	.94	.94
76	2.21	17	5.0	.69	.74	.71	1.5
76	2.21	12	5.0	1.04	1.04	1.04	1.5
76	2.21	10	6.0	5.	1.5	3.25	1.5
76	2.21	10	5.0	1.04	1.25	1.15	1.5
76	2.21	10	5.0	1.39	1.25	1.32	1.5
76	2.21		.0	1.83	1.16	1.49	1.5
77	1.76	16	4.0	.67	.63	.65	1.06
77	1.76	11	5.0	1.04	1.14	1.09	1.06
77	1.76	10	5.0	1.04	1.25	1.15	1.06
77	1.76	12	5.0	.83	1.04	.94	1.06
77	1.76	8	5.0	2.08	1.56	1.82	1.06
77	1.76	17	5.0	.69	.74	.71	1.06
77	1.76		.0	1.06	1.06	1.06	1.06
78	2.	12	5.0	.83	1.04	.94	1.31
78	2.	6	5.0	2.08	2.08	2.08	1.31
78	2.	6	3.0	1.25	1.25	1.25	1.31
78	2.	11	6.0	1.25	1.36	1.31	1.31
78	2.	15	5.0	.83	.83	.83	1.31
78	2.	13	8.0	1.33	1.54	1.44	1.31
78	2.		.0	1.26	1.35	1.31	1.31
79	1.9	6	4.0	1.11	1.67	1.39	1.54
79	1.9	8	5.0	1.39	1.56	1.48	1.54
79	1.9	8	5.0	1.39	1.56	1.48	1.54
79	1.9	8	4.0	1.11	1.25	1.18	1.54
79	1.9	6	5.0	2.08	2.08	2.08	1.54
79	1.9		.0	1.42	1.63	1.52	1.54
80	2.8	9	6.0	1.67	1.67	1.67	1.78
80	2.8	5	3.0	1.25	1.5	1.38	1.78
80	2.8	5	5.0	2.08	2.5	2.29	1.78
80	2.8		.0	1.67	1.89	1.78	1.78
81	3.9	7	4.0	1.67	1.43	1.55	2.35
81	3.9	3	5.0	4.17	4.17	4.17	2.35
81	3.9	6	3.0	1.25	1.25	1.25	2.35
81	3.9		.0	2.36	2.28	2.32	2.35
82	.55	14	4.0	.67	.71	.69	.78
82	.55	14	4.0	.56	.71	.63	.78
82	.55	13	5.0	.83	.96	.9	.78
82	.55	13	4.0	.83	.77	.8	.78
82	.55	12	4.0	.83	.83	.83	.78

Continued on next page

116

Table B.5: Solids Mobilization Experimental Data — Large Flume Study — Part 2. — Continued

EXP	D_UP	FRMS	DIST	V_1	V_2	$\bar{V}$	$V_{computed}$
82	.55		.0	.74	.8	.77	.78
83	.99	16	6.0	.83	.94	.89	.76
83	.99	14	4.0	.67	.71	.69	.76
83	.99	14	4.0	.67	.71	.69	.76
83	.99	13	4.0	.83	.77	.8	.76
83	.99	15	4.0	.67	.67	.67	.76
83	.99		.0	.73	.76	.75	.76
84	1.22	9	4.0	1.11	1.11	1.11	1.07
84	1.22	13	4.0	.67	.77	.72	1.07
84	1.22	11	5.0	1.04	1.14	1.09	1.07
84	1.22	10	5.0	1.04	1.25	1.15	1.07
84	1.22	10	6.0	1.	1.5	1.25	1.07
84	1.22		.0	.97	1.15	1.06	1.07
85	1.3	9	4.0	1.11	1.11	1.11	1.11
85	1.3	8	4.0	1.11	1.25	1.18	1.11
85	1.3	10	5.0	1.39	1.25	1.32	1.11
85	1.3	11	5.0	1.04	1.14	1.09	1.11
85	1.3	13	5.0	.69	.96	.83	1.11
85	1.3	10	5.0	1.04	1.25	1.15	1.11
85	1.3		.0	1.06	1.16	1.11	1.11
86	1.44	15	4.0	.56	.67	.61	1.
86	1.44	12	5.0	1.04	1.04	1.04	1.
86	1.44	11	5.0	1.04	1.14	1.09	1.
86	1.44	8	4.0	1.11	1.25	1.18	1.
86	1.44	15	4.0	.67	.67	.67	1.
86	1.44	9	5.0	1.39	1.39	1.39	1.
86	1.44		.0	.97	1.03	1.	1.
87	2.1	11	5.0	1.04	1.14	1.09	1.22
87	2.1	7	3.0	1.25	1.07	1.16	1.22
87	2.1	8	5.0	1.39	1.56	1.48	1.22
87	2.1	6	3.0	1.25	1.25	1.25	1.22
87	2.1	9	4.0	1.11	1.11	1.11	1.22
87	2.1	8	4.0	1.11	1.25	1.18	1.22
87	2.1		.0	1.19	1.23	1.21	1.22
88	2.2	10	5.0	1.39	1.25	1.32	.59
88	2.2	9	5.0	1.39	1.39	1.39	.59
88	2.2	8	4.0	1.67	1.25	1.46	.59
88	2.2	7	4.0	1.11	1.43	1.27	.59
88	2.2	7	4.0	1.67	1.43	1.55	.59
88	2.2		.0	1.44	1.35	1.4	.59
89	2.1	9	5.0	1.39	1.39	1.39	.53
89	2.1	11	5.0	1.04	1.14	1.09	.53
89	2.1	16	6.0	.71	.94	.83	.53
89	2.1	10	7.0	1.46	1.75	1.6	.53
89	2.1	16	9.0	1.5	1.41	1.45	.53
89	2.1	8	6.0	1.67	1.88	1.77	.53
89	2.1		.0	1.29	1.42	1.36	.53
90	2.7	10	5.0	1.39	1.71	1.55	1.81
90	2.7	4	4.0	1.67	2.5	2.08	1.81
90	2.7	8	6.0	1.67	1.88	1.77	1.81

Continued on next page

117

Table B.5: Solids Mobilization Experimental Data — Large Flume Study — Part 2. — Continued

EXP	D_UP	FRMS	DIST	V_1	V_2	$\bar{V}$	$V_{computed}$
90	2.7	12	7.0	1.17	1.46	1.31	1.81
90	2.7	5	7.0	5.83	3.5	4.67	1.81
90	2.7	7	3.0	.83	1.07	.95	1.81
90	2.7		.0	1.86	1.73	1.8	1.81
91	3.2	6	3.0	1.25	1.25	1.25	1.33
91	3.2	11	5.0	1.04	1.14	1.09	1.33
91	3.2	12	8.0	1.67	1.67	1.67	1.33
91	3.2	4	3.0	1.25	1.88	1.56	1.33
91	3.2	8	3.0	1.25	.94	1.09	1.33
91	3.2		.0	1.29	1.37	1.33	1.33

Table B.6: Solids Mobilization Experimental Data — Large Flume Study — Part 3.

[EXP is the experiment number; SIZE is the size of the bed material (S=small, L=Large);TR_m is the motion of the bed material at tracer time; BED_m is the overall bed motion; STATUS is the culvert status after tracers have passed ; Fr_{tr} is a Froude number computed from the tracer velocities; Fr_{comp} is a Froude number computed from the nominal discharge.

EXP	SIZE	TR_m	BED_m	STATUS	Fr_{tr}	Fr_{comp}
1	S	NO	SALT	FREE	.69	.56
1	S	NO	SALT	FREE	.69	.56
1	S	NO	SALT	FREE	.69	.73
1	S	NO	SALT	FREE	.69	.49
1	S	NO	SALT	FREE	.69	.96
1	S	NO	SALT	FREE	.69	.85
1	S	NO	SALT	FREE	.69	.69
2	S	NO	SALT	FREE	.45	.45
2	S	NO	SALT	FREE	.45	.49
2	S	NO	SALT	FREE	.45	.4
2	S	NO	SALT	FREE	.45	.47
2	S	NO	SALT	FREE	.45	.47
2	S	NO	SALT	FREE	.45	.41
2	S	NO	SALT	FREE	.45	.45
3-A	S	NO	NO	FREE	.35	.28
3-A	S	NO	NO	FREE	.35	.31
3-A	S	NO	NO	FREE	.35	.59
3-A	S	NO	NO	FREE	.35	.34
3-A	S	NO	NO	FREE	.35	.32
3-A	S	NO	NO	FREE	.35	.26
3-A	S	NO	NO	FREE	.35	.35
3-B	S	NO	NO	FREE	.43	.37
3-B	S	NO	NO	FREE	.43	.33
3-B	S	NO	NO	FREE	.43	.48
3-B	S	NO	NO	FREE	.43	.74
3-B	S	NO	NO	FREE	.43	.34
3-B	S	NO	NO	FREE	.43	.3
3-B	S	NO	NO	FREE	.43	.43
4-A	S	NO	NO	FREE	.48	.42
4-A	S	NO	NO	FREE	.48	.63
4-A	S	NO	NO	FREE	.48	.47
4-A	S	NO	NO	FREE	.48	.41
4-A	S	NO	NO	FREE	.48	.51
4-A	S	NO	NO	FREE	.48	.65
4-A	S	NO	NO	FREE	.48	.49
4-B	S	NO	NO	FREE	.5	.52
4-B	S	NO	NO	FREE	.5	.34
4-B	S	NO	NO	FREE	.5	.56
4-B	S	NO	NO	FREE	.5	.5
4-B	S	NO	NO	FREE	.5	.55
4-B	S	NO	NO	FREE	.5	.76
4-B	S	NO	NO	FREE	.5	.49
5	S	YES	YES	FREE	.63	.85
5	S	YES	YES	FREE	.63	.62

119

Table B.6: Solids Mobilization Experimental Data — Large Flume Study — Part 3. — Continued

EXP	SIZE	TR_m	BED_m	STATUS	Fr_{tr}	Fr_{comp}
5	S	YES	YES	FREE	.63	.51
5	S	YES	YES	FREE	.63	.62
5	S	YES	YES	FREE	.63	.61
5	S	YES	YES	FREE	.63	.57
5	S	YES	YES	FREE	.63	.63
6-A	S	YES	YES	CLOG	.9	.82
6-A	S	YES	YES	CLOG	.9	.82
6-A	S	YES	YES	CLOG	.9	1.12
6-A	S	YES	YES	CLOG	.9	.71
6-A	S	YES	YES	CLOG	.9	.91
6-A	S	YES	YES	CLOG	.9	1.01
6-A	S	YES	YES	CLOG	.9	.9
6-B	S	YES	YES	SELF_CLEAR	.71	.76
6-B	S	YES	YES	SELF_CLEAR	.71	.76
6-B	S	YES	YES	SELF_CLEAR	.71	.66
6-B	S	YES	YES	SELF_CLEAR	.71	.62
6-B	S	YES	YES	SELF_CLEAR	.71	.73
6-B	S	YES	YES	SELF_CLEAR	.71	.71
7	S	YES	YES	CLOG	.62	.6
7	S	YES	YES	CLOG	.62	.75
7	S	YES	YES	CLOG	.62	.6
7	S	YES	YES	CLOG	.62	.6
7	S	YES	YES	CLOG	.62	.57
7	S	YES	YES	CLOG	.62	.64
7	S	YES	YES	CLOG	.62	.52
7	S	YES	YES	CLOG	.62	.62
8	S	NO	NO	FREE	.26	.26
8	S	NO	NO	FREE	.26	.23
8	S	NO	NO	FREE	.26	.22
8	S	NO	NO	FREE	.26	.22
8	S	NO	NO	FREE	.26	.27
8	S	NO	NO	FREE	.26	.19
8	S	NO	NO	FREE	.26	.24
9	S	NO	NO	1BBL_OPEN	.41	.4
9	S	NO	NO	1BBL_OPEN	.41	.43
9	S	NO	NO	1BBL_OPEN	.41	.38
9	S	NO	NO	1BBL_OPEN	.41	.4
9	S	NO	NO	1BBL_OPEN	.41	.38
9	S	NO	NO	1BBL_OPEN	.41	.43
9	S	NO	NO	1BBL_OPEN	.41	.41
10	S	SALT	SALT	1BBL_OPEN	.46	.43
10	S	SALT	SALT	1BBL_OPEN	.46	.5
10	S	SALT	SALT	1BBL_OPEN	.46	.35
10	S	SALT	SALT	1BBL_OPEN	.46	.41
10	S	SALT	SALT	1BBL_OPEN	.46	.52
10	S	SALT	SALT	1BBL_OPEN	.46	.52
10	S	SALT	SALT	1BBL_OPEN	.46	.46
11	S	SALT	SALT	1BBL_OPEN	.58	.56
11	S	SALT	SALT	1BBL_OPEN	.58	.58
11	S	SALT	SALT	1BBL_OPEN	.58	.54

Continued on next page

Table B.6: Solids Mobilization Experimental Data — Large Flume Study — Part 3. — Continued

EXP	SIZE	TR_m	BED_m	STATUS	Fr_{tr}	Fr_{comp}
11	S	SALT	SALT	1BBL_OPEN	.58	.63
11	S	SALT	SALT	1BBL_OPEN	.58	.6
11	S	SALT	SALT	1BBL_OPEN	.58	.57
11	S	SALT	SALT	1BBL_OPEN	.58	.58
12	S	NO	SALT	1BBL_OPEN	.5	.51
12	S	NO	SALT	1BBL_OPEN	.5	.59
12	S	NO	SALT	1BBL_OPEN	.5	.46
12	S	NO	SALT	1BBL_OPEN	.5	.46
12	S	NO	SALT	1BBL_OPEN	.5	.48
12	S	NO	SALT	1BBL_OPEN	.5	.51
12	S	NO	SALT	1BBL_OPEN	.5	.48
12	S	NO	SALT	1BBL_OPEN	.5	.49
13	S	NO	SALT	SELF_CLEAR	.48	.57
13	S	NO	SALT	SELF_CLEAR	.48	.45
13	S	NO	SALT	SELF_CLEAR	.48	.45
13	S	NO	SALT	SELF_CLEAR	.48	.49
13	S	NO	SALT	SELF_CLEAR	.48	.52
13	S	NO	SALT	SELF_CLEAR	.48	.47
13	S	NO	SALT	SELF_CLEAR	.48	.48
14	S	NO	NO	FREE	.56	.58
14	S	NO	NO	FREE	.56	.61
14	S	NO	NO	FREE	.56	.48
14	S	NO	NO	FREE	.56	.48
14	S	NO	NO	FREE	.56	.58
14	S	NO	NO	FREE	.56	.5
14	S	NO	NO	FREE	.56	.54
15	S	NO	YES	FREE	.6	.66
15	S	NO	YES	FREE	.6	.54
15	S	NO	YES	FREE	.6	.59
15	S	NO	YES	FREE	.6	.54
15	S	NO	YES	FREE	.6	.62
15	S	NO	YES	FREE	.6	.56
15	S	NO	YES	FREE	.6	.6
16	S	NO	YES	FREE	.52	.51
16	S	NO	YES	FREE	.52	.59
16	S	NO	YES	FREE	.52	.46
16	S	NO	YES	FREE	.52	.56
16	S	NO	YES	FREE	.52	.56
16	S	NO	YES	FREE	.52	.46
16	S	NO	YES	FREE	.52	.52
17	S	NO	YES	FREE	.32	.29
17	S	NO	YES	FREE	.32	.31
17	S	NO	YES	FREE	.32	.31
17	S	NO	YES	FREE	.32	.37
17	S	NO	YES	FREE	.32	.31
17	S	NO	YES	FREE	.32	.3
17	S	NO	YES	FREE	.32	.34
17	S	NO	YES	FREE	.32	.32
18	S	NO	YES	FREE	1.08	.45
18	S	NO	YES	FREE	1.08	.57

Continued on next page

121

Table B.6: Solids Mobilization Experimental Data — Large Flume Study — Part 3. — Continued

EXP	SIZE	TR_m	BED_m	STATUS	Fr_{tr}	Fr_{comp}
18	S	NO	YES	FREE	1.08	.57
18	S	NO	YES	FREE	1.08	.49
18	S	NO	YES	FREE	1.08	.47
18	S	NO	YES	FREE	1.08	.52
18	S	NO	YES	FREE	1.08	.47
18	S	NO	YES	FREE	1.08	.51
19	S	NO	YES	FREE	.43	.45
19	S	NO	YES	FREE	.43	.46
19	S	NO	YES	FREE	.43	.38
19	S	NO	YES	FREE	.43	.45
19	S	NO	YES	FREE	.43	.46
19	S	NO	YES	FREE	.43	.45
19	S	NO	YES	FREE	.43	.44
20	S	NO	YES	FREE	.45	.42
20	S	NO	YES	FREE	.45	.44
20	S	NO	YES	FREE	.45	.39
20	S	NO	YES	FREE	.45	.44
20	S	NO	YES	FREE	.45	.48
20	S	NO	YES	FREE	.45	.43
20	S	NO	YES	FREE	.45	.43
21	S	NO	YES	FREE	.44	.4
21	S	NO	YES	FREE	.44	.39
21	S	NO	YES	FREE	.44	.38
21	S	NO	YES	FREE	.44	.38
21	S	NO	YES	FREE	.44	.39
21	S	NO	YES	FREE	.44	.43
21	S	NO	YES	FREE	.44	.4
22	S	YES	YES	FREE	.5	.53
22	S	YES	YES	FREE	.5	.58
22	S	YES	YES	FREE	.5	.45
22	S	YES	YES	FREE	.5	.51
22	S	YES	YES	FREE	.5	.41
22	S	YES	YES	FREE	.5	.4
22	S	YES	YES	FREE	.5	.48
23	S	YES	YES	FREE	.52	.65
23	S	YES	YES	FREE	.52	.52
23	S	YES	YES	FREE	.52	.46
23	S	YES	YES	FREE	.52	.46
23	S	YES	YES	FREE	.52	.54
23	S	YES	YES	FREE	.52	.46
23	S	YES	YES	FREE	.52	.51
24	S	NO	YES	CLOG	.48	.61
24	S	NO	YES	CLOG	.48	.51
24	S	NO	YES	CLOG	.48	.49
24	S	NO	YES	CLOG	.48	.43
24	S	NO	YES	CLOG	.48	.49
24	S	NO	YES	CLOG	.48	.46
24	S	NO	YES	CLOG	.48	.5
25	S	YES	YES	FREE	.16	.14
25	S	YES	YES	FREE	.16	.2

Continued on next page

Table B.6: Solids Mobilization Experimental Data — Large Flume Study — Part 3. — Continued

EXP	SIZE	TR_m	BED_m	STATUS	Fr_{tr}	Fr_{comp}
25	S	YES	YES	FREE	.16	.13
25	S	YES	YES	FREE	.16	.08
26	S	NO	YES	CLOG	.56	.66
26	S	NO	YES	CLOG	.56	.63
26	S	NO	YES	CLOG	.56	.6
26	S	NO	YES	CLOG	.56	.24
26	S	NO	YES	CLOG	.56	.74
26	S	NO	YES	CLOG	.56	.55
26	S	NO	YES	CLOG	.56	.57
27	S	NO	YES	CLOG	.58	.58
27	S	NO	YES	CLOG	.58	.52
27	S	NO	YES	CLOG	.58	.64
27	S	NO	YES	CLOG	.58	.58
27	S	NO	YES	CLOG	.58	.55
27	S	NO	YES	CLOG	.58	.58
27	S	NO	YES	CLOG	.58	.57
28	S	YES	YES	CLOG	.51	.61
28	S	YES	YES	CLOG	.51	.5
28	S	YES	YES	CLOG	.51	.43
28	S	YES	YES	CLOG	.51	.46
28	S	YES	YES	CLOG	.51	.48
28	S	YES	YES	CLOG	.51	.61
28	S	YES	YES	CLOG	.51	.51
29	S	YES	YES	CLOG	.45	.27
29	S	YES	YES	CLOG	.45	.25
29	S	YES	YES	CLOG	.45	.58
29	S	YES	YES	CLOG	.45	.64
29	S	YES	YES	CLOG	.45	.59
29	S	YES	YES	CLOG	.45	.44
29	S	YES	YES	CLOG	.45	.46
30	S	YES	YES	CLOG	.77	.79
30	S	YES	YES	CLOG	.77	.86
30	S	YES	YES	CLOG	.77	.78
30	S	YES	YES	CLOG	.77	.58
30	S	YES	YES	CLOG	.77	.79
30	S	YES	YES	CLOG	.77	.79
30	S	YES	YES	CLOG	.77	.77
31	S	YES	YES	CLOG	.82	.61
31	S	YES	YES	CLOG	.82	.72
31	S	YES	YES	CLOG	.82	.42
31	S	YES	YES	CLOG	.82	.58
32	S	YES	YES	CLOG	.55	.54
33	S	NO	NO	FREE	.01	.18
33	S	NO	NO	FREE	.01	.17
33	S	NO	NO	FREE	.01	.25
33	S	NO	NO	FREE	.01	.22
33	S	NO	NO	FREE	.01	.17
33	S	NO	NO	FREE	.01	.18
33	S	NO	NO	FREE	.01	.17
33	S	NO	NO	FREE	.01	.2

Continued on next page

123

Table B.6: Solids Mobilization Experimental Data — Large Flume Study — Part 3. — Continued

EXP	SIZE	TR_m	BED_m	STATUS	Fr_{tr}	Fr_{comp}
34	S	NO	YES	CLOG	.01	.26
34	S	NO	YES	CLOG	.01	.2
34	S	NO	YES	CLOG	.01	.23
34	S	NO	YES	CLOG	.01	.22
34	S	NO	YES	CLOG	.01	.23
34	S	NO	YES	CLOG	.01	.24
34	S	NO	YES	CLOG	.01	.23
35	S	NO	NO	FREE	.29	.25
35	S	NO	NO	FREE	.29	.3
35	S	NO	NO	FREE	.29	.33
35	S	NO	NO	FREE	.29	.27
35	S	NO	NO	FREE	.29	.29
35	S	NO	NO	FREE	.29	.29
36	S	NO	YES	CLOG	.65	.76
36	S	NO	YES	CLOG	.65	.73
36	S	NO	YES	CLOG	.65	.46
36	S	NO	YES	CLOG	.65	.64
36	S	NO	YES	CLOG	.65	.65
37	S	NO	YES	CLOG	.64	.61
37	S	NO	YES	CLOG	.64	.67
37	S	NO	YES	CLOG	.64	.73
37	S	NO	YES	CLOG	.64	.61
37	S	NO	YES	CLOG	.64	.64
37	S	NO	YES	CLOG	.64	.58
37	S	NO	YES	CLOG	.64	.64
38	S	YES	YES	CLOG	.61	.55
38	S	YES	YES	CLOG	.61	.61
38	S	YES	YES	CLOG	.61	.6
38	S	YES	YES	CLOG	.61	.66
38	S	YES	YES	CLOG	.61	.66
38	S	YES	YES	CLOG	.61	.55
38	S	YES	YES	CLOG	.61	.61
39	S	YES	YES	CLOG	.51	.62
39	S	YES	YES	CLOG	.51	.53
39	S	YES	YES	CLOG	.51	.46
39	S	YES	YES	CLOG	.51	.47
39	S	YES	YES	CLOG	.51	.52
40	S	YES	YES	SELF_CLEAR	.95	.89
40	S	YES	YES	SELF_CLEAR	.95	.96
40	S	YES	YES	SELF_CLEAR	.95	.96
40	S	YES	YES	SELF_CLEAR	.95	.96
40	S	YES	YES	SELF_CLEAR	.95	.94
41	S	YES	YES	SELF_CLEAR	.75	.87
41	S	YES	YES	SELF_CLEAR	.75	.69
41	S	YES	YES	SELF_CLEAR	.75	.69
41	S	YES	YES	SELF_CLEAR	.75	.75
42	S	YES	YES	SELF_CLEAR	.68	.68
42	S	YES	YES	SELF_CLEAR	.68	.65
42	S	YES	YES	SELF_CLEAR	.68	.68
42	S	YES	YES	SELF_CLEAR	.68	.67

Table B.6: Solids Mobilization Experimental Data — Large Flume Study — Part 3. — Continued

EXP	SIZE	TR_m	BED_m	STATUS	Fr_{tr}	Fr_{comp}
43	S	NO	NO	FREE	.2	.23
43	S	NO	NO	FREE	.2	.21
43	S	NO	NO	FREE	.2	.19
43	S	NO	NO	FREE	.2	.14
43	S	NO	NO	FREE	.2	.23
43	S	NO	NO	FREE	.2	.18
43	S	NO	NO	FREE	.2	.2
44	S	NO	NO	FREE	.31	.31
44	S	NO	NO	FREE	.31	.29
44	S	NO	NO	FREE	.31	.36
44	S	NO	NO	FREE	.31	.32
44	S	NO	NO	FREE	.31	.28
44	S	NO	NO	FREE	.31	.31
44	S	NO	NO	FREE	.31	.31
45	S	NO	NO	FREE	.27	.3
45	S	NO	NO	FREE	.27	.27
45	S	NO	NO	FREE	.27	.28
45	S	NO	NO	FREE	.27	.28
45	S	NO	NO	FREE	.27	.26
45	S	NO	NO	FREE	.27	.29
45	S	NO	NO	FREE	.27	.28
46	S	NO	NO	FREE	.35	.36
46	S	NO	NO	FREE	.35	.31
46	S	NO	NO	FREE	.35	.34
46	S	NO	NO	FREE	.35	.39
46	S	NO	NO	FREE	.35	.34
46	S	NO	NO	FREE	.35	.34
46	S	NO	NO	FREE	.35	.35
47	S	NO	NO	FREE	.34	.33
47	S	NO	NO	FREE	.34	.3
47	S	NO	NO	FREE	.34	.32
47	S	NO	NO	FREE	.34	.43
47	S	NO	NO	FREE	.34	.33
47	S	NO	NO	FREE	.34	.33
47	S	NO	NO	FREE	.34	.34
48	S	NO	NO	FREE	.4	.39
48	S	NO	NO	FREE	.4	.4
48	S	NO	NO	FREE	.4	.46
48	S	NO	NO	FREE	.4	.4
48	S	NO	NO	FREE	.4	.36
48	S	NO	NO	FREE	.4	.38
48	S	NO	NO	FREE	.4	.4
49	S	NO	NO	FREE	.4	.35
49	S	NO	NO	FREE	.4	.38
49	S	NO	NO	FREE	.4	.38
49	S	NO	NO	FREE	.4	.44
49	S	NO	NO	FREE	.4	.42
49	S	NO	NO	FREE	.4	.39
50	S	YES	YES	SELF_CLEAR	.37	.41
50	S	YES	YES	SELF_CLEAR	.37	.36

Continued on next page

Table B.6: Solids Mobilization Experimental Data — Large Flume Study — Part 3. — Continued

EXP	SIZE	TR_m	BED_m	STATUS	Fr_{tr}	Fr_{comp}
50	S	YES	YES	SELF_CLEAR	.37	.37
50	S	YES	YES	SELF_CLEAR	.37	.34
50	S	YES	YES	SELF_CLEAR	.37	.37
50	S	YES	YES	SELF_CLEAR	.37	.37
50	S	YES	YES	SELF_CLEAR	.37	.37
51	S	NO	YES	NO_MATL	.45	.39
51	S	NO	YES	NO_MATL	.45	.47
51	S	NO	YES	NO_MATL	.45	.54
51	S	NO	YES	NO_MATL	.45	.44
51	S	NO	YES	NO_MATL	.45	.43
51	S	NO	YES	NO_MATL	.45	.43
51	S	NO	YES	NO_MATL	.45	.45
52	S	NO	YES	NO_MATL	.43	.41
52	S	NO	YES	NO_MATL	.43	.38
52	S	NO	YES	NO_MATL	.43	.55
52	S	NO	YES	NO_MATL	.43	.44
52	S	NO	YES	NO_MATL	.43	.41
52	S	NO	YES	NO_MATL	.43	.38
52	S	NO	YES	NO_MATL	.43	.43
53	S	NO	YES	NO_MATL	.36	.36
53	S	NO	YES	NO_MATL	.36	.41
53	S	NO	YES	NO_MATL	.36	.36
53	S	NO	YES	NO_MATL	.36	.34
53	S	NO	YES	NO_MATL	.36	.36
53	S	NO	YES	NO_MATL	.36	.35
53	S	NO	YES	NO_MATL	.36	.37
54	L	NO	NO	FREE	.35	.34
54	L	NO	NO	FREE	.35	.46
54	L	NO	NO	FREE	.35	.34
54	L	NO	NO	FREE	.35	.25
54	L	NO	NO	FREE	.35	.38
54	L	NO	NO	FREE	.35	.35
55	L	NO	NO	FREE	.58	.68
55	L	NO	NO	FREE	.58	.5
55	L	NO	NO	FREE	.58	.5
55	L	NO	NO	FREE	.58	.47
55	L	NO	NO	FREE	.58	.71
55	L	NO	NO	FREE	.58	.57
56	L	NO	NO	FREE	.64	.65
56	L	NO	NO	FREE	.64	.65
56	L	NO	NO	FREE	.64	.61
56	L	NO	NO	FREE	.64	.68
56	L	NO	NO	FREE	.64	.61
56	L	NO	NO	FREE	.64	.64
57	L	NO	YES	FREE	.53	.57
57	L	NO	YES	FREE	.53	.45
57	L	NO	YES	FREE	.53	.56
57	L	NO	YES	FREE	.53	.43
57	L	NO	YES	FREE	.53	.59
57	L	NO	YES	FREE	.53	.52

Continued on next page

Table B.6: Solids Mobilization Experimental Data — Large Flume Study — Part 3. — Continued

EXP	SIZE	TR_m	BED_m	STATUS	Fr_{tr}	Fr_{comp}
58	L	NO	YES	FREE	.53	.71
58	L	NO	YES	FREE	.53	.5
58	L	NO	YES	FREE	.53	.59
58	L	NO	YES	FREE	.53	.42
58	L	NO	YES	FREE	.53	.42
58	L	NO	YES	FREE	.53	.53
59	L	NO	YES	CLOG	.5	.51
59	L	NO	YES	CLOG	.5	.45
59	L	NO	YES	CLOG	.5	.54
59	L	NO	YES	CLOG	.5	.6
59	L	NO	YES	CLOG	.5	.48
59	L	NO	YES	CLOG	.5	.5
60	L	NO	YES	CLOG	.64	.66
60	L	NO	YES	CLOG	.64	.47
60	L	NO	YES	CLOG	.64	.59
60	L	NO	YES	CLOG	.64	.75
60	L	NO	YES	CLOG	.64	.7
60	L	NO	YES	CLOG	.64	.63
61	L	YES	YES	CLOG	.78	.43
61	L	YES	YES	CLOG	.78	.98
61	L	YES	YES	CLOG	.78	.7
61	L	YES	YES	CLOG	.78	.93
61	L	YES	YES	CLOG	.78	.71
61	L	YES	YES	CLOG	.78	1.12
61	L	YES	YES	CLOG	.78	.82
61	L	YES	YES	CLOG	.78	.53
61	L	YES	YES	CLOG	.78	.78
62	L	NO	NO	FREE	.41	.37
62	L	NO	NO	FREE	.41	.42
62	L	NO	NO	FREE	.41	.41
62	L	NO	NO	FREE	.41	.38
62	L	NO	NO	FREE	.41	.45
62	L	NO	NO	FREE	.41	.41
63	L	NO	NO	FREE	.48	.51
63	L	NO	NO	FREE	.48	.45
63	L	NO	NO	FREE	.48	.45
63	L	NO	NO	FREE	.48	.47
63	L	NO	NO	FREE	.48	.5
63	L	NO	NO	FREE	.48	.48
64	L	NO	NO	FREE	.43	.38
64	L	NO	NO	FREE	.43	.45
64	L	NO	NO	FREE	.43	.43
64	L	NO	NO	FREE	.43	.48
64	L	NO	NO	FREE	.43	.38
64	L	NO	NO	FREE	.43	.43
65	L	NO	NO	FREE	.4	.42
65	L	NO	NO	FREE	.4	.33
65	L	NO	NO	FREE	.4	.39
65	L	NO	NO	FREE	.4	.4
65	L	NO	NO	FREE	.4	.43

Continued on next page

127

Table B.6: Solids Mobilization Experimental Data — Large Flume Study — Part 3. — Continued

EXP	SIZE	TR_m	BED_m	STATUS	Fr_{tr}	Fr_{comp}
65	L	NO	NO	FREE	.4	.39
66	L	NO	NO	FREE	.45	.45
66	L	NO	NO	FREE	.45	.38
66	L	NO	NO	FREE	.45	.48
66	L	NO	NO	FREE	.45	.4
66	L	NO	NO	FREE	.45	.45
66	L	NO	NO	FREE	.45	.43
67	L	NO	NO	FREE	.61	.69
67	L	NO	NO	FREE	.61	.63
67	L	NO	NO	FREE	.61	.55
67	L	NO	NO	FREE	.61	.66
67	L	NO	NO	FREE	.61	.49
67	L	NO	NO	FREE	.61	.6
68	L	NO	NO	FREE	.3	.38
68	L	NO	NO	FREE	.3	.21
68	L	NO	NO	FREE	.3	.23
68	L	NO	NO	FREE	.3	.33
68	L	NO	NO	FREE	.3	.35
68	L	NO	NO	FREE	.3	.3
69	L	NO	NO	FREE	.28	.31
69	L	NO	NO	FREE	.28	.28
69	L	NO	NO	FREE	.28	.27
69	L	NO	NO	FREE	.28	.26
69	L	NO	NO	FREE	.28	.25
69	L	NO	NO	FREE	.28	.27
70	L	NO	NO	FREE	.31	.3
70	L	NO	NO	FREE	.31	.28
70	L	NO	NO	FREE	.31	.27
70	L	NO	NO	FREE	.31	.35
70	L	NO	NO	FREE	.31	.34
70	L	NO	NO	FREE	.31	.31
71	L	NO	NO	FREE	.36	.32
71	L	NO	NO	FREE	.36	.38
71	L	NO	NO	FREE	.36	.38
71	L	NO	NO	FREE	.36	.32
71	L	NO	NO	FREE	.36	.4
71	L	NO	NO	FREE	.36	.36
72	L	NO	NO	FREE	.29	.39
72	L	NO	NO	FREE	.29	.21
72	L	NO	NO	FREE	.29	.24
72	L	NO	NO	FREE	.29	.32
72	L	NO	NO	FREE	.29	.31
72	L	NO	NO	FREE	.29	.3
73	L	NO	NO	FREE	.24	.33
73	L	NO	NO	FREE	.24	.19
73	L	NO	NO	FREE	.24	.2
73	L	NO	NO	FREE	.24	.19
73	L	NO	NO	FREE	.24	.24
73	L	NO	NO	FREE	.24	.23
74	L	NO	NO	FREE	.36	.46

Continued on next page

128

Table B.6: Solids Mobilization Experimental Data — Large Flume Study — Part 3. — Continued

EXP	SIZE	TR_m	BED_m	STATUS	Fr_{tr}	Fr_{comp}
74	L	NO	NO	FREE	.36	.44
74	L	NO	NO	FREE	.36	.4
74	L	NO	NO	FREE	.36	.35
74	L	NO	NO	FREE	.36	.36
75	L	NO	NO	FREE	.38	.24
75	L	NO	NO	FREE	.38	.44
75	L	NO	NO	FREE	.38	.45
75	L	NO	NO	FREE	.38	.43
75	L	NO	NO	FREE	.38	.34
75	L	NO	NO	FREE	.38	.38
76	L	NO	YES	FREE	.57	.27
76	L	NO	YES	FREE	.57	.4
76	L	NO	YES	FREE	.57	1.24
76	L	NO	YES	FREE	.57	.44
76	L	NO	YES	FREE	.57	.5
76	L	NO	YES	FREE	.57	.57
77	L	NO	YES	FREE	.43	.26
77	L	NO	YES	FREE	.43	.44
77	L	NO	YES	FREE	.43	.47
77	L	NO	YES	FREE	.43	.38
77	L	NO	YES	FREE	.43	.74
77	L	NO	YES	FREE	.43	.29
77	L	NO	YES	FREE	.43	.43
78	L	NO	YES	CLOG	.45	.32
78	L	NO	YES	CLOG	.45	.71
78	L	NO	YES	CLOG	.45	.43
78	L	NO	YES	CLOG	.45	.45
78	L	NO	YES	CLOG	.45	.28
78	L	NO	YES	CLOG	.45	.49
78	L	NO	YES	CLOG	.45	.45
79	L	NO	YES	CLOG	.43	.39
79	L	NO	YES	CLOG	.43	.41
79	L	NO	YES	CLOG	.43	.41
79	L	NO	YES	CLOG	.43	.33
79	L	NO	YES	CLOG	.43	.58
79	L	NO	YES	CLOG	.43	.42
80	L	YES	YES	CLOG	.46	.43
80	L	YES	YES	CLOG	.46	.35
80	L	YES	YES	CLOG	.46	.59
80	L	YES	YES	CLOG	.46	.46
81	L	NO	YES	CLOG	.48	.32
81	L	NO	YES	CLOG	.48	.86
81	L	NO	YES	CLOG	.48	.26
81	L	NO	YES	CLOG	.48	.48
82	L	NO	NO	FREE	.43	.38
82	L	NO	NO	FREE	.43	.35
82	L	NO	NO	FREE	.43	.5
82	L	NO	NO	FREE	.43	.45
82	L	NO	NO	FREE	.43	.46
82	L	NO	NO	FREE	.43	.43

Continued on next page

129

Table B.6: Solids Mobilization Experimental Data — Large Flume Study — Part 3. — Continued

EXP	SIZE	TR_m	BED_m	STATUS	Fr_{tr}	Fr_{comp}
83	L	NO	NO	FREE	.36	.42
83	L	NO	NO	FREE	.36	.32
83	L	NO	NO	FREE	.36	.32
83	L	NO	NO	FREE	.36	.38
83	L	NO	NO	FREE	.36	.31
83	L	NO	NO	FREE	.36	.35
84	L	NO	NO	FREE	.48	.5
84	L	NO	NO	FREE	.48	.32
84	L	NO	NO	FREE	.48	.49
84	L	NO	NO	FREE	.48	.51
84	L	NO	NO	FREE	.48	.56
84	L	NO	NO	FREE	.48	.48
85	L	NO	NO	FREE	.54	.54
85	L	NO	NO	FREE	.54	.57
85	L	NO	NO	FREE	.54	.64
85	L	NO	NO	FREE	.54	.52
85	L	NO	NO	FREE	.54	.4
85	L	NO	NO	FREE	.54	.55
85	L	NO	NO	FREE	.54	.54
86	L	NO	NO	FREE	.49	.3
86	L	NO	NO	FREE	.49	.51
86	L	NO	NO	FREE	.49	.54
86	L	NO	NO	FREE	.49	.58
86	L	NO	NO	FREE	.49	.33
86	L	NO	NO	FREE	.49	.69
86	L	NO	NO	FREE	.49	.49
87	L	NO	NO	FREE	.3	.27
87	L	NO	NO	FREE	.3	.29
87	L	NO	NO	FREE	.3	.37
87	L	NO	NO	FREE	.3	.31
87	L	NO	NO	FREE	.3	.28
87	L	NO	NO	FREE	.3	.29
87	L	NO	NO	FREE	.3	.3
88	L	YES	YES	CLOG	.16	.37
88	L	YES	YES	CLOG	.16	.39
88	L	YES	YES	CLOG	.16	.41
88	L	YES	YES	CLOG	.16	.35
88	L	YES	YES	CLOG	.16	.43
88	L	YES	YES	CLOG	.16	.39
89	L	NO	YES	CLOG	.15	.39
89	L	NO	YES	CLOG	.15	.3
89	L	NO	YES	CLOG	.15	.23
89	L	NO	YES	CLOG	.15	.45
89	L	NO	YES	CLOG	.15	.4
89	L	NO	YES	CLOG	.15	.49
89	L	NO	YES	CLOG	.15	.38
90	L	YES	YES	CLOG	.41	.35
90	L	YES	YES	CLOG	.41	.47
90	L	YES	YES	CLOG	.41	.4
90	L	YES	YES	CLOG	.41	.3

Continued on next page

130

Table B.6: Solids Mobilization Experimental Data — Large Flume Study — Part 3. — Continued

EXP	SIZE	TR_m	BED_m	STATUS	Fr_{tr}	Fr_{comp}
90	L	YES	YES	CLOG	.41	1.06
90	L	YES	YES	CLOG	.41	.22
90	L	YES	YES	CLOG	.41	.41
91	L	YES	YES	CLOG	.27	.26
91	L	YES	YES	CLOG	.27	.22
91	L	YES	YES	CLOG	.27	.34
91	L	YES	YES	CLOG	.27	.32
91	L	YES	YES	CLOG	.27	.22
91	L	YES	YES	CLOG	.27	.27

C. University of Houston — Numerical Modeling Supplementary Material

Table C.1: Rainfall event from November 2000 used by Wang and Krou (2008) for hydrologic and hydraulic computations of Johnson Fork Creek.

Hour	411017	413270	414670	415312	417243
60	0.0	0.0	0.0	0.0	0.0
61	0.0	0.0	0.0	0.0	0.0
62	0.0	0.0	0.0	0.0	0.0
63	0.0	0.0	0.2	0.0	0.0
64	0.0	0.9	0.6	1.5	0.2
65	0.0	0.0	0.0	0.1	0.0
66	0.1	0.0	0.0	0.0	0.4
67	0.0	0.0	0.0	0.0	0.7
68	0.0	0.0	0.0	0.0	0.0
69	0.0	0.0	0.0	0.0	0.0
70	0.0	0.0	0.0	0.0	0.0
71	0.0	0.0	0.0	0.0	0.0
72	0.0	0.0	0.0	0.0	0.2
73	0.0	0.0	0.0	0.3	0.1
74	0.0	0.0	0.0	0.5	0.1
75	0.0	1.0	0.0	0.4	0.1
76	0.4	0.2	0.6	0.0	0.0
77	0.7	0.4	0.0	0.0	0.0
78	1.4	0.4	0.1	0.6	0.0
79	1.4	0.7	0.0	0.1	0.1
80	0.7	0.1	0.1	0.0	0.0
81	0.6	0.0	0.8	0.0	0.0
82	0.3	0.0	0.7	0.0	0.0
83	0.4	0.1	0.8	0.0	0.0
84	0.3	0.3	0.7	0.0	0.0
85	0.3	0.1	0.9	0.3	0.0
86	0.3	0.0	0.3	0.2	0.2
87	0.2	0.0	0.0	0.1	0.3
88	0.0	0.0	0.0	0.0	0.4
89	0.0	0.1	0.2	0.0	0.3
90	0.2	0.0	0.4	0.1	0.2
91	0.2	0.0	0.2	0.4	0.2
92	0.0	0.0	0.2	0.3	0.3
93	0.0	0.0	0.0	0.2	0.2
94	0.1	0.1	0.0	0.0	0.0
95	0.0	0.0	0.0	0.0	0.0
Total	7.6	4.4	6.8	5.1	4.0
Average	0.21	0.12	0.19	0.14	0.11
Latitude	31.07	30.56	30.27	30.4	30.35
Longitude	-99.2	-100.07	-99.48	-99.35	-98.53
Distance	103.952	104.632	103.983	103.897	103.098
Weighted Avg	21.945	12.788	19.641	14.719	11.455
Average = 0.155 in/hr, Total = 5.43 in					
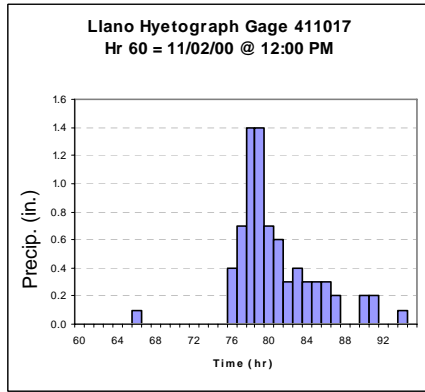
(a) Hyetographs for Raingage 411017.
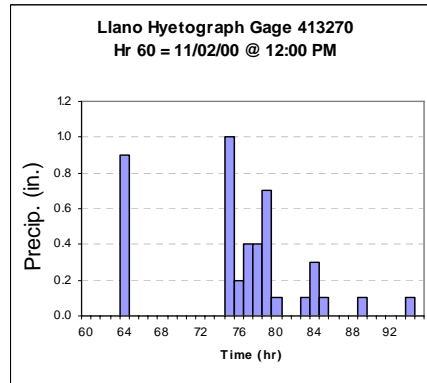
(b) Hyetograph for Raingage 413270.
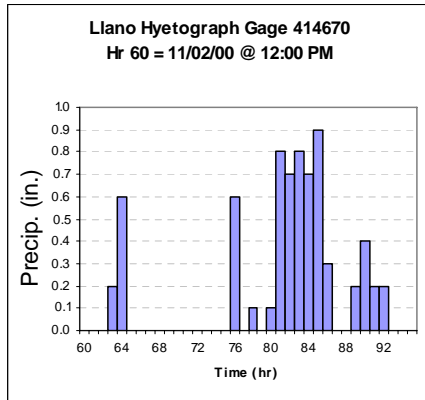
(c) Hyetographs for Raingages 414670.
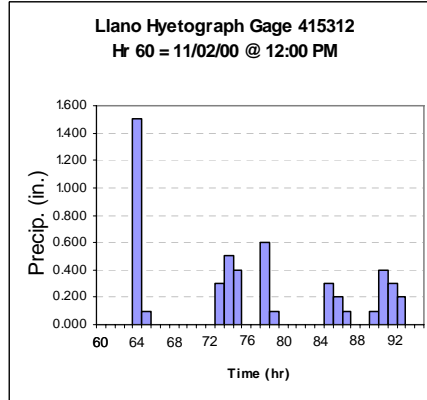
(d) Hyetograph for Raingage 415312.
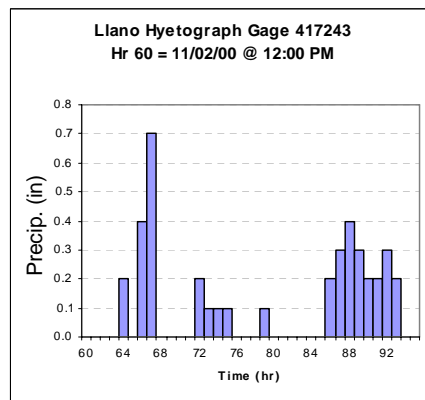
(e) Hyetograph for Raingage 417243.

Figure C.1: Hyetographs from Raingages 411017, 413270, 414670, 415312, and 417243 for the event of November 2, 2000, from Wang and Krou (2008).

134

Table C.2: MUSLE factors from GIS watershed analysis (Wang and Krou, 2008).

LUCODE	LEVEL2	CN	CI	CII	CIII	C
11	RESIDENTIAL	89	0.1	0.1	1	0.01
12	COMMERCIAL AND SERVICES	95	0.1	0.1	1	0.01
14	TRANS, COMM, UTIL	98	0.1	0.1	1	0.01
16	MXD URBAN OR BUILT-UP	90	0.8	0.1	1	0.08
17	OTHER URBAN OR BUILT-UP	90	0.8	0.1	1	0.08
21	CROPLAND AND PASTURE	89	0.8	0.3	1	0.24
22	ORCH,GROV,VNYRD,NURS,ORN	85	0.8	0.18	1	0.144
23	CONFINED FEEDING OPS	80	0.8	0.3	1	0.24
24	OTHER AGRICULTURAL LAND	85	0.8	0.18	1	0.144
31	HERBACEOUS RANGELAND	80	0.8	0.2	1	0.16
32	SHRUB & BRUSH RANGELAND	80	0.8	0.3	1	0.24
33	MIXED RANGELAND	80	0.8	0.3	1	0.24
41	DECIDUOUS FOREST LAND	83	0.5	0.8	1	0.4
42	EVERGREEN FOREST LAND	77	0.5	0.8	1	0.4
43	MIXED FOREST LAND	83	0.5	0.7	1	0.35
53	RESERVOIRS	100	1	1	1	1
73	SANDY AREA (NON-BEACH)	70	1	1	1	1
75	STRIP MINES	91	1	1	1	1
76	TRANSITIONAL AREAS	98	1	1	1	1

Table C.3: Watershed geologic group and soil erodibility (Wang and Krou, 2008).

Rock formation	Description	Area (acre)	UNIT	Erodibilty
Atokan and Morrowan Series	Carbonate and fossils	5857	PP1	0.1
Cambrian	Old rock	8890	C	0.05
Fredericksburg Group	Limestone with cracks	241002	lK2	0.6
Lower Ordovician (Canadian)	Sandstone, silestone	5074	O1	0.14
Paragneiss and schist	Metamorphic rock	344047	Ym	0.05
Trinity group	Sand, gravel, clay, limestone	218708	lK1	0.05
Washita Group	Carbonates	57048	lK3	0.1
Younger Y granitic rocks	Young granite	25981	Yg2	0

Table C.4: University of Houston MUSLE results (Wang and Krou, 2008).

ID	Area (acre)	Area (mi²)	Length (m)	Slope (%)	Slope Angle	LS	Erod. K	Crop C	S (SCS)	Lag Time (hr)	Time TR (hr)	Q_V (in)	Q_V (ac-ft)	Q_p (cfs)	MUSLE (ton)
1	87158	136	146295	0.45	0.0045	2.69	0.0405	0.26	2.26	62.9	80.4	3.44	24963	820.1	33431
2	35766	56	94128	1.7	0.017	7.46	0.0528	0.287	2.26	22.8	40.3	3.43	10220	671.8	72290
3	41378	65	93371	1.1	0.011	4.98	0.0347	0.244	2.44	29.2	46.7	3.31	11406	670.3	28737
4	50354	79	100365	0.47	0.0047	2.48	0.0441	0.26	2.32	46.1	63.6	3.39	14220	598.4	20505
5	32162	50	106791	1.1	0.011	5.18	0.0505	0.263	2.37	32	49.5	3.37	9026	491.4	34500
6	46092	72	106980	1.1	0.011	5.19	0.0343	0.31	2.33	31.8	49.3	3.4	13060	706.7	41659
7	31710	50	76549	0.45	0.0045	2.21	0.0409	0.248	2.31	37.9	55.4	3.4	8984	432.8	10459
8	7329	11	40448	0.45	0.0045	1.83	0.0303	0.284	2.34	22.9	40.4	3.39	2072	137.2	1695
9	10267	16	55569	1.1	0.011	4.26	0.0346	0.24	2.24	18.5	36	3.46	2964	215.8	6001
10	44031	69	89591	0.47	0.0047	2.4	0.0418	0.214	2.33	42.2	59.7	3.39	12443	557.9	13811
11	17089	27	56514	1.1	0.011	4.28	0.0501	0.277	2.4	19.3	36.8	3.34	4762	350.7	17251
12	21010	33	64831	0.45	0.0045	2.11	0.0079	0.276	2.39	33.7	51.2	3.35	5865	310.2	1400
13	753	1	9829	0.62	0.0062	1.54	0.008	0.357	2.55	6.6	24.1	3.28	205	23.7	49
14	29222	46	75415	0.6	0.006	2.77	0.1103	0.266	2.28	32.2	49.7	3.41	8316	444.5	36759
15	15952	25	62374	0.62	0.0062	2.69	0.026	0.265	2.46	28.2	45.7	3.31	4401	263.7	4383
16	9876	15	45552	0.54	0.0054	2.19	0.0287	0.247	2.4	28.3	40.8	3.34	2746	183.2	2292
17	25391	40	62941	0.54	0.0054	2.41	0.0162	0.25	2.39	30.1	47.6	3.34	7076	403.7	3831
18	24630	38	61996	0.74	0.0074	3.11	0.1969	0.297	2.12	23.9	41.4	3.52	7233	449.5	76656
19	31037	48	67099	0.74	0.0074	3.18	0.1431	0.297	2.07	25.2	42.7	3.56	9205	549.3	72939
20	65863	103	127393	0.62	0.0062	3.33	0.044	0.252	2.39	49.3	66.8	3.35	18371	745.8	34760
21	16020	25	58215	0.62	0.0062	2.63	0.0144	0.25	2.42	26.5	44	3.32	4432	275.1	2300
22	18254	29	64075	0.54	0.0054	2.42	0.0207	0.251	2.36	30.3	47.8	3.36	5115	288.6	3416
23	54660	85	107736	0.87	0.0087	4.22	0.247	0.322	2.11	34.3	51.8	3.52	16056	798.4	305001
24	10627	17	39881	2	0.02	23.79	0.1243	0.301	2.25	10.5	28	3.43	3037	286.7	179124
25	9035	14	40637	2	0.02	24.02	0.129	0.308	2.22	10.6	28.1	3.45	2598	243	160714
26	24572	38	74092	2	0.02	32.43	0.1875	0.312	2.15	16.9	34.4	3.5	7170	540.3	881283
27	5376	8	32510	0.47	0.0047	1.77	0.05	0.236	2.37	18.9	36.4	3.36	1506	111.7	1673
28	31286	49	78251	0.74	0.0074	3.34	0.234	0.295	2.15	29	46.5	3.51	9139	508.7	118560
29	4913	8	23626	0.47	0.0047	1.61	0.05	0.24	2.46	14.9	32.4	3.3	1351	114.6	1476
30	28604	45	72202	1.7	0.017	6.89	0.075	0.285	2.41	19	36.5	3.33	7936	592.6	76265
31	32054	50	69367	0.47	0.0047	2.22	0.05	0.26	2.32	34.3	51.8	3.39	9048	467.5	14110
32	9722	15	41393	1.7	0.017	5.83	0.0385	0.386	1.88	10.8	28.3	3.75	3037	259.6	16526
33	47814	75	92048	0.47	0.0047	2.42	0.0662	0.291	2.31	42.9	60.4	3.4	13540	598.5	32775
34	16738	26	68800	2	0.02	31.25	0.091	0.311	2.2	16.1	33.6	3.46	4830	376.6	269409
35	11858	19	43284	2	0.02	24.79	0.05	0.309	2.22	11.2	28.7	3.45	3411	312.9	86391
36	3310	5	21169	0.87	0.0087	2.59	0.0753	0.315	2.11	9.3	26.8	3.53	973	93.3	3490
37	30555	48	72580	0.87	0.0087	3.75	0.1877	0.305	2.11	25	42.5	3.53	8985	543.7	113605
38	35759	56	81464	0.87	0.0087	3.88	0.2696	0.309	2.18	27.9	45.4	3.48	10360	596.1	194805
39	17601	28	58782	0.87	0.0087	3.52	0.3016	0.318	2.12	21.2	38.7	3.52	5159	344.3	101229
40	30818	48	78062	0.47	0.0047	2.3	0.0905	0.273	2.48	39	56.5	3.29	8448	412.5	24954
41	31922	50	70690	0.47	0.0047	2.24	0.1097	0.318	2.36	35.1	52.6	3.37	8972	458.8	37496
42	44451	69	91670	0.87	0.0087	4.02	0.2256	0.309	2.48	32.6	50.1	3.29	12194	671.1	197763
43	21372	33	54057	2	0.02	27.7	0.0644	0.314	2.27	13.5	31	3.42	6095	521.8	232550
44	27958	44	61240	2	0.02	29.48	0.1961	0.347	2.61	16	33.5	3.21	7488	631.8	1040897
45	78122	122	106791	2	0.02	38.93	0.304	0.36	2.69	25.3	42.8	3.17	20665	1380.7	6060301
46	29816	47	76738	0.47	0.0047	2.29	0.2243	0.364	2.77	40.7	58.2	3.12	7744	387.4	75306
47	70140	110	115675	0.87	0.0087	4.31	0.3195	0.354	2.58	40	57.5	3.25	18987	922	527046
48	26241	41	63697	0.87	0.0087	3.6	0.254	0.324	2.33	23.6	41.1	3.38	7399	482.6	131624
49	20357	32	63697	0.87	0.0087	3.6	0.2709	0.352	2.68	25.3	42.8	3.17	5379	359.5	108328
50	22721	36	60862	0.47	0.0047	2.14	0.2477	0.37	2.6	32.7	50.2	3.22	6104	342.4	64471
51	16833	26	54813	0.47	0.0047	2.07	0.2264	0.358	2.74	30.9	48.4	3.13	4392	263	39595
52	43786	68	84866	0.47	0.0047	2.36	0.2311	0.369	2.86	44.8	62.3	3.06	11160	531.1	118802
53	25961	41	55002	0.47	0.0047	2.07	0.2977	0.377	2.91	32	49.5	3.03	6552	396.8	86462
54	19975	31	59349	0.47	0.0047	2.12	0.3585	0.389	2.86	33.7	51.2	3.06	5096	295.2	80935
55	48997	77	85244	0.47	0.0047	2.36	0.1651	0.358	2.71	43.8	61.3	3.16	12900	604.7	96094
56	45631	71	85055	0.47	0.0047	2.36	0.1303	0.379	2.92	45.4	62.9	3.03	11505	549	71214
57	34930	55	73147	0.47	0.0047	2.26	0.1027	0.35	2.83	39.6	57.1	3.07	8946	462.6	39141

Table C.5: Annual maximum peaks from for Gage 08150000 — Llano River near Junction, Texas (Wang and Krou, 2008).

Year	Q_p (cfs)	Year	Q_p (cfs)
1916	11100	1960	35500
1917	192	1961	55700
1918	14900	1962	385
1919	35700	1963	1630
1920	13700	1964	26400
1921	880	1965	8180
1922	16100	1966	13800
1923	60400	1967	658
1924	85500	1968	16600
1925	76900	1969	1610
1926	5600	1970	21600
1927	607	1971	19800
1928	32000	1972	8750
1929	2100	1973	6570
1930	2770	1974	97800
1931	89700	1975	4180
1932	106000	1976	25700
1933	15800	1977	41600
1934	4720	1978	76700
1935	319000	1979	3770
1936	158000	1980	139000
1937	2000	1981	19900
1938	137000	1982	129000
1939	74400	1983	163
1940	6000	1984	213
1941	7250	1985	106000
1942	43000	1986	36600
1943	10000	1987	12700
1944	8640	1988	54300
1945	3270	1989	324
1946	1290	1990	50300
1947	4540	1991	24000
1948	122000	1992	5370
1949	12100	1993	289
1950	568	1994	5720
1951	5320	1995	2200
1952	2540	1998	53100
1953	5030	1999	409
1954	3090	2000	158000
1955	36800	2001	49700
1956	1020	2002	4310
1957	40500	2003	11200
1958	63600	2004	120000
1959	17500		

Table C.6: Results from fitting Pearson Type III distribution to the logarithms of annual peak discharge from Llano River near Junction, Texas (Wang and Krou, 2008).

T (yrs)	$1/T$	K_T	y_T	Q_p (cfs)
2	0.5	0.07556	9.44	12543
5	0.2	0.85558	10.88	53205
10	0.1	1.22202	11.56	104896
100	0.01	1.98585	12.98	431786

Table C.7: Cross sections used by University of Houston researchers for HEC-RAS modeling (Wang and Krou, 2008).

Segment	Section	Manning's n	Dwn. Stream Length (m)	Bottom Elev. (m)	Bottom Slope (m/m)
	24057	0.02	243.99	548.94	0.00201
1	23813	0.02	236.9	548.45	0.0019
2	23576	0.15	414.44	548	0.00036
3	23162	0.15	916.31	547.85	0.00206
4	22245	0.15	429.85	545.96	0.00612
5	21816	0.15	1214.79	543.33	0.00073
6	20601	0.15	1310.91	542.44	0.00491
7	19290	0.15	1183.95	536	0.00422
8	18106	0.04	289.89	531	0
9	17816	0.04	265.72	531	0
10	17550	0.04	891.18	531	0.00112
11	16659	0.04	723.99	530	0.00195
12	15935	0.04	804.39	528.59	0.00571
13	15131	0.04	1255.9	524	0
14	13875	0.15	9.26	524	0
15	13866	0.15	18.44	524	0
16	13847	0.15	20.05	524	0
17	13827	0.014	826.71	524	0
18	13000	0.15	720.09	524	-0.00179
19	12280	0.014	9.02	525.29	-0.00665
20	12271	0.014	18.34	525.35	-0.00709
21	12253	0.014	22.53	525.48	-0.00666
22	12230	0.014	1683.17	525.63	0.00394
23	10547	0.15	1524.39	519	0.00218
24	9023	0.15	9.4	515.67	0.00426
25	9013	0.15	19.41	515.63	0.00464
26	8994	0.15	21.01	515.54	0.00476
27	8973	0.15	493.82	515.44	0.00605
28	8479	0.15	334.22	512.45	0.00135
29	8145	0.15	1300.64	512	0.00153
30	6844	0.15		510.01	

Table C.8: Results from University of Houston particle-size distribution (Wang and Krou, 2008).

Particle Fraction	Grid Sampling (mm)	Volumetric Sampling (mm)		
		Layer 0–2 in.	Layer 2–4 in.	Layer 4–6 in.
$d_{15.9}$	9.2	–	5.75	8
d_{35}	16.5	27	12.56	15.1
d_{50}	24.2	42	16.5	22
d_{65}	35	51	22.3	33
$d_{84.1}$	64	65	39	54
d_{90}	77.5	67.5	46.5	60.5

D. FM 335 Structure

The purpose of this section is to present Mr. George "Rudy" Herrmann's analysis of the FM 335 crossing. There were two reports, the primary report (Herrmann, 2008a) and the supplemental report (Herrmann, 2008b). The text of these reports are included.

Report of Observations and Recommendations: RM 335 and Un-named Stream

Real County, Texas
Reconnaissance on 3 April, 2007

George R. Herrmann, P.E., P.H.

Introduction

This site is located where RM 335 crosses an un-named ephemeral stream, approximately 5,700 feet south of the crossing of the Nueces river known colloquially as "Ben Williams Crossing." The site is located in Real County, closely adjacent to the Nueces River, which forms the boundary with Edwards County. Figure 1 is an overhead image of the site, and Figure 2 is a site map, including delineation of the drainage area.

The site consists of a concrete armored "low water" type stream crossing, where the majority of flow overtops the roadway for floods of substantial flow rate. At the time of observation (approximately 1330 CDT on 3 April, 2007) the crossing had sustained heavy damage from a recent flood event.
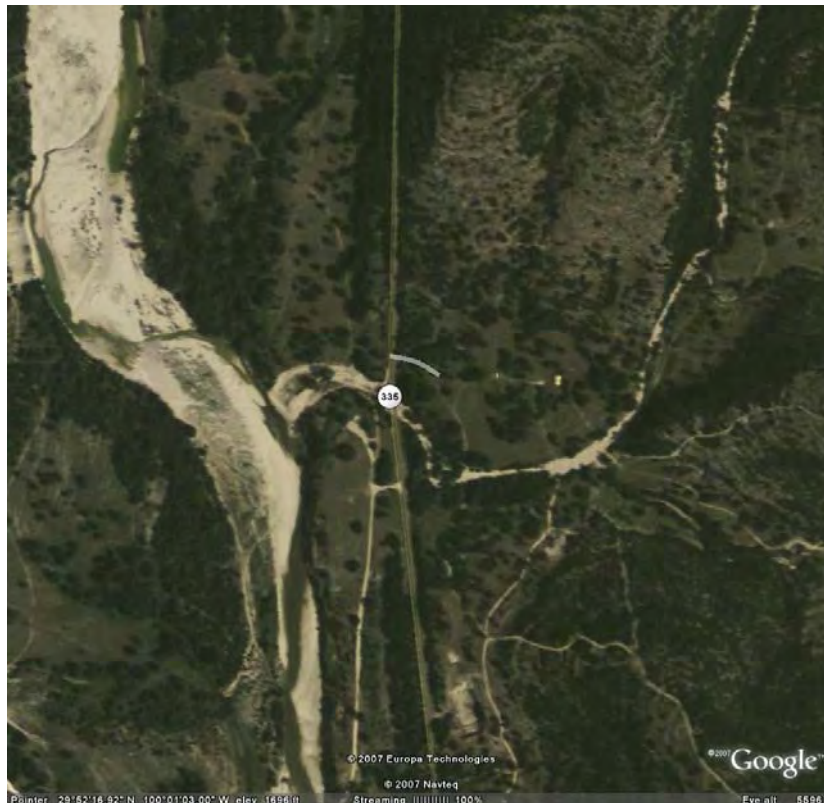
Figure 1
Overhead Image of the site (from Google Earth).
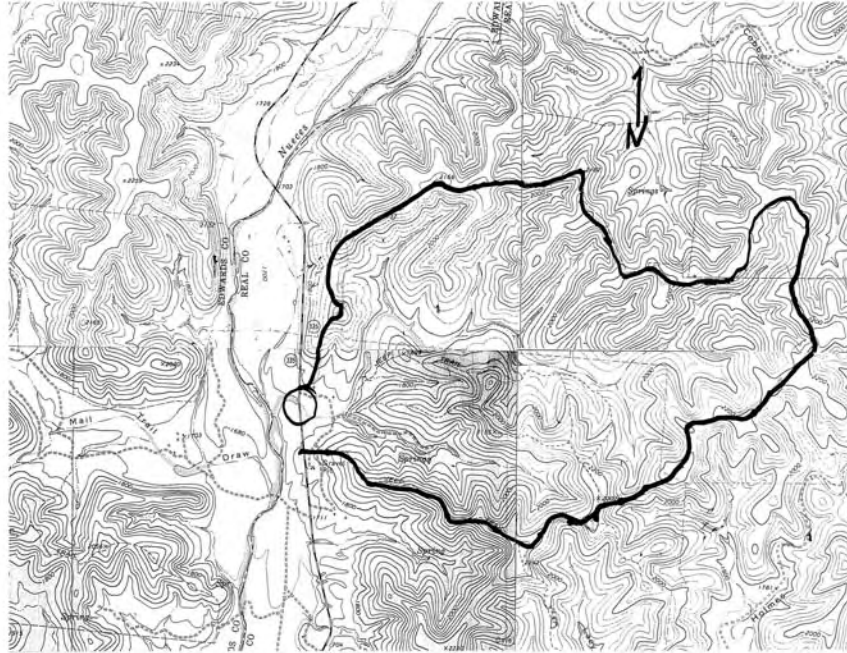
Figure 2
Site map, assembled from USGS 71/2 min. quad sheets.

General Conditions

The stream at this site is a low-order stream that drains approximately 2.7 square miles of Edwards Plateau terrain directly from the valley walls adjacent to the Nueces, across a relatively short floodplain terrace on which the site is located, directly into the main stem of the Nueces River. As such, it shows a steep gradient, and appears to transport colluvial material directly from the valley wall slopes to the river. Local geology is dominated by massive limestone outcrops- soil development is thin and spotty. Alluvial and colluvial deposits provide the medium for most of the local vegetation. Runoff potential is high, because of lack of soil structure.

Local climatology favors mesoscale convective events as the dominant rainfall generation mechanism. Sort duration, high intensity rainfall from these events combines with the local geology and topography to result in a well-deserved reputation for "flashy" ephemeral streams. It is not uncommon for years to pass between significant runoff events. Peak flow rates during those that do occur can be quite high for short periods of time.

Because of a poorly understood peculiarity of the local geology, streams in this area tend to exhibit an extraordinarily high gravel load. The presence in such quantity and behavior of this material under conditions of flood flow is the subject of current study, but is not yet well understood.

Site Conditions

The site under examination exhibits many features common to similar stream crossings on low-volume roadways in this area. At the time of design and construction of the roadway, interruption of service for short periods during flood events was apparently considered an acceptable consequence of saving money on bridge- or culvert-type drainage structures. The flashy nature of local streams dictates that large, expensive structures are needed to provide even modest performance as gauged by frequency of overtopping. Extended periods of drought reduce the overall financial efficiency of such structures. As a result, many crossings are simply armored sag vertical curves, often with a small corrugated metal culvert pipe as a relief structure to prevent long-term ponding of water upstream of the roadway embankment. The primary conveyance is over-the-road flow.

At this particular site, there appears (from observation only) to be a difference in elevation of the gravel in the streambed downstream to upstream of approximately 7-8 feet. Concrete slope paving failed and was transported away on the downstream slope of the embankment, allowing undermining of the roadway and the displacement of roadway embankment material. Figures 3 shows the upstream, and Figure 4 the downstream side of the road.

Figure 3
Upstream side of the road, looking south.

Figure 4
Downstream side of the road, looking south.

A portion of a 24" corrugated, galvanized metal pipe is visible in the eroded face of the roadway embankment, although it appears completely clogged with gravel and debris. Interestingly, a considerable amount of what appears to be bed material has been backwashed into the eroded area and deposited against the eroded face- including particles of considerable size (up to 1 foot) to a height of approximately 6 feet from streambed level. No sign of the upstream end of the culvert pipe is evident. (see Figure 5)

At the time of reconnaissance, flow sufficient to sustain the surface flow downstream (of the order of 2-3 cfs) was visible issuing from beneath the roadway embankment. This indicates both a difference in hydraulic head from upstream to downstream, and a very high permeability. No surface water was visible upstream.

Bed material present was characteristic of the area. This is coarse gravel to cobble sized, primarily subangular to subrounded material, generally light in color.

Figure 5
Cavity and exposed roadway fill, downstream side of roadway. Note
backwashed bed material deposited against eroded embankment.
Water at the bottom of picture is "spring" flow outward from the
gravel.

Conclusions

There is a considerable difference (several feet) in elevation between the upstream and
downstream mean streambeds. The stream cross section downstream appears
characteristic of streams in the area, being slightly incised into a soft, caliche material. It
is probably influenced in morphology by backwater effects from the Nueces during flood
events on the main stem. Indications are that the difference in elevation is attributable to
gravel accumulation on the upstream side of the crossing, caused primarily by the
existence of the crossing itself. At times of flood flow and overtopping of the roadway,
flow is distributed laterally along the roadway rather than being concentrated in the
bankfull channel. Stream power is significantly reduced. Material carried in the bed load
is inhibited from continuing downstream and accumulates. The small culvert pipe cannot
provide a conduit for the transport of such quantities of large material. Eventually, bed
material accumulates above the culvert pipe, clogs it, and renders it useless.

Structures such as this were evidently designed with the idea in mind that they only
needed to conduct water from one side of the roadway to the other. This has been, and
continues to be, the overwhelmingly dominant philosophy in drainage engineering.
There is considerable evidence that failure to accommodate the passage of bed material
from one side of the roadway to the other led to appreciable alteration of the fluvial

configuration in the vicinity of these structures. We are now in the situation of paying the price for this oversight, which originally occurred many years ago. At the time, and given the state of knowledge, the approach was reasonable.

Future construction at these sites should include accommodation of the passage of bed material, in addition to water. Not only should arriving bed material be permitted to pass, but that which has accumulated over the years must somehow be metered out and allowed to pass, returning the stream to a condition and state more resembling that prior to construction. Some thought and management will be needed to accomplish the controlled release of accumulated material.

Recommendations

It is obvious that a small culvert through the roadway embankment is a futile gesture. It should be equally obvious that accommodating all flow over the roadway probably compounds existing problems. As stated before, arriving bed material should be allowed to pass the roadway, and the existing accumulation allowed to diffuse over time.

Current wisdom is that net sediment transport is dominated by small quantities of movement on a frequent basis, rather than by catastrophic floods. Sediment movement by frequent, small floods overwhelms the quantities moved by infrequent, large floods by "persistence." Given that fact, it is not necessary to accommodate large floods to deal with sediment accumulation, but it should pay to attempt to optimize the effects of the most frequent flow events.

The standard shapes for culvert-type structures in Texas are circular pipes and rectangular boxes. Single circular structures exhibit a performance curve that is "steeper" in slope when head of water is graphed on the ordinate versus discharge on the abscissa, as compared to natural channels. In order to obtain sufficient performance, multiple barrels are needed, which distributes flow over a wide lateral distance. However, single pipes confine flow to a narrow width, maintaining a high-velocity jet, and consequently stream power for the movement of sediment. Boxes, conversely, exhibit a shallower curve over the performance range, but for quite small flows, width is again too great to allow stream power to be maintained.

As an alternative, I suggest the installation of a single, large, horizontal elliptical concrete pipe. This would be a compromise between the high-head performance of a box, and the focusing of velocity of a pipe, to maintain stream power.

A cursory examination of the elliptical concrete pipe tables shows that pipes of heights of 63" to 77" and height-to-width ratios around 0.64 are available, which would be roughly appropriate.*

In response to the existing accumulation, and in anticipation of metering that accumulation out over years, I suggest a drop-type inlet be constructed of gabion baskets, designed and constructed such that the top gabion layer is approximately one foot below

6

the mean upstream streambed elevation. Over several years, that one foot of material should be moved through the structure, leaving the bed lower. When that is observed, another layer of gabions can be removed, releasing more material over the ensuing years. Over the course of a decade or so, the accumulated material can be dealt with, after which the stream should resume the natural profile..

The elliptical pipe might be set such that the physical invert elevation is ½ to 1 foot below the downstream mean bed elevation. This would allow a shallow accumulation of material inside of the pipe without elevating the stream bottom, allowing material to react to the natural series of forces that initiates bed material movement.

The idea of using elliptical pipe rather than more conventional circular or rectangular shapes, and of metering the accumulated gravel downstream by use of a stacked gabion inlet both stem from knowledge gained during an ongoing research project. The close scrutiny of similar sites in the same geographic area has dramatically increased our understanding of situations like this.

*Located in the online "Concrete Pipe Design Manual", Table 4, p. 115.
www.concrete-pipe.org
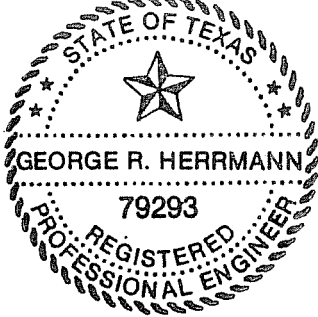
The seal appearing on this document
was authorized by
George R. Herrmann, P.E., 79293
on
4 April 2007

I hereby certify that this document was prepared by me or under my direct supervision, and I am duly certified and registered as a Professional Hydrologist under the Rules and Regulations of the American Institute of Hydrology

George R. Herrmann, P.E., Professional Hydrologist, Certificate 06-H-1679, Certified and Registered by The American Institute of Hydrology

Supplementary Report:
Subsequent Actions, Observations, and Conditions,
RM 335 and Un-named Stream

Real County, Texas
Reconnaissance on 6 August, 2008
Supplement to Report from Reconnaissance on 3 April, 2007

George R. Herrmann, P.E., P.H.

Introduction

This report continues the documentation of actions and occurrences at a previously
examined damaged stream/roadway crossing site, and is attached to a previous report. It
documents the subsequent repair of the damaged crossing and the events and decisions
surrounding it.

Update on Previous Recommendations

In the previous report, I suggested the installation of a single, large, horizontal elliptical
pipe as a compromise between high-head performance and focused velocity at low flows.
Appendix A details and illustrates some examples of the logic behind that
recommendation. However, it was found that elliptical concrete pipe was not
manufactured in the state of Texas at the time or currently, and would require
considerable time and expense to manufacture or obtain. An emergency contract was
authorized for repair, which implied that time was of the essence. The use of that
configuration was therefore not practical. The "pipe arch" shape was considered, but
would have had to be manufactured in the size desired, which was not compatible with
the emergency schedule. It was considered necessary to use off-the-shelf components.
However, rather than abandon the ideas upon which the recommendation for elliptical
pipe was made, an alternative was sought.

Design of the Replacement Structure

As elaborated on in Appendix A, it was considered desirable to use a conduit that
presents a curved boundary and thus appropriate growth characteristics of the important
flow properties for sediment transport. It was considered important that small flows not
be divided or distributed over large lateral widths, making the traditional installation of
multiple barrels on the same grade and elevation undesirable.

An innovative solution to this set of constraints was to construct a multiple-barrel
structure of off-the-shelf circular concrete pipe of two different diameters, matching the
pipe soffit elevations rather than flow lines as is traditional with multi-barrel culverts. An
illustration of this concept is shown in figure S1. By doing so, we were able to maintain
the desirable aspects of the growth curves for the important flow characteristics of a
large, single circular pipe at low flows, while providing additional discharge capacity for
water flow at higher depths. It was hypothesized that near-boundary velocity vectors

would be focused and optimized along the center of the approach and departure channels, as well as in the center (main) conduit even under high flows, providing good conduct of gravel- to cobble-size particles through the structure throughout a considerable flow depth range.

The structure as built is composed of a single 72" circular concrete pipe flanked on both sides by 42" circular concrete supplemental pipes. Since the supplemental pipes are set with soffits matching the main pipe, their flow lines are 30" above that of the main pipe and conduct no flow until water reaches a depth of 30 inches at the upstream end of the structure. The availability of emergency funds necessitated the specification of materials for estimation purposes on a moment's notice. The sizes were therefore selected based on nothing more than an educated and informed best-guess. I had previously gone through the exercise in Appendix A and therefore had considerable information, but I had not analyzed the particular configuration that I specified.

As noted in the original report and shown in Figures 3 and 4 of that document, there was a considerable difference in elevation (approximately 8 feet) from the upstream side of the crossing to the downstream side, composed of gravel accumulated on the upstream side. The entire effort was centered on the idea of allowing gravel already accumulated to be released downstream, and to prevent future recurrence of that accumulation. The immediate release of the accumulated gravel was thought to be potentially undesirable, as such a volume may clog even a very large conduit. For that reason, the original plan included a drop-inlet-like structure upstream composed of gabion baskets that could be removed in layers to affect a controlled release of gravel over a period of years. The actual project plans were done by Dennis M. "Marshall" Heap, P.E. of the TxDOT Junction Area Office, upon my recommendation of a configuration. Drawings showing the approximate geometry of the installation as planned are shown in Figure S1. As will be described later, the gabion basket inlet was unnecessary and was not constructed.
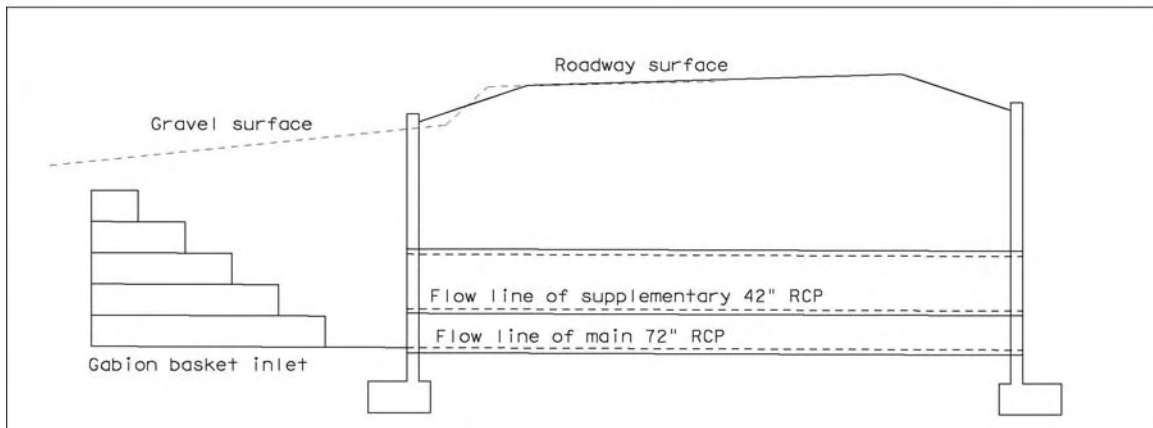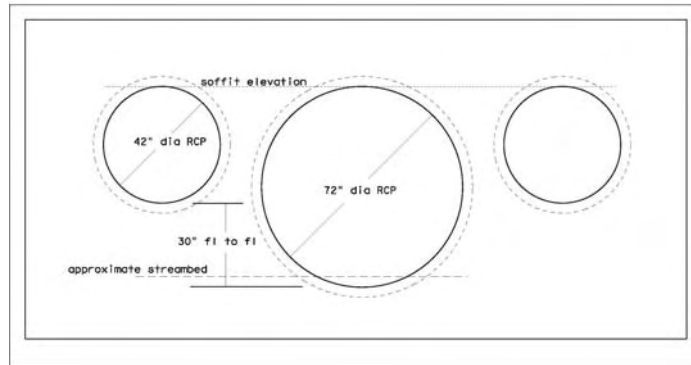
Figure S1
Approximate pipe configuration

Construction and Subsequent Performance

The crossing as it existed on the date of the second reconnaissance is shown in Figures S2- S6. Construction of the replacement crossing was undertaken in a timely manner, proceeding as specified. As can be seen in Figure S2, gravel had to be removed from the upstream side to facilitate the construction process. After the installation of the pipes and the substantial completion of the crossing itself but prior to the construction of the upstream gabion basket gravel metering inlet, there was a rainfall and associated runoff event of moderate but undocumented magnitude.   Upon the recession of flow, project personnel observed that the preponderance of the gravel stored upstream had apparently already been transported away, leaving the stream in a condition substantially closer to that prior to the presence of the accumulation. This indicated that fears of ill effects from the immediate release of such a volume of gravel were unfounded, and as a result the gabion structure was omitted.

The photographs in Figures S2-S3 may be compared to those in Figures 3 and 4 of the original report to gage the changes in the stream above the crossing.

Figure S2
Upstream side of the completed replacement crossing, looking south.
This photograph is comparable to Figure 3 in the original report.

Figure S3
Upstream side of the completed replacement crossing, looking slightly upstream.
Note the re-establishment of visible banks in the upstream channel.

Figure S4
Downstream channel, second reconnaissance

Figures S5-S6 document the structure as built and as in place on August 6, 2008.

Figure S5- Downstream end

Figure S6- Upstream end

Information on occurrences during construction was relayed to me in conversation by Lewis Nowlin, P.E., Junction Area Engineer

The speed with which this situation began to remedy itself when provided with favorable conditions was surprising. With no real way of knowing how long it took for the gravel then present to accumulate, taking years to remedy would not have been surprising. This can be construed as evidence of the magnitude of gravel transport potential in streams like this.

At the time of the second reconnaissance, the structure appeared to be functioning better than anticipated to move both water and gravel. Both the upstream and downstream channels appear to be progressing in the direction of natural configuration. Considering the sheer mass of sediment transported away from the crossing in approximately one year, I am very encouraged with the conditions I observed.

Attached as Figures S7 and S8 are photographs that were taken by Junction Area Office personnel immediately following the event mentioned. Figure S7 is a view upstream from the roadway; the former height of the gravel accumulation can be seen as a line on the top of the rock at the extreme left, and in the remaining gravel accumulated around vegetation on the far right. Figure S8 is a picture of cobble-size material in the culvert barrel. The transport of particles of this size is difficult to explain theoretically, but obviously occurs with some regularity in cases like this.

Figure S7- Looking upstream from the crossing just after the event mentioned.

Figure S8
Cobbles in the Center Barrel

Discussion and Conclusions

As stated earlier, a detailed analysis was not done on the actual configuration prior to installation. With some thought, though, it is evident that such an analysis should not be difficult. The performance curve of a 72" pipe on the slope in question holds until the upstream depth reaches the flow lines of the smaller barrels. At that point, the performance curve of a pair of 42" pipes, with initial conditions at that elevation, can be added to the curve of the 72" pipe by superposition. Thus might a set of performance curves for any combination of pipes be constructed and compared to one another, and possibly to the bankfull cross section of a stream.

In theory, there may be no limit to the combination of sizes and offset elevations of barrels that can be combined in this manner. In that way, a performance curve might be matched to any need. In practicality, some restrictions might occur due to the flow division/distribution phenomenon discussed with respect to double-barrel structures in Appendix A. However, by combining this concept with horizontal elliptical pipe (if it were to become available), a great deal of flexibility might be obtained.

This concept appears to hold considerable promise for the treatment of similar situations. It could easily be extended to any type of culvert in the interest of establishing or re-

establishing something resembling natural sediment throughput and processes. In my opinion, it warrants considerable further research, both physical modeling and conceptual development.

The seal appearing on this document
was authorized by
George R. Herrmann, P.E., 79293
on
21 August 2008

I hereby certify that this document was prepared by me or under my direct supervision, and I am duly certified and registered as a Professional Hydrologist under the Rules and Regulations of the American Institute of Hydrology

George R. Herrmann, P.E., Professional Hydrologist, Certificate 06-H-1679, Certified and Registered by The American Institute of Hydrology

George R. Herrmann

Appendix A- Performance Curves of Various Conduits

Figures A1, A2, and A3 illustrate the phenomenon of interest; the relative performance of conduits of different shape but of roughly comparable size. Identical "hydraulic size" is impossible because of the difference in geometry.

The conduit conditions compared were a single 72" X 113" horizontal ellipse, a single 72" circle, a double 72" circle, and a rectangular box shape 7.4' wide and 6' high. The choice of a nonsensical box width of 7.4' was made in order to give a flow area identical to the 72" X113" horizontal ellipse in order to make the closest comparison possible. The choice of both single and double circular pipes was made for a similar reason- to bracket the performance of the elliptical pipe.
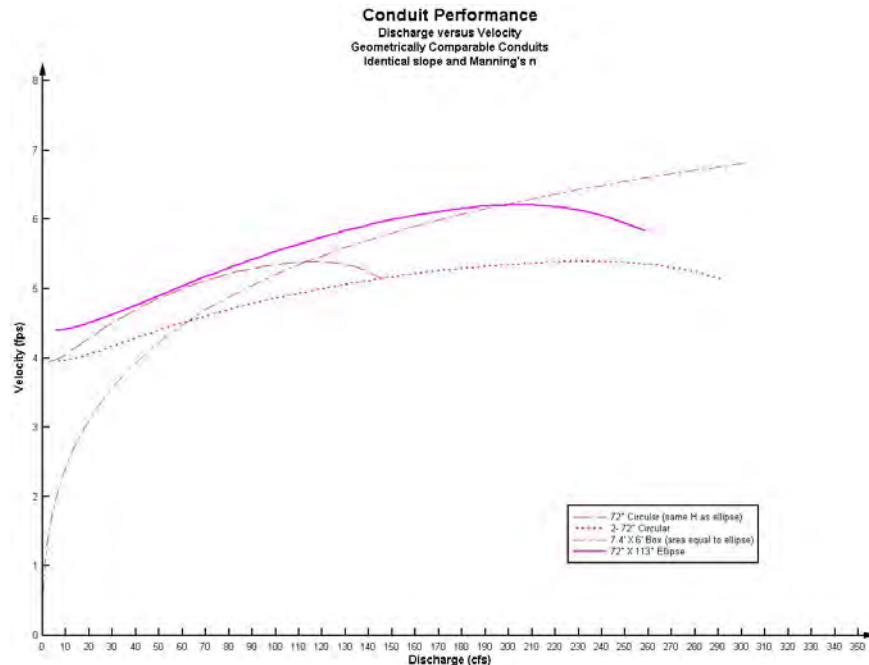
Figure A1
Graph of velocity vs. discharge for various conduit configurations.

Figure A1 is a graph of velocity on the ordinate versus discharge on the abscissa. Note that all of the curved-boundary sections exhibit a performance curve that is not monotonic increasing, while the rectangular section demonstrates a curve that is. The curved sections show a limb of diminishing velocity. This is a well-known phenomenon due to the increase in wetted perimeter compared to area as water level exceeds the springline of the pipe.
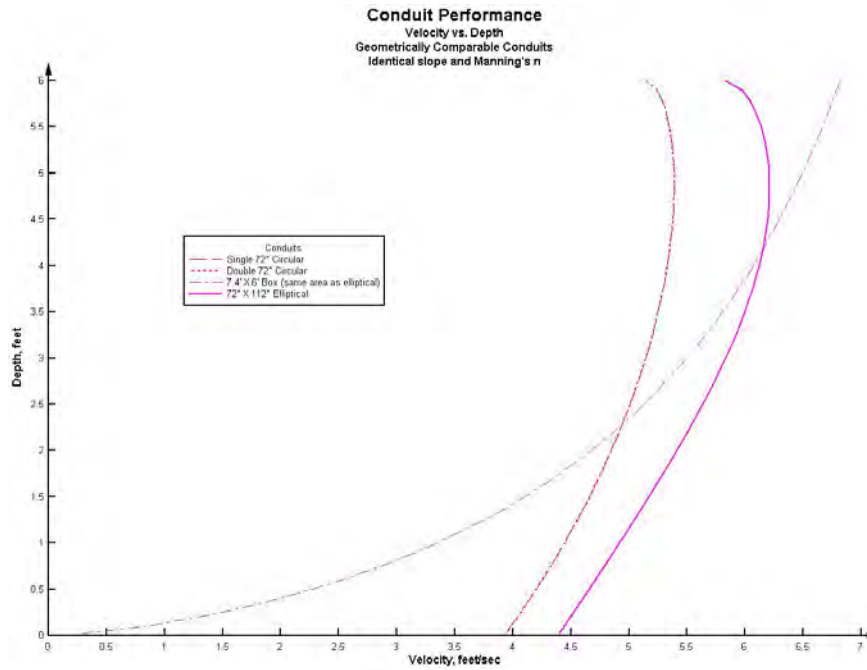
Figure A2
Graph of depth vs. velocity for the same conduit configurations.
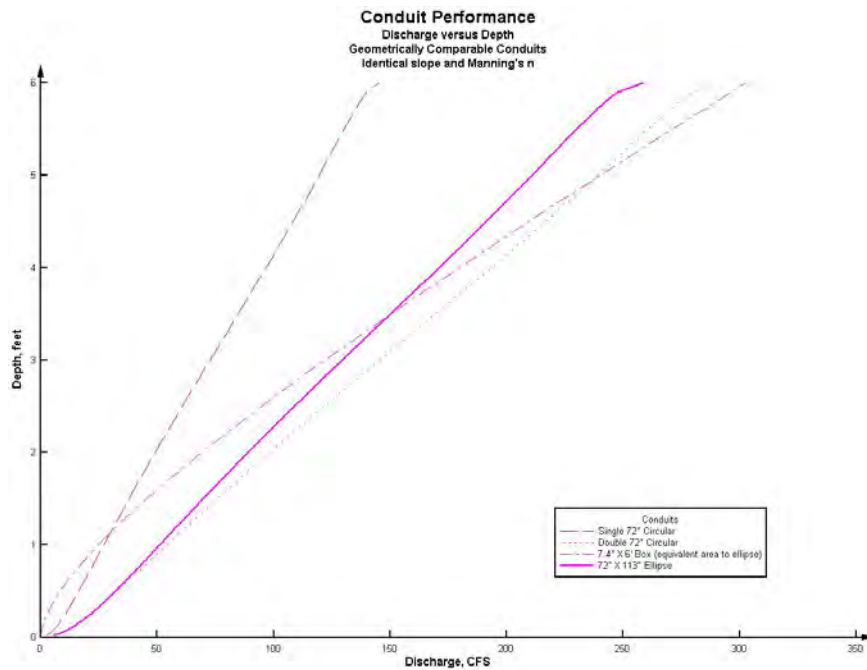
Figure A3
Graph of depth vs. discharge for the same conduit configurations.

The horizontal ellipse exhibits the greatest velocity immediately upon the beginning of perceptible discharge. This translates to a similar maximum position in the depth vs. velocity graph, Figure A2. On Figure A3, the depth vs. discharge graph, the horizontal ellipse and the double circular configuration are very similar at small depths and discharges, with the double circle carrying more discharge at higher depths, due obviously to its greater area. With this configuration, low flows are focused in a single jet through the structure. If the structure is roughly similar in configuration to the approach and departure channels, a reasonably uninterrupted jet can be expected above, through, and below the structure.

A single circular conduit exhibits a smaller initial velocity value, gains faster, diminishes faster, and reaches full flow at a much lower discharge than the other sections. This is shown in both the velocity vs. discharge and depth vs. velocity graphs. It also exhibits the most rapid growth of depth with discharge and of course reaches full flow at a lower discharge than the other configurations. The approach, through-structure, and departure streamlines would be similar in nature to those discussed for the ellipse.

The double circle exhibits a velocity vs. discharge curve that is simply the curve for the single conduit stretched along twice the discharge. The depth vs. velocity curve is identical to that for a single circular, while the depth vs. discharge curve shows a slope that is half that for the single circle. All of the above property relationships between the single and double circles should be intuitively obvious. One that is also obvious but the importance of which is less obvious is that flow is split between two loci in the double configuration. Velocity in the approach and departure channels in this configuration will be distributed over a width somewhat greater than the center-to-center spacing of the conduits, ultimately dividing near the upstream face of a structure. The magnitude of this effect is uncertain, but intuitively it should reduce stream power in the approach and departure reaches.

As might be expected, all of the graphs for a rectangular box structure are dramatically different from those for the curved-boundary shapes. The velocity vs. discharge curve is a continuous, monotonically increasing curve similar in appearance to a logarithmic curve (concave downward), with an initial value of zero. Maximum capacity is the greatest by virtue of flow area being greatest, but velocity does not reach a value similar to the initial value of the other shapes until discharge is roughly 25% of maximum capacity. That velocity is also distributed over the entire structure width, rather than being focused in the center. The depth vs. velocity curve does not approach that of the other shapes until depth is almost half of the structure height. The shape of that curve is monotonically increasing with an upward concavity and an initial velocity value of zero. Depth versus discharge for the rectangular structure is also a monotonically increasing, concave-downward curve. For very small discharge, depth is greater than the other shapes because of the increased wetted perimeter of the wide section. It crosses that of the single circular first, followed by the ellipse, then the double circular, terminating at the highest discharge for full flow of the configurations investigated. However, it must

be stressed that for the rectangular structure all flows, are distributed over a much greater lateral width than for any other shape. This is especially important for small flows.

If all we were trying to move was water, the rectangular box appears to be the most efficient shape to fit within specific height and lateral width constraints. That should be intuitive, in that specific single-valued constraints on each axis of a two-dimensional orthogonal plane defines a rectangle. The truth of this is ubiquitous in highway drainage and the number of box culverts in place. The prevailing thought behind culvert design is now and always has been that water was the only important material moving across the landscape in streams. The movement of suspended sediment moving in water can be considered as a fluid- movement is simply incidental to the movement of the water. Bedload sediment is not so simple; bedload material moves as a distinctly different material phase.

If we depart from that prevailing thought and acknowledge that streams also move sediment by bedload transport mechanisms, then we see that we must accommodate the movement of that sediment of all types through highway structures. The ability of flow to move sediment is a function of both the velocity and depth of that flow. Neither absolute velocity nor absolute depth can be considered dominant; the relationship between them must be managed, and managed across a wide range of flow discharges. No single point on the depth/discharge/velocity relationship constitutes a satisfactory criterion, we must pay close attention to shape of the curves involved. In short, we must not inhibit water from moving sediment through our structures at small to moderate discharges. Studying the nature of curves such as those shown is a step in that process.